Characterization of the small *Arabidopsis thaliana* GTPase and ADP-ribosylation factor-like 2 protein TITAN 5

Inga Mohr[1], Amin Mirzaiebadizi[2], Sibaji K. Sanyal[1], Pichaporn Chuenban[1], Mohammad R. Ahmadian[2], Rumen Ivanov[1] and Petra Bauer[1,3]

[1]Institute of Botany, Heinrich Heine University, 40225 Düsseldorf, Germany.
[2]Institute of Biochemistry and Molecular Biology II, Medical Faculty and University Hospital Düsseldorf, Heinrich Heine University, Düsseldorf, Germany
[3]Cluster of Excellence on Plant Sciences, Heinrich Heine University, 40225 Düsseldorf, Germany.

Author contributions: I.M., M.R.A., R.I., and P.B. conceived the project; I.M., A.M., S.K.S., P.C., M.R.A., R.I. and P.B. designed experiments, supervised the research and analyzed data; I.M., A.M., S.K.S., and P.C. performed experiments and analyzed data; I.M. wrote the manuscript; I.M., A.M., M.R.A., R.I., and P.B. edited the manuscript; P.B. acquired funding. R.I. and P.B. agreed to serve as the author responsible for contact and communication.

Highlights

- The small ARF-like GTPase TTN5 has a very rapid intrinsic nucleotide exchange capacity with a conserved nucleotide switching mechanism
- Biochemical data classified TTN5 as a non-classical small GTPase, likely present in GTP-loaded active form in the cell
- YFP-TTN5 is dynamically associated with vesicle transport and different processes of the endomembrane system, requiring the active form of TTN5

Running title

ARF-like GTPase TTN5 functions

Abstract

Small GTPases function by conformational switching ability between GDP- and GTP-bound states in rapid cell signaling events. The ADP-ribosylation factor (ARF) family is involved in vesicle trafficking. Though evolutionarily well conserved, little is known about ARF and ARF-like GTPases in plants. Here, we characterized biochemical properties and cellular localization of the essential small ARF-like GTPase TITAN 5/HALLIMASCH/ARL2/ARLC1 (hereafter termed TTN5) from *Arabidopsis thaliana*. Two TTN5 variants were included in the study with point mutations at conserved residues, suspected to be functional for nucleotide exchange and GTP hydrolysis, $TTN5^{T30N}$ and $TTN5^{Q70L}$. We found that TTN5 had a very rapid intrinsic nucleotide exchange capacity with a conserved nucleotide switching mechanism. TTN5 acted as a non-classical small GTPase with a remarkably low GTP hydrolysis activity, suggesting it is likely present in GTP-loaded active form in the cell. We analyzed signals from yellow fluorescent protein (YFP)-tagged TTN5 and from *in situ* immunolocalization of hemagglutine-tagged HA_3-TTN5 in Arabidopsis seedlings and in a transient expression system. Together with colocalization using endomembrane markers and pharmacological treatments the microscopic analysis suggests that TTN5 can be present at the plasma membrane and dynamically associated with membranes of vesicles, Golgi stacks and multivesicular bodies.

While the TTN5^{Q70L} variant showed similar GTPase activities and localization behavior as wild-type TTN5, the TTN5^{T30N} mutant differed in some aspects.

Hence, the unusual capacity of rapid nucleotide exchange activity of TTN5 is linked with cell membrane dynamics, likely associated with vesicle transport pathways in the endomembrane system.

Keywords

TTN5; ARF-like; ARL2; endomembrane; GTPase; plasma membrane; vesicle

Abbreviations

Arabidopsis	*Arabidopsis thaliana*
ARF-like / ARL	ADP-ribosylation factor-like
BFA	brefeldin A
EE	early endosomes
GAP	GTPase-activating protein
GEF	guanine nucleotide exchange factor
MVB	multivesicular body
TGN	*trans*-Golgi network
TTN5	TITAN 5

Introduction

A large variety of regulatory processes in signal transduction depends on guanine nucleotide-binding proteins of the GTPase family. Following the identification of common oncogenes (*HRAS, KRAS* and *NRAS*) a new class of GTPases has been recognized, that became known as the RAS superfamily of small GTPases (Bos 1988, Hall 1990, Kahn et al. 1992). RAS proteins have many conserved members in the eukaryotic kingdom. The RAS superfamily consists of five subfamilies in mammals: the Rat sarcoma (RAS), RAS homologs (RHO), RAS-like proteins in the brain (RAB), Ras-related nuclear proteins (RAN) and ADP-ribosylation factor (ARF) subfamilies (Kahn et al. 1992, Ahmadi et al. 2017). In *Arabidopsis thaliana* (Arabidopsis) only four families are represented, the ROP (Rho of plants), RAB, RAN and the ARF (Vernoud et al. 2003). The subfamilies are classified by sequence identity and characteristic sequence motifs with well-conserved regulatory functions within the cell (Kahn et al. 1992). Many mammalian small GTPases act as molecular switches in signal transduction. They switch from inactive GDP-loaded to active GTP-loaded GTPase form. The different activity states enable them to form differential complexes with proteins or act in tethering complexes to the target membrane. Small GTPases have usually low intrinsic GDP/GTP exchange and GTP hydrolysis activity and require the regulation by guanine nucleotide exchange factors (GEFs) and GTPase-activating proteins (GAPs). GEFs are potentially recruited to the inactive, GDP-bound GTPase at their site of action and accelerate GDP/GTP exchange leading to GTPase activation. GTP binding induces a conformational change of two regions referred to as switch I and II. The active, GTP-loaded GTPases exert their function *via* direct interaction with their effectors (Sztul et al. 2019, Nielsen 2020, Adarska et al. 2021) until their inactivation by GAPs, which stimulate the hydrolysis of GTP. Most of the known protein interactions important for their signaling functions occur in the active conformation of the GTPases. Members of the ARF family contain a conserved glycine at position 2 (Gly-2) for the characteristic *N*-myristoylation of an amphipathic helix (Kahn et al. 1992). ARF GTPases are often involved in vesicle-mediated endomembrane trafficking in mammalian cells and yeast (Just and Peränen 2016).

In plants, the activities of small GTPases and their functional environments in the plant cells are by far not understood well and only described in a very rudimentary manner. In particular, the ARF family of small GTPases is surprisingly poorly described in plants, although the Arabidopsis ARF family consists of twelve ARF, seven ARF-like and the associated SAR1 proteins (Singh et al. 2018). The best-studied plant ARF-GTPases, SAR1 and ARF1, act in the anterograde and retrograde vesicle transport between the endoplasmic reticulum (ER) and the Golgi. SAR1 is involved in COPII trafficking from the ER to the Golgi, whereas ARF1 participates in the opposite COPI pathway (Singh et al. 2018, Nielsen 2020). Another ARF-like protein, ARL1, has perhaps a role in endosome-to-Golgi trafficking (Latijnhouwers et al. 2005, Stefano et al. 2006). These roles of ARF1 and SAR1 in COPI and II vesicle formation within the endomembrane system are well conserved in eukaryotes which raises the question of whether other plant ARF members are also involved in functioning of the endomembrane system. A recent study showed Golgi-related localization for some ARF and ARF-like proteins (Niu et al. 2022) promoting a general involvement of the ARF family in the endomembrane system.

TITAN 5 (TTN5)/HALLIMASCH (HAL)/ARF-LIKE 2 (ARL2), ARLC1, from here on referred to as TTN5, is essential in plant development. It was identified in two independent screens for abnormal embryo mutants. The *ttn5* loss-of-function mutants are arrested soon after cell division of the fertilized egg cell, indicating a fundamental, potentially housekeeping role in cellular activities (Mayer et al. 1999, McElver et al. 2000, Lloyd and Meinke 2012). TTN5 is closely related in sequence to human ADP-ribosylation factor-like 2 (HsARL2). HsARL2 has high nucleotide dissociation rates, being up to 4000-fold faster compared to RAS (Hanzal-Bayer et al. 2005, Veltel et al. 2008). HsARL2 is associated with different functions in cells, ranging from microtubule development, also identified for yeast and Caenorhabditis homologs (Bhamidipati et al. 2000, Fleming et al. 2000, Radcliffe et al. 2000, Antoshechkin and Han 2002, Tzafrir et al. 2002, Mori and Toda 2013), adenine nucleotide transport in mitochondria (Sharer et al. 2002) and control of phosphodiesterase activity in cilia (Ismail et al. 2011, Fansa and Wittinghofer 2016). It is thought that HsARL2 requires fast-acting nucleotide exchange and participates in different cellular processes that depend on developmental and tissue-specific factors. With regard to the plant ortholog, it is still completely unknown, which cellular roles TTN5 fulfills in plants. Until today, the function of this small plant GTPase remains elusive at the molecular level. Besides lacking knowledge of the physiological context, the GTPase characteristics and properties of the TTN5 enzyme are not yet demonstrated.

Here, we show by stopped-flow fluorimetry kinetic assays that TTN5 is a functional small GTPase with conserved GTP hydrolysis and very fast nucleotide exchange characteristics. Based on fluorescence microscopy combined with pharmacological treatments, TTN5 may be located at the plasma membrane and within the endomembrane system. Our study enables future investigation of the cellular-physiological functions of this small GTPase.

Results

TTN5 exhibited atypical characteristics of rapid nucleotide exchange and slow GTP hydrolysis

There is a higher sequence similarity of TTN5 with its animal ARL2 ortholog than to any Arabidopsis ARF/ARL proteins (Figure 1A) (McElver et al. 2000, Vernoud et al. 2003). Several observations indicate that TTN5 plays a fundamental and essential role in cellular activities. Loss of function of TTN5 causes a very early embryo-arrest phenotype (Mayer et al. 1999, McElver et al. 2000). An essential TTN5 function is also reflected by its regulation and ubiquitous gene expression during plant development and in the root epidermis revealed in

134 public RNA-seq data sets of organ and single cell analysis of roots (Supplementary Figure
135 S1A, B). *TTN5* is strongly expressed during early embryo development where cell division, cell
136 elongation and cell differentiation take place (Supplementary Figure S1C). Hence, *TTN5* is
137 expressed and presumably functional in very fundamental processes in cells with stronger
138 expression when cells grow and divide.
139 The molecular switch functions can be presumed for TTN5 based on its sequence similarity
140 and structural prediction (Figure 1B, C). HsARL2 has a fast GDP/GTP exchange characteristic
141 (Hanzal-Bayer et al. 2005, Veltel et al. 2008). However, it had not been known whether the
142 plant TTN5 has similar or different GTPase characteristics as its animal counterparts. In this
143 study, we characterized the nucleotide binding and GTP hydrolysis properties of $TTN5^{WT}$ and
144 two of its mutants, $TTN5^{T30N}$ and $TTN5^{Q70L}$, using heterologously expressed and purified
145 proteins and *in vitro* biochemical assays, as previously established for human GTPases
146 (Eberth and Ahmadian 2009). The experimental workflow is illustrated in Supplementary
147 Figure S2A-E. The dominant-negative $TTN5^{T30N}$ is assumed to preferentially bind GEFs,
148 sequestering them from their proper context, while the constitutively active $TTN5^{Q70L}$ is thought
149 to be defective in hydrolyzing GTP. Equivalent mutants have been frequently used and
150 characterized in previous studies (Scheffzek et al. 1997, Zhou et al. 2006, Newman et al.
151 2014). We monitored the real-time kinetics of the interactions of fluorescent guanine
152 nucleotides using stopped-flow fluorimetry suited for very rapid enzymatic reactions (Figure
153 2A-C). 2-deoxy-3-O-N-methylanthraniloyl-deoxy-GDP (mdGDP) and GppNHp (mGppNHp), a
154 non-hydrolyzable GTP analog, were used to mimic GDP and GTP binding to TTN5 proteins.
155 This approach allowed us to monitor real-time kinetics and quantify nucleotide association and
156 dissociation characteristics of small GTPases, such as HsARL2 and HsARL3 (Hillig et al. 2000,
157 Hanzal-Bayer et al. 2005, Veltel et al. 2008, Zhang et al. 2018). The kinetics allow us to
158 determine the association rate constant (k_{on}) and the dissociation rate constant (k_{off}),
159 respectively. The k_{on} value is defined as the rate of nucleotide binding to the GTPase to form
160 the GTPase-nucleotide complex (Figure 2B) whereas the k_{off} value describes the rate of
161 nucleotide dissociation from the GTPase (Figure 2C). We found that TTN5 proteins were able
162 to bind both nucleotides, with the exception of mGppNHp binding by $TTN5^{T30N}$ (Supplementary
163 Figures S3A-F, S4A-E). $TTN5^{Q70L}$ revealed the highest k_{on} value for mGDP binding (0.401 $\mu M^{-1}s^{-1}$),
164 which was 9-fold higher compared to $TTN5^{WT}$ (0.044 $\mu M^{-1}s^{-1}$) and $TTN5^{T30N}$ (0.048 $\mu M^{-1}s^{-1}$),
165 respectively (Figure 2D; Supplementary Figure S3D-F). The k_{on} values for mGppNHp
166 binding were 2-fold lower for $TTN5^{WT}$ (0.029 $\mu M^{-1}s^{-1}$) and $TTN5^{Q70L}$ (0.222 $\mu M^{-1}s^{-1}$) compared
167 to those for mGDP binding, respectively (Figure 2E; Supplementary Figure S4C, D). The
168 differences in k_{on} for the respective nucleotide binding were small. However, $TTN5^{Q70L}$ showed
169 a 7.5-fold faster mGppNHp binding than $TTN5^{WT}$. A remarkable observation was that we were
170 not able to monitor the kinetics of mGppNHp association with $TTN5^{T30N}$ but observed its
171 dissociation (k_{off} = 0.026 s^{-1}; Figure 2E). To confirm the binding capability of $TTN5^{T30N}$ with
172 mGppNHp, we measured the mGppNHp fluorescence in real-time before and after titration of
173 nucleotide-free $TTN5^{T30N}$. As shown in Supplementary Figure S4B, the binding of mGppNHp
174 to $TTN5^{T30N}$ occurs so fast that it was not possible to resolve the rate of association.
175 We next measured the dissociation (k_{off}) of mdGDP and mGppNHp from the TTN5 proteins in
176 the presence of excess amounts of GDP and GppNHp, respectively (Figure 2C) and found
177 interesting differences (Figure 2D, E; Supplementary Figures S3G-I, S4F-H). First, $TTN5^{WT}$
178 showed a k_{off} value (0.012 s^{-1} for mGDP) (Figure 2D; Supplementary Figure S3G), which was
179 100-fold faster than those obtained for classical small GTPases, including RAC1 (Haeusler et
180 al. 2006) and HRAS (Gremer et al. 2011), but very similar to the k_{off} value of HsARF3 (Fasano
181 et al. 2022). Second, the k_{off} values for mGDP and mGppNHp, respectively, were in a similar

182 range between TTN5^{WT} (0.012 s^{-1} mGDP and 0.001 s^{-1} mGppNHp) and TTN5^{Q70L} (0.025 s^{-1}
183 mGDP and 0.006 s^{-1} mGppNHp), respectively, but the k_{off} values differed 10-fold between the
184 two nucleotides mGDP and mGppNHp in TTN5^{WT} (k_{off} = 0.012 s^{-1} versus k_{off} = 0.001 s^{-1}; Figure
185 2D, E; Supplementary Figure S3G, I, S4F, H). Thus, mGDP dissociated from proteins 10-fold
186 faster than mGppNHp. Third, the mGDP dissociation from TTN5^{T30N} (k_{off} = 0.149 s^{-1}) was 12.5-
187 fold faster than that of TTN5^{WT} and 37-fold faster than the mGppNHp dissociation of TTN5^{T30N}
188 (k_{off} = 0.004 s^{-1}) (Figure 2D, E; Supplementary Figure S3H, S4G). Mutants of CDC42, RAC1,
189 RHOA, ARF6, RAD, GEM and RAS GTPases, equivalent to TTN5^{T30N}, display decreased
190 nucleotide binding affinity and therefore tend to remain in a nucleotide-free state in a complex
191 with their cognate GEFs (Erickson et al. 1997, Ghosh et al. 1999, Radhakrishna et al. 1999,
192 Jung and Rösner 2002, Kuemmerle and Zhou 2002, Wittmann et al. 2003, Nassar et al. 2010,
193 Huang et al. 2013, Chang and Colecraft 2015, Fisher et al. 2020, Shirazi et al. 2020). Since
194 TTN5^{T30N} exhibits fast guanine nucleotide dissociation, these results suggest that TTN5^{T30N}
195 may also act in either a dominant-negative or fast-cycling manner as reported for other GTPase
196 mutants (Fiegen et al. 2004, Wang et al. 2005, Fidyk et al. 2006, Klein et al. 2006, Soh and
197 Low 2008, Sugawara et al. 2019, Aspenström 2020).
198 The dissociation constant (K_d) is calculated from the ratio k_{off}/k_{on}, which inversely indicates
199 the affinity of the interaction between proteins and nucleotides (the higher K_d, the lower affinity).
200 Interestingly, TTN5^{WT} binds mGppNHp (K_d = 0.029 µM) 10-fold tighter than mGDP (K_d =
201 0.267 µM), a difference, which was not observed for TTN5^{Q70L} (K_d for mGppNHp = 0.026 µM,
202 K_d for mGDP = 0.061 µM) (Figure 2D, E). The lower affinity of TTN5^{WT} for mdGDP compared
203 to mGppNHp brings us one step closer to the hypothesis that classifies TTN5 as a non-
204 classical GTPase with a tendency to accumulate in the active (GTP-bound) state (Jaiswal et
205 al. 2013). The K_d value for the mGDP interaction with TTN5^{T30N} was 11.5-fold higher
206 (3.091 µM) than for TTN5^{WT}, suggesting that this mutant exhibited faster nucleotide exchange
207 and lower affinity for nucleotides than TTN5^{WT}. Similar as other GTPases with a T30N
208 exchange, TTN5^{T30N} may behave in a dominant-negative manner in signal transduction
209 (Vanoni et al. 1999).

210 To get hints on the functionalities of TTN5 during the complete GTPase cycle, it was crucial
211 to determine its ability to hydrolyze GTP. Accordingly, the catalytic rate of the intrinsic GTP
212 hydrolysis reaction, defined as k_{cat}, was determined by incubating 100 µM GTP-bound TTN5
213 proteins at 25°C and analyzing the samples at various time points using a reversed-phase
214 HPLC column (Figure 2F; Supplementary Figure S5). The determined k_{cat} values were quite
215 remarkable in two respects (Figure 2G). First, all three TTN5 proteins, TTN5^{WT}, TTN5^{T30N} and
216 TTN5^{Q70L}, showed quite similar k_{cat} values (0.0015 s^{-1}, 0.0012 s^{-1}, 0.0007 s^{-1}; Figure 2G;
217 Supplementary Figure S5). The GTP hydrolysis activity of TTN5^{Q70L} was quite high (0.0007 s^{-}
218 ^{1}). This was unexpected because, as with most other GTPases, the glutamine mutations at the
219 corresponding position drastic impair hydrolysis, resulting in a constitutively active GTPase in
220 cells (Hodge et al. 2020, Matsumoto et al. 2021). Second, the k_{cat} value of TTN5^{WT} (0.0015 s^{-}
221 ^{1}) although quite low as compared to other GTPases (Jian et al. 2012, Esposito et al. 2019),
222 was 8-fold lower than the determined k_{off} value for mGDP dissociation (0.012 s^{-1}) (Figure 2E).
223 This means that a fast intrinsic GDP/GTP exchange versus a slow GTP hydrolysis can have
224 drastic effects on TTN5 activity in resting cells, since TTN5 can accumulate in its GTP-bound
225 form, unlike the classical GTPase (Jaiswal et al. 2013). To investigate this scenario, we pulled
226 down GST-TTN5 protein from bacterial lysates in the presence of an excess amount of
227 GppNHp in the buffer using glutathione beads and measured the nucleotide-bound form of
228 GST-TTN5 using HPLC. As shown in Figure 2H, isolated GST-TTN5 increasingly bonds
229 GppNHp, indicating that the bound nucleotide is rapidly exchanged for free nucleotide (in this

230 case GppNHp). This is not the case for classical GTPases, which remain in their inactive GDP-
231 bound forms under the same experimental conditions (Walsh et al. 2019, Hodge et al. 2020).

232 In summary, the TTN5 sequence not only contains conserved regions necessary for
233 nucleotide binding but theTTN5 protein also binds nucleotides detectably. Interestingly, the
234 slow intrinsic GTP hydrolysis rates in combination with the high dissociation rates for GDP
235 suggest that TTN5 tends to exist in a GTP-loaded form. A fast intrinsic GDP/GTP exchange
236 and a slow GTP hydrolysis can have drastic effects on TTN5 activity in cells under
237 resting/unstimulated conditions, as TTN5 can accumulate in its GTP-bound form, unlike the
238 classical GTPases (Jaiswal et al. 2013). On the other hand, the originally suspected
239 constitutively active TTN5^{Q70L} still has intrinsic GTPase activity, while the T30N variant exhibits
240 a low affinity for mGDP. Therefore, we propose that TTN5 exhibits the typical functions of a
241 small GTPase based on *in vitro* biochemical activity studies, including guanine nucleotide
242 association and dissociation, but emphasizes its divergence among the ARF GTPases by its
243 kinetics.
244

245 **TTN5 may be a highly dynamic protein and localize to different intracellular**
246 **compartments**

247 Several ARF GTPases function in vesicle transport and are located at various membranous
248 sites linked with the endomembrane compartments in eukaryotes (Vernoud et al. 2003).
249 Localization had not been comprehensively studied for TTN5. To obtain hints where in a cell
250 TTN5 may be localized, we first created transgenic Arabidopsis lines constitutively expressing
251 YFP-tagged TTN5 (pro35S::YFP-TTN5) and its two mutant forms (pro35S::YFP-TTN5^{T30N},
252 pro35S::YFP-TTN5^{Q70L}) and investigated the localization in 6-day-old seedlings in the
253 epidermis of cotyledons, hypocotyls, root hair zone and in root tips (Figure 3A; Supplementary
254 Figure S6A). The microscopic observations were made in different planes of the tissues, e.g.
255 inside the cells across the vacuoles (Supplementary Figure S6) and underneath the plasma
256 membrane at the cell peripheries (Figure 3). We chose the investigation of YFP-TTN5 in the
257 epidermis as this is a tissue where *TTN5* transcripts were detected in plants (Supplementary
258 Figure S1B). YFP signals in YFP-TTN5 seedlings were detected in the nucleus, in the
259 cytoplasm and at or in close proximity to the plasma membrane in the epidermal cotyledon
260 cells (Supplementary Figure S6B). The same localization patterns were found for mutant YFP-
261 TTN5 signals (Supplementary Figure S6C-D). The YFP-signals in YFP-TTN5, YFP-TTN5^{T30N}
262 and YFP-TTN5^{Q70L} seedlings were also present in a similar pattern in the stomata (Figure 3B-
263 D). In hypocotyls of seedlings, intracellular YFP signal was observed in nuclei and in close
264 proximity to or at the plasma membrane with all three YFP-TTN5 forms (Supplementary Figure
265 S6E-G). Investigation of the root hair zone showed YFP signals in the cytoplasm and at the
266 plasma membrane of root hairs (Supplementary Figure S6H-J). In the root tip, YFP signal was
267 detectable inside the cytoplasm and in nuclei (Supplementary Figure S6K). The pattern was
268 similar for YFP-TTN5^{T30N} and YFP-TTN5^{Q70L} (Supplementary Figure S6L-M). Fluorescent
269 signal in YFP-TTN5, YFP-TTN5^{T30N} and YFP-TTN5^{Q70L} seedlings inside the cytoplasm was
270 confined to punctate structures indicating that the signals were present in cytosolic vesicle-like
271 structures together with free signals in the cytosol. This localization pattern was also present
272 in leaf epidermal cells and stomata of the cotyledons (Figure 3B-D), in the hypocotyls (Figure
273 3E-G) and in the cells of the root hair zones and in the root hairs (Figure 3H-J). These observed
274 structures point to an association of TTN5 with vesicle and endomembrane trafficking. A closer
275 inspection of the dynamics of these structures in the leaf epidermis of cotyledons showed high
276 mobility of fluorescent signal within the cells (Supplementary Video Material S1A-C), likewise
277 in hypocotyl cells (Supplementary Video Material S1D). Interestingly, the mobility of these

punctate structures differed within the cells when the mutant YFP-TTN5^{T30N} was observed in hypocotyl epidermis cells, but not in the leaf epidermis cells (Supplementary Video Material S1E, compare with S1B) nor was it the case for the YFP-TTN5^{Q70L} mutant (Supplementary Video Material S1F, compare with S1E). We detected approximately half of the cells within the hypocotyl epidermis with slowed-down or completely arrested movement for YFP-TTN5^{T30N}, in contrast to YFP-TTN5 and YFP-TTN5^{Q70L} (Supplementary Video Material S1D-F). This loss of fluorescence signal mobility in YFP-TTN5^{T30N} seedlings may be a consequence of missing effector interaction. We did not observe the blocked mobility for fluorescent signals in cells expressing YFP-TTN5, YFP-TTN5^{T30N} and YFP-TTN5^{Q70L} in the root elongation zone (Supplementary Video Material S1G-I). No mobility of YFP fluorescence signal was visible in root tip cells for any YFP-TTN5 form (Supplementary Video Material S1J-L).

To evaluate the Arabidopsis data and to better visualize YFP-TTN5, we expressed YFP-TTN5 constructs transiently in *Nicotiana benthamiana* leaf epidermis cells. We found that fluorescent signals in YFP-TTN5-, YFP-TTN5^{T30N}- and YFP-TTN5^{Q70L}-expressing cells were also all localized at or in close proximity to the plasma membrane and in several cytosolic punctate structures, apart from the nucleus, similar to Arabidopsis cotyledons, hypocotyls and root hair zones (Figure 3K-N; Supplementary Figure S6N-Q). Additionally, YFP signals were also detected in a net-like pattern typical for ER localization (Figure 3M, N). This showed that localization of fluorescent signal was similar between Arabidopsis epidermis cells and *N. benthamiana* leaf epidermis.

It should be noted that the 35S promoter-driven YFP-TTN5 constructs did not complement the embryo-lethal phenotype of *ttn5-1* (Supplementary Figure S7A, B). We also found multiple YFP bands in α-GFP Western blot analysis using YFP-TTN5 Arabidopsis seedlings. Besides the expected and strong 48 kDa YFP-TTN5 band, we observed three weak bands ranging between 26 to 35 kDa (Supplementary Figure S7C). We cannot explain the presence of these small protein bands. They might correspond to free YFP, to proteolytic products or potentially to proteins produced from aberrant transcripts with perhaps alternative translation start or stop sites. On the other side, a triple hemagglutinin-tagged HA_3-TTN5 driven by the 35S promoter did complement the embryo-lethal phenotype of *ttn5-1* (Supplementary Figure S7D, E). α-HA Western blot control performed with plant material from HA_3-TTN5 seedlings showed a single band at the correct size, but no band that was 13 to 18 kDa smaller (Supplementary Figure S7D). Hence, the inability of YFP-TTN5 to complement the embryo-lethal phenotype was presumably due to the YFP-tag which was rather large compared with the small GTPase and larger than the relatively small HA_3-tag. Interestingly, HA_3-TTN5^{T30N} seedlings presented a root length phenotype, whereas HA_3-TTN5 and HA_3-TTN5^{Q70L} seedlings had no obvious phenotype compared to wild type plants. HA_3-TTN5^{T30N} roots were shorter than those of HA_3-TTN5^{Q70L} and HA_3-TTN5, which can be due to the atypical biochemical TTN5^{T30N} characteristics (Figure 3O).

To verify that the localization patterns observed with the YFP-TTN5 constructs are representative of a functional TTN5, we performed immunofluorescence staining against the HA_3-tag in roots of HA_3-TTN5 seedlings and compared the localization patterns (Figure 3P). Alexa 488-labeled α-HA antibody staining reflected HA_3-TTN5 localization and signals were visible in root cells and root hairs as expected. Signals were mostly present in punctate structures close to the plasma membrane and in the cytosol (Figure 3P), fitting with above described fluorescence signals obtained with the YFP-TTN5 plants.

For a more detailed investigation of HA_3-TTN5 subcellular localization, we then performed co-immunofluorescence staining with an Alexa 488-labeled antibody recognizing the Golgi and TGN marker ARF1, while detecting HA_3-TTN5 with an Alexa 555-labeled antibody (Robinson

326 et al. 2011, Singh et al. 2018) (Figure 4A). ARF1-Alexa 488 staining was clearly visible in
327 punctate structures representing presumably Golgi stacks (Figure 4A, Alexa 488), as
328 previously reported (Singh et al. 2018). Similar structures were obtained for HA_3-TTN5-Alexa
329 555 staining (Figure 4A, Alexa 555). But surprisingly, colocalization analysis demonstrated that
330 the HA_3-TTN5-labeled structures were mostly not colocalizing and thus distinct from the ARF1-
331 labeled ones (Figure 4A). Yet the HA_3-TTN5- and ARF1-labeled structures were in close
332 proximity to each other (Figure 4A). We hypothesized that the HA_3-TTN5 structures can be
333 connected to intracellular trafficking steps. To test this, we performed brefeldin A (BFA)
334 treatment, a commonly used tool in cell biology for preventing dynamic membrane trafficking
335 events and vesicle transport involving the Golgi. BFA is a fungal macrocyclic lactone that leads
336 to a loss of *cis*-cisternae and accumulation of Golgi stacks, known as BFA-induced
337 compartments, up to the fusion of the Golgi with the ER (Ritzenthaler et al. 2002, Wang et al.
338 2016). For a better identification of BFA bodies, we additionally used the dye FM4-64, which
339 can emit fluorescence in a lipophilic membrane environment. FM4-64 marks the plasma
340 membrane in the first minutes following application to the cell, then may be endocytosed and
341 in the presence of BFA become accumulated in BFA bodies (Bolte et al. 2004). We observed
342 BFA bodies positive for both, HA_3-TTN5-Alexa 488 and FM4-64 signals (Figure 4B). Similar
343 patterns were observed for YFP-TTN5-derived signals in YFP-TTN5-expressing roots (Figure
344 4C). Hence, HA_3-TTN5 and YFP-TTN5 can be present in similar subcellular membrane
345 compartments.
346 We did not observe any staining in nuclei or ER when performing HA_3-TTN5
347 immunostaining (Figure 3P; Figure 4A, B), as was the case for fluorescence signals in YFP-
348 TTN5-expressing cells. Presumably, this can indicate that either the nuclear and ER signals
349 seen with YFP-TTN5 correspond to the smaller proteins detected, as described above, or that
350 immunostaining was not suited to detect them. Hence, we focused interpretation on patterns
351 of localization overlapping between the fluorescence staining with YFP-labeled TTN5 and with
352 HA_3-TTN5 immunostaining, such as the particular signal patterns in the specific punctate
353 membrane structures.
354 Taken together, signals of YFP-TTN5 and HA_3-TTN5 were located in multiple membrane
355 compartments in the epidermis of different Arabidopsis organs and of *N. benthamiana* leaves,
356 including the particular ring-like punctate structures and vesicles. Fluorescence signals in YFP-
357 TTN5 and YFP-TTN5^{Q70L}-expressing seedlings displayed high mobility in the cells, as
358 expected from a function of a GTPase in the active state in dynamic processes such as vesicle
359 trafficking. In contrast to that, fluorescence signals in YFP-TTN5^{T30N} were less mobile, in line
360 with the root length phenotype conferred by HA_3-TTN5 ^{T30N}, speaking in favor of the observed
361 kinetics for TTN5^{T30N} with a very fast nucleotide exchange rate and loss of affinity to
362 nucleotides. Altogether, TTN5 intracellular localization seems complex, indicating that TTN5
363 may have multiple cellular functions as an active GTPase as it can be associated with different
364 intracellular structures of the endomembrane system.
365
366 **TTN5 may associate with components of the cellular endomembrane system**
367 The overlapping localization of HA_3-TTN5 and YFP-TTN5 signals prompted us to better
368 resolve the membrane structures and compartments. The endomembrane system is highly
369 dynamic in the cell. Well-established fluorescent endomembrane markers and
370 pharmacological treatments help to determine the nature of individual components of the
371 system in parallel to colocalization studies with proteins of interest such as TTN5. We
372 conducted the colocalization experiments in *N. benthamiana* leaf epidermis. We just described
373 above that fluorescence signals were comparable between *N. benthamiana* leaf epidermis and

374 Arabidopsis cotyledons or root epidermis. Moreover, it represents an established system for
375 functional association of fluorescent proteins with multiple endomembrane components and
376 optimal identification of membrane structures (Brandizzi et al. 2002, Hanton et al. 2009).
377 At first, we further investigated the endoplasmic reticulum (ER)-Golgi connection. This site is
378 characteristic of association with small GTPases like the already tested ARF1, involved in
379 COPI vesicle transport from Golgi to the ER (Just and Peränen 2016). This time, we tested
380 another Golgi marker, the soybean (*Glycine max*) protein α-1,2 mannosidase 1 (GmMan1).
381 GmMan1 is a glycosidase that acts on glycoproteins at the *cis*-Golgi, facing the ER (Figure
382 5A). GmMan1-mCherry-positive Golgi stacks are visible as nearly round punctuate structures
383 throughout the whole cell (Nelson et al. 2007, Wang et al. 2016). Fluorescence signals in leaf
384 discs, transiently expressing YFP-TTN5 and its mutant variants, partially colocalized with
385 GmMan1-mCherry signals at the Golgi stacks (Figure 5B-D). We also observed YFP
386 fluorescence signals in the form of circularly shaped ring structures with a fluorescence-
387 depleted center. These structures can be of vacuolar origin as described for similar fluorescent
388 rings in Tichá et al. (2020) for ANNI-GFP. Further, quantitative analysis reflected the visible
389 colocalization of the GmMan1 marker and YFP fluorescence with Pearson coefficients 0.63
390 (YFP-TTN5), 0.65 (YFP-TTN5^{T30N}) and 0.68 (YFP-TTN5^{Q70L}) (Supplementary Figure S8A; see
391 also similar results obtained with overlap coefficients), indicating a strong correlation between
392 the two signals. We performed an additional object-based analysis to compare overlapping
393 YFP fluorescence signals in YFP-TTN5-expressing leaves with GmMan1-mCherry signals
394 (YFP/mCherry ratio) and *vice versa* (mCherry/YFP ratio). We detected 24 % overlapping YFP-
395 fluorescence signals for TTN5 with Golgi stacks, while in YFP-TTN5^{T30N} and YFP-TTN5^{Q70L}-
396 expressing leaves, signals only shared 16 and 15 % overlap with GmMan1-mCherry-positive
397 Golgi stacks (Supplementary Figure S8B). Some YFP-signals did not colocalize with the
398 GmMan1 marker. This effect appeared more prominent in leaves expressing YFP-TTN5^{T30N}
399 and less for YFP-TTN5^{Q70L}, compared to YFP-TTN5 (Figure 5B-D). Indeed, we identified 48 %
400 GmMan1-mCherry signal overlapping with YFP-positive structures in YFP-TTN5^{Q70L} leaves,
401 whereas 43 and only 31 % were present with YFP fluorescence signals in YFP-TTN5 and YFP-
402 TTN5^{T30N}-expressing leaves, respectively (Supplementary Figure S8B), indicating a smaller
403 amount of GmMan1-positive Golgi stacks colocalizing with YFP signals for YFP-TTN5^{T30N}.
404 Hence, the GTPase-active TTN5 forms are likely more present at *cis*-Golgi stacks compared
405 to TTN5^{T30N}.
406 Next, we evaluated the Golgi localization by BFA treatment. The action of BFA causes a
407 corresponding redistribution of GmMan1-mCherry (Ritzenthaler et al. 2002, Wang et al. 2016)
408 (Figure 5E). We found that upon BFA treatment, GmMan1-mCherry signal was present in the
409 ER and in BFA-induced compartments. YFP-signal of YFP-TTN5 constructs showed partially
410 matching localization with GmMan1-mCherry upon BFA treatment suggesting a connection of
411 TTN5 to Golgi localization (Figure 5F-H). Hence, the colocalization with GmMan1-mCherry
412 and BFA treatment was indicative of YFP signals localizing to Golgi stacks upon YFP-TTN5
413 expression, while the lower association of mostly the YFP-TTN5^{T30N} mutant form with this
414 membrane compartment was noted.
415 Second, we investigated localization to the endocytic compartments, endosomes of the
416 *trans*-Golgi network (TGN) and multivesicular bodies (MVBs) using the marker RFP-ARA7
417 (RABF2B), a small RAB-GTPase present there (Kotzer et al. 2004, Lee et al. 2004, Stierhof
418 and El Kasmi 2010, Ito et al. 2016) (Figure 5I). These compartments play a role in sorting
419 proteins between the endocytic and secretory pathways, with MVBs developing from the TGN
420 and representing the final stage in transport to the vacuole (Valencia et al. 2016, Heucken and
421 Ivanov 2018). Colocalization studies revealed that YFP signal in YFP-TTN5-expressing leaves

422 was present at RFP-ARA7-positive MVBs (Figure 5J). Noticeably, overlaps between RFP-
423 ARA7 and YFP fluorescence signals upon TTN5^{T30N} expression were lower than for the other
424 TTN5 forms (Figure 5J-L; Supplementary Figure S8C, D). We obtained a Pearson coefficient
425 for the pair of either YFP fluorescence upon YFP-TTN5 or YFP-TTN5^{Q70L} expression with RFP-
426 ARA7 of 0.78, whereas a coefficient of only 0.59 was obtained with YFP-TTN5^{T30N} confirming
427 the visual observation (Supplementary Figure S8C; see also similar results for overlap
428 coefficients). Object-based analysis showed that, RFP-ARA7-positive structures had an
429 overlap with YFP fluorescence in YFP-TTN5-expressing (29 %) leaves and even more with
430 YFP-TTN5^{Q70L} (75 %) signals unlike with YFP-TTN5^{T30N} signals (21 %) (Supplementary Figure
431 S8D). Based on this, signals of YFP-TTN5^{Q70L} and YFP-TTN5 tended to colocalize better with
432 ARA7-positive compartments than YFP-TTN5^{T30N}.
433 To test MVB localization, we treated plant cells with wortmannin, a common approach to
434 studying endocytosis events. Wortmannin is a fungal metabolite that inhibits
435 phosphatidylinositol-3-kinase (PI3K) function and thereby causes swelling of the MVBs (Cui et
436 al. 2016) (Figure 5M). RFP-ARA7-expressing cells showed the expected typical wortmannin-
437 induced formation of doughnut-like shaped MVBs (Jaillais et al. 2008). The YFP fluorescence
438 signals in YFP-TTN5-expressing leaves partially colocalized with these structures (Figure 5N-
439 P) indicating that fluorescence signals upon YFP-TTN5 expression and the two mutants are
440 present in MVBs. YFP signals in YFP-TTN5Q70L-expressing leaf discs were located even to
441 a greater extent to MVBs than in wild-type YFP-TTN5 and much more than in YFP-TTN5^{T30N}-
442 expressing cells, suggesting an active role of YFP-TTN5^{Q70L} in MVBs, for example in the lytic
443 degradation pathway or the recycling of proteins, similar to ARA7 (Kotzer et al. 2004).
444 Finally, to investigate a possible connection of TTN5 with the plasma membrane, we
445 colocalized YFP signals of the YFP-TTN5 constructs with the dye FM4-64, which can emit
446 fluorescence in a lipophilic membrane environment and marks the plasma membrane in the
447 first minutes following application to the cell (Bolte et al. 2004) (Figure 6A). Fluorescence
448 signals for all three forms of TTN5 colocalized with FM4-64 at the plasma membrane in a
449 similar manner (Figure 6B-D). To further investigate plasma membrane localization, we
450 performed mannitol-induced plasmolysis. YFP signals for all three YFP-TTN5 constructs were
451 then located similarly to FM4-64-stained Hechtian strands, thread-like structures attached to
452 the apoplast visible upon plasmolysis and surrounded by plasma membrane (Figure 6E-G).
453 In summary, these colocalization experiments showed that YFP signals upon YFP-TTN5
454 expression were found in different membrane sites of the endomembrane system, including
455 Golgi, MVBs and plasma membrane. We figured that similar to other ARF proteins, this pattern
456 can indicate that TTN5 might participate in a highly dynamic vesicle trafficking process. Indeed,
457 when we recorded the dynamic movement of YFP signals inside *N. benthamiana* leaf
458 epidermis cells, YFP-TTN5 and YFP-TTN5^{Q70L} derived signals colocalized with GmMan1-
459 mCherry and revealed high motion over time, while, again, this was less the case for the YFP-
460 TTN5^{T30N} construct (Supplementary Video Material S1M-O).
461 One potential cellular trafficking route is the degradation pathway to the vacuole. We,
462 therefore, investigated fluorescence localization upon YFP-TTN5 transient expression in late
463 endosomal compartments that might be involved in vacuolar targeting. FM4-64 is used as a
464 marker for membranes of late endosomal compartment and vacuole targeting, since following
465 plasma membrane visualization FM4-64-stained endocytic vesicles become apparent at later
466 stages as well as vacuolar membrane staining (Ueda et al. 2001, Emans et al. 2002,
467 Dhonukshe et al. 2007, Ivanov and Vert 2021). Hence, we colocalized YFP signals with FM4-
468 64-positive compartments at later time points. Next to colocalization of YFP fluorescence in
469 YFP-TTN5-expressing leaves with FM4-64 at the plasma membrane, we detected

470 colocalization with fluorescent compartments in the cell, which was similar for the two mutant
471 forms (Figure 6H-J). This indicates that YFP-TTN5 may be involved in the targeting of
472 endocytosed plasma membrane material, irrespective of the mutations.
473 In summary, YFP signals upon YFP-TTN5 and YFP-TTN5^{Q70L} expression were dynamic
474 and colocalized with endomembrane structures, whereas fluorescence signal in YFP-
475 TTN5^{T30N}-expressing leave discs tended to be less mobile and dynamic and colocalized less.

476 **Discussion**

477 This work provides evidence that the small ARF-like GTPase TTN5 has a very rapid intrinsic
478 nucleotide exchange capacity with a conserved nucleotide switching mechanism. TTN5 might
479 be primarily present in a GTP-loaded active form in a cell. TTN5 might be also a dynamic
480 protein inside cells with respect to its localization to membrane structures, which can be a hint
481 on association with vesicle transport and different processes of the endomembrane system.
482 The active TTN5^{Q70L} mutant was capable of nucleotide switching and might be mostly similarly
483 localized as TTN5 in a cell. The TTN5^{T30N} mutant, on the other hand, was affected by a lower
484 nucleotide exchange capacity than the other TTN5 forms. It differed significantly in localization
485 properties and its dynamics, albeit depending on cell types. TTN5^{T30N} also conferred a root
486 length phenotype. Therefore, the GTP-bound state that we presume for TTN5 is most likely
487 very critical for protein localization and dynamics in cells.
488

489 **TTN5 exhibits characteristic GTPase functions**

490 TTN5 was classified as an ARL2 homolog of the ARF GTPases based on its sequence
491 similarity. The sequence analysis suggested nucleotide binding (McElver et al. 2000) which is
492 reinforced by structural prediction suggesting the formation of a nucleotide-binding pocket by
493 the binding motifs. Nucleotide association and dissociation of TTN5, TTN5^{T30N} and TTN5^{Q70L}
494 indicated that TTN5 along with the two mutant forms can bind guanine nucleotides. The k_{on}
495 values of TTN5^{T30N} and TTN5 were nearly the same, indicating no effect of the mutation on the
496 GDP-binding characteristics as was expected in the absence of a GEF. The k_{on} value for
497 TTN5^{Q70L} was clearly higher than that of the wild-type form, indicating that this mutant can bind
498 GDP faster than TTN5 to form the nucleotide-bound form. Compared with other members of
499 the Ras superfamily, it was in the range of HRAS (Hanzal-Bayer et al. 2005) and around ten
500 times slower than the fast association of RAC1 (Jaiswal et al. 2013). Intrinsic nucleotide
501 exchange measurements of TTN5 and TTN5^{Q70L} have shown remarkably fast nucleotide
502 exchange rates, when compared to other well-studied RAS proteins. The intrinsic nucleotide
503 exchange reaction rates for RAC1, RAC2 and RAC3 have been mentioned around 40.000 s
504 (Haeusler et al. 2006). Our data show that TTN5 is faster in nucleotide exchange rate and very
505 similar to that of human ARL2 (Hanzal-Bayer et al. 2005, Veltel et al. 2008). This suggests that
506 TTN5 quickly replaces GDP for GTP and transforms from an inactive to an active state. This
507 behavior indicates that TTN5 presumably should not require interaction with GEFs for
508 activation in cells. This can also be an explanation for the case of TTN5^{Q70L}. Small GTPases
509 with substitutions of the glutamine of the switch II region (*e.g.*, Glu-71 for HsARF1 and ARL1,
510 Glu-61 for HRAS) are constitutively active (Zhang et al. 1994, Van Valkenburgh et al. 2001,
511 Karnoub and Weinberg 2008). Accordingly, TTN5^{Q70L} is likely to exchange GDP rapidly to GTP
512 and switch itself to stay in an active form as suggested by the fast intrinsic nucleotide exchange
513 rate. Interestingly, TTN5^{T30N} resulted in an even higher dissociation rate constant k_{off}. The
514 calculated K_d confirmed the higher nucleotide-binding affinity for GDP of TTN5 and TTN5^{Q70L}
515 compared with TTN5^{T30N}. Reports on human ARL2, ARF6 and ARL4D showed that their
516 corresponding T30N mutants led to a decreased affinity to GDP similar to TTN5^{T30N} (Macia et
517 al. 2004, Hanzal-Bayer et al. 2005, Li et al. 2012).

518 Interestingly, a comparison of mdGDP with mGppNHp revealed a higher GTP affinity for all
519 three versions, with the highest for TTN5^{Q70L}. These high GTP affinities in combination with the
520 fast GDP exchange rates and extremely slow hydrolysis pinpointed to a GTP-loaded TTN5
521 even in the rested state, which is very uncommon for small GTPases. This atypical behavior
522 is already reported for a few non-classical RHO GTPases like RHOD or RIF (Jaiswal et al.
523 2013). This unusual GTP-bound active state along with the lacking *N*-myristoylation and
524 phylogenetic distances (Boisson et al. 2003, Vernoud et al. 2003) strengthens that there are
525 major differences between TTN5 and other ARF family members. The similarity between the
526 wild type and TTN5^{Q70L} is consistent with the previous report on human ARL2 in which wild-
527 type and Q70L proteins showed only a little difference in binding affinity (Hanzal-Bayer et al.
528 2005). Additionally, an equivalent ratio of nucleotide affinity was found between HRAS and
529 HRAS^{Q61L}, but with a much higher affinity typical for small GTPases (Der et al. 1986). Since
530 Gln-70 at the switch II region is important for GAP-stimulated GTP hydrolysis (Cherfils and
531 Zeghouf 2013), we assume that nucleotide exchange activity is unaffected by this amino acid
532 substitution.
533 To date, no GEF protein for TTN5 is reported. The Arabidopsis genome encodes only two
534 of the five mammalian GEF subgroups, namely the large ARF-GEF subgroups, the BFA-
535 inhibited GEF (BIG) and the Golgi Brefeldin A (BFA)-resistance factor 1 (GBF/GNOM) family
536 (Memon 2004, Wright et al. 2014, Brandizzi 2018). Potential interactions with these proteins
537 are of high interest and can also point to functions of TTN5 as a co-GEF as it is proposed for
538 HsARL3 and HsARL2 with their effector BART by stabilizing the active GTPase (ElMaghloob
539 et al. 2021). Especially, interactions at the nucleotide-binding site, which are prevented in the
540 TTN5^{T30N} mutant, will be of great interest to study further functions and interaction partners of
541 TTN5.
542 Taken together, the categorization as a non-classical GTPase has three implications:
543 First, the very slow hydrolysis rate predicts the existence of a TTN5-GAP. Second, TTN5^{T30N}
544 may function as a dominant-negative mutant and in the presence of a GEF, it cannot bind
545 GDP. Third, the TTN5^{Q70L} hydrolysis rate is not decreased.
546

547 **TTN5 may act in the endomembrane system**

548

549 The localization data on YFP- and HA$_3$-TTN5 suggest that it may be localized at different
550 cellular membrane compartments which is typical for the ARF-like GTPase family (Memon
551 2004, Sztul et al. 2019) and supports potential involvement of TTN5 in endomembrane
552 trafficking. We based the TTN5 localization data on tagging approaches with two different
553 detection methods to enhance reliability of specific protein detection. Even though YFP-TTN5
554 did not complement the embryo-lethality of a *ttn5* loss of function mutant, we made several
555 observations that suggest YFP-TTN5 signals to be meaningful at various membrane sites.
556 YFP-TTN5 may not complement due to differences in TTN5 levels and interactions in some
557 cell types, which were hindering specifically YFP-TTN5 but not HA$_3$-TTN5. In a previous study,
558 overexpression of ARF1 did not affect intracellular localization compared to endogenous
559 tagged-ARF1 but differed in function to form tubulated structures (Bottanelli et al. 2017).
560 Though constitutively driven, the YFP-TTN5 expression may be delayed or insufficient at the
561 early embryonic stages resulting in the lack of embryo-lethal complementation. On the other
562 hand, the very fast nucleotide exchange activity may be hindered by the presence of a large
563 YFP-tag in comparison with the small HA$_3$-tag which is able to rescue the embryo-lethality. The
564 lack of complementation represents a challenge for the localization of small GTPases with
565 rapid nucleotide exchange in plants. Despite of these limitations, we made relevant

566 observations in our data that made us believe that YFP signals in YFP-TTN5-expressing cells
567 at membrane sites can be meaningful. At first, using pharmacological treatments and
568 colocalization with known membrane compartment markers, we noted that various particular
569 membrane compartments showed YFP signals, such as the punctate small ring-like structures
570 resembling previously reported ANNI-GFP staining (Tichá et al. 2020), large ring-like
571 structures resulting from wortmannin treatment and BFA bodies, all of which are meaningful
572 for studies of vesicle transport and plasma membrane protein regulation processes (Wang et
573 al. 2009, Suo et al. 2021). Furthermore, the fluorescence signals obtained with YFP-TTN5
574 constructs also depended on T30 and Q70 residues. Point mutant YFP-TTN5 forms, and
575 particularly the YFP-TTN5^{T30N} had partly quite distinct fluorescence localization patterns, such
576 as reduced mobility in certain cells and differing degrees of colocalization with the utilized
577 markers. Next to this, HA_3-TTN5^{T30N} seedlings showed reduced root growth which may be due
578 to the same reasons as the altered localization and mobility. Since TTN5^{T30N} has, based on
579 the enzyme kinetic results, a very fast nucleotide exchange rate and lost affinity to nucleotides
580 compared to TTN5, these differing YFP fluorescence patterns of the YFP-TTN5^{T30N} construct
581 at membrane sites and the effect on root growth are not unexpected to occur. Hence, we
582 considered these specific YFP localization signals at membrane sites for valid interpretation,
583 especially when supported by HA_3-TTN5 immunodetection.
584 Following up, colocalization analysis showed that both *cis*-Golgi and MVB-positive
585 structures colocalized to a higher proportion with YFP signals of the YFP-TTN5^{Q70L} construct
586 compared with signals in YFP-TTN5T30N-expressing cells. This could be an indicator of the
587 site of TTN5 action, considering our knowledge of the activation of ARF GTPases and ARL
588 proteins in other organisms which show high TTN5 sequence similarity. They are usually
589 recruited or move to their place of action upon interacting with their specific GEF, which leads
590 to GDP to GTP exchange-dependent activation (Sztul et al. 2019, Nielsen 2020, Adarska et
591 al. 2021). Though our biochemical data implies no need for a typical GTPase-GEF interaction
592 for activation, GEF interaction can be still important for the localization. Most of the effector-
593 GTPase interactions take place in their GTP-bound form (Sharer and Kahn 1999, Hanzal-
594 Bayer et al. 2005). One exception is the role of TTN5 sequence-based homologs in microtubule
595 dynamics. ARL2/Alp41-GDP interacts with Cofactor D/Alp1^{D} (Bhamidipati et al. 2000, Mori and
596 Toda 2013). Another possibility is a hindrance of dimerization by the T30N mutation. ARF1
597 protein dimer formation is important for the formation of free vesicles (Beck et al. 2009, Beck
598 et al. 2011) associated with cell mobility which was disturbed in YFP-TTN5^{T30N}-expressing
599 cells. The colocalization of YFP fluorescence in YFP-TTN5-expressing cells with ARA7-
600 positive structures even still in the wortmannin-induced swollen state, triggered by the
601 homotypic fusion of MVBs (Wang et al. 2009), may indicate that TTN5 performs similar
602 functions in relation to ARA7. ARA7 is involved in cargo transport in the endocytic pathway to
603 the vacuole, with a role, for example, in the endocytosis of plasma membrane material (Ueda
604 et al. 2001, Sohn et al. 2003, Kotzer et al. 2004, Ebine et al. 2011). The colocalization of FM4-
605 64-labeled endocytosed vesicles with fluorescence in YFP-TTN5-expressing cells may
606 indicate that TTN5 is involved in endocytosis and the possible degradation pathway into the
607 vacuole. Our data on colocalization with the different markers support the hypothesis that TTN5
608 may have functions in vesicle trafficking.
609 A potential explanation of the YFP localization to similar compartments in YFP-TTN5- and
610 YFP-TTN5^{Q70L}-expressing cells compared to fluorescence signal of YFP-TTN5^{T30N} expression
611 can be based on a special feature of TTN5 in the ARF family. ARF GTPases are mostly
612 myristoylated on Gly-2, which is essential for their membrane binding. TTN5 as well as ARL2
613 and ARL3 lack this myristoylation though Gly-2 is present (Boisson et al. 2003, Kahn et al.

614 2006). ARL2 and ARL3 are still able to bind membranes, probably only by their N-terminal
615 amphipathic helix as it was established for SAR1, with an ARL2 membrane-binding efficiency
616 being nucleotide-independent (Lee et al. 2005, Kapoor et al. 2015). We suggest similar
617 behavior for TTN5, as detected YFP signals localized to membranous compartments. Based
618 on the varying colocalization degrees, with the fluorescence signals of YFP-TTN5^{T30N} construct
619 being less prominent at the Golgi and MVBs, compared to YFP-TTN5 and YFP-TTN5^{Q70L}, we
620 hypothesize that different membrane localization could be associated with a nucleotide- or
621 nucleotide exchange-dependent process. In a nucleotide-free or GDP-bound state, TTN5 may
622 be predominantly present close to the plasma membrane, while in an active GTP-bound state,
623 which according to enzyme kinetics should be the regular one, is dynamically linked with the
624 endomembrane system. Interestingly, with respect to the intracellular dynamics, we observed
625 that the TTN5^{T30N} mutant had a different behavior in different organ types. This could be due
626 to differing GEFs being differentially expressed. Likewise, it is conceivable that the
627 constitutively expressed TTN5 has different effector binding partners.
628 This broad diversity of biological functions of proteins with high sequence similarity to TTN5
629 associated with a variety of signaling cascades is also reflected by very different protein
630 partners for that. Few orthologs of human ARL2 interaction partners are present in Arabidopsis.
631 It is therefore exceedingly interesting to identify interacting proteins to determine whether TTN5
632 performs similar functions as HsARL2 or what other role it may play. Such interactions might
633 also explain why TTN5 is essential in plants with regard to a potential GTP-dependence for
634 TTN5 function which fits to already known functions of other ARF GTPases (Sztul et al. 2019,
635 Nielsen 2020, Adarska et al. 2021). In addition, ARF proteins are affected by a similar set of
636 GEFs and GAPs, indicating an interconnected network in ARF signaling. ARF double
637 knockdowns revealed specific phenotypes, suggesting redundancy in the ARF family
638 (Volpicelli-Daley et al. 2005, Kondo et al. 2012, Nakai et al. 2013, Adarska et al. 2021). The
639 investigation of the TTN5 connection in the ARF family might reveal a missing link in ARF
640 signaling and cell traffic.
641
642 **Conclusion**
643 In this study, we identified TTN5 as a functional GTPase of the ARF-like family. TTN5 had
644 not only sequence similarity with human ARL2 but also, both these two proteins share a very
645 rapid nucleotide exchange capacity in contrast to other characterized ARF/ARL proteins. TTN5
646 has a faster nucleotide dissociation rate to a slower GTP hydrolysis rate and a higher affinity
647 to GTP compared to GDP. Thus, TTN5 is a non-classical GTPase that most likely accumulates
648 in a GTP-bound state in cells in line with certain cellular phenotypes and protein localization
649 data. The nucleotide exchange capacity affected the localization and dynamics of YFP-tagged
650 TTN5 protein forms and associated TTN5 with the endomembrane system. In the future, the
651 identification of potential TTN5 GEF, GAP and effector proteins as well as other interaction
652 partners and particularly potential plasma membrane target proteins as cargo for vesicle
653 transport will be of great interest to clarify the potential roles of TTN5 in endomembrane
654 trafficking and whole-plant physiological contexts.
655
656 **Material & Methods**

657 **Arabidopsis plant material and growth conditions**
658 The Arabidopsis *ttn5-1* mutant was previously described (McElver et al. 2000).
659 Heterozygous seedlings were selected by genotyping using the primers TTN5 intron1 fwd and
660 pDAP101 LB1 (Supplementary Table S1). For pro35S::YFP-TTN5 and pro35S::HA_3-TTN5
661 constructs, *TTN5*, *TTN5^{T30N}* and *TTN5^{Q70L}* coding sequences were amplified with B1 and B2

662 attachment sites for Gateway cloning (Life Technologies) using the primer TITAN5 n-ter B1
663 and TITAN5 stop B2 (Supplementary Table S1). The obtained PCR fragments were cloned *via*
664 BP reaction (Life Technologies) into pDONR207 (Invitrogen). pro35S::YFP-TTN5 and
665 pro35S::HA_3-TTN5 constructs were created *via* LR reaction (Life Technologies) with the
666 destination vector pH7WGY2 (Karimi et al. 2005) and pALLIGATOR2 (Bensmihen et al. 2004),
667 respectively. Agrobacteria were transformed with obtained constructs and used for stable
668 Arabidopsis transformation (adapted by (Clough and Bent 1998). Arabidopsis seeds were
669 sterilized with sodium hypochlorite solution (6 % Sodium hypochlorite and 0.1 % Triton X-100)
670 and stored for 24 hours at 4°C for stratification. Seedlings were grown upright on half-strength
671 Hoagland agar medium (1.5 mM $Ca(NO_3)_2$, 0.5 mM KH_2PO_4, 1.25 mM KNO_3, 0.75 mM $MgSO_4$,
672 1.5 µM $CuSO_4$, 50 µM H_3BO_3, 50 µM KCl, 10 µM $MnSO_4$, 0.075 µM $(NH_4)_6Mo_7O_{24}$, 2 µM
673 $ZnSO_4$, 50 µM FeNaEDTA and 1 % sucrose, pH 5.8, supplemented with 1.4 % Plant agar
674 (Duchefa)] in growth chambers (CLF Plant Climatics) under long-day condition (16 hours light
675 at 21°C, 8 hours darkness at 19°C). Seedlings were grown for six days (six-day system) or 10
676 days (10-day system) or 17 days with the last three days on fresh plates (two-week system).
677 Root length measurement were performed using JMicroVision: Image analysis toolbox for
678 measuring and quantifying components of high-definition images. Version 1.3.4
679 (https://jmicrovision.github.io, Roduit, N.)
680 *Nicotiana benthamiana* plants were grown on soil for 2-4 weeks in a greenhouse facility
681 under long-day conditions (16 hours of light, 8 hours of darkness).
682
683 **Point mutant generation of *TTN5***
684 pDONR207:TTN5 was used as a template for site-directed *TTN5* mutagenesis. Primers
685 T5T30Nf and T5T30Nr (Supplementary Table S1) were used to amplify the entire vector
686 generating the $TTN5^{T30N}$ coding sequence and primers TQ70Lf and T5Q70Lr (Supplementary
687 Table S1) were used to amplify the entire vector generating the $TTN5^{Q70L}$ coding sequence.
688 The PCR amplifications were run using the following conditions: 95°C, 30 s; 18 cycles of 95°C,
689 30 s/ 55°C, 1 min/ 72°C 8 min; 72°C, 7 min. The completed reaction was treated with 10 units
690 of DpnI endonuclease for 1 h at 37°C and then used for *E. coli* transformation. Successful
691 mutagenesis was confirmed by Sanger sequencing.
692
693 ***In vitro* GTPase activity assays**
694 An overview of protein expression and purification is shown in Supplementary Figure S2A.
695 Recombinant pGEX-4T-1 bacterial protein expression vectors (Amersham, Germany)
696 containing coding sequences for *TTN5*, $TTN5^{T30N}$ and $TTN5^{Q70L}$ were transferred into *E. coli*
697 BL21 (DE3) Rosetta strain (Invitrogen, Germany). Following induction of GST-TTN5 fusion
698 protein expression according to standard procedures. Cell lysates were obtained after cell
699 disruption with a probe sonicator (Bandelin sonoplus ultrasonic homogenizer, Germany) using
700 a standard buffer (300 mM NaCl, 3 mM Dithiothreitol (DTT), 10 mM $MgCl_2$, 0.1 mM GDP, 1 %
701 Glycerol and 50 mM Tris-HCl, pH 7.4). GST-fusion proteins were purified by loading total
702 bacterial lysate on a preequilibrated glutathione Sepharose column (Sigma, Germany) using
703 fast performance liquid chromatography system (Cytiva, Germany) (Step 1, affinity-purified
704 GST-TTN5 protein fraction). GST-tagged protein fractions were incubated with thrombin
705 (Sigma, Germany) at 4°C overnight for cleavage of the GST-tag (Step 2, GST cleavage) and
706 applied again to the affinity column (Step 3, yielding TTN5 protein fraction). Purified proteins
707 were concentrated using 10 kDa ultra-centrifugal filter Amicon (Merck Millipore, Germany). The
708 quality and quantity of proteins were analyzed by SDS-protein gel electrophoresis (Bio-Rad),
709 UV/Vis spectrometer (Eppendorf, Germany) and high-performance liquid chromatography

710 (HPLC) using a reversed-phase C18 column (Sigma, Germany) and a pre-column (Nucleosil
711 100 C18, Bischoff Chromatography) as described (Eberth and Ahmadian 2009)
712 (Supplementary Figure S2B-D).
713 Nucleotide-free TTN5 protein was prepared from the TTN5 protein fraction (Eberth and
714 Ahmadian 2009) as illustrated in Supplementary Figure S2E. 0.5 mg TTN5 protein was
715 combined with 1 U of agarose bead-coupled alkaline phosphatase (Sigma Aldrich, Germany)
716 for degradation of bound GDP to GMP and Pi in the presence of 1.5-fold molar excess of non-
717 hydrolyzable GTP analog GppCp (Jena Bioscience, Germany). After confirmation of GDP
718 degradation by HPLC, 0.002 U snake venom phosphodiesterase (Sigma Aldrich, Germany)
719 per mg TTN5 was added to cleave GppCp to GMP, G and Pi. The reaction progress of
720 degradation of nucleotides was analyzed by HPLC using 30 µM TTN5 in 30 µl injection volume
721 (Beckman Gold HPLC, Beckman Coulter). After completion of the reaction, in order to remove
722 the agarose bead-coupled alkaline phosphatase, the solution was centrifuged for 10 min at
723 10000 *g*, 4°C, which was followed by snap freezing and thawing cycles to inactivate the
724 phosphodiesterase. mdGDP (2-deoxy-3-O-N-methylanthraniloyl GDP)- and mGppNHp 2'/3'-
725 O-(N-Methyl-anthraniloyl)-guanosine-5'-[(β,γ)-imido]triphosphate)-bound TTN5, $TTN5^{T30N}$ and
726 $TTN5^{Q70L}$ were prepared by incubation of nucleotide-free forms with fluorescent nucleotides
727 (Jena Bioscience, Germany) in a molar ratio of 1 to 1.2. The solution was purified from excess
728 amount of mdGDP and mGppNHp by using prepacked gel-filtration NAP-5 Columns (Cytiva,
729 Germany) to remove unbound nucleotides. Protein and nucleotide concentration were
730 determined using the Bradford reagent (Sigma Aldrich, Germany) and HPLC, respectively.
731 All kinetic fluorescence measurements including nucleotide association and dissociation
732 reactions were monitored on a stopped-flow instrument system SF-61, HiTech Scientific (TgK
733 Scientific Limited, UK) and SX20 MV (Applied Photophysics, UK) at 25°C using nucleotide
734 exchange buffer (10 mM K_2HPO_4/KH_2PO_4, pH 7.4, 5 mM $MgCl_2$, 3 mM DTT, 30 mM Tris/HCl,
735 pH 7.5) (Eberth and Ahmadian 2009). Fluorescence was detected at 366 nm excitation and
736 450 nm emission using 408 nm cut-off filter for mant-nucleotides (Hemsath and Ahmadian
737 2005).
738 To determine the intrinsic nucleotide exchange rate, k_{off}, 0.2 µM mdGDP- and mGppNHp-
739 bound proteins were combined with a 200-fold molar excess of 40 µM non-fluorescent GDP in
740 two different set of experiments, respectively. The decay of the fluorescence intensity
741 representing mdGDP and mGppNHp dissociation and replacement by non-fluorescent
742 nucleotide were recorded over time (Supplementary Figure S2G). Moreover, to determine the
743 nucleotide association rate, k_{on}, of mdGDP and mGppNHp to the nucleotide-free GTPase,
744 0.2 µM fluorescent nucleotides were mixed with different concentrations of nucleotide-free
745 TTN5 variants. The increase in the fluorescent intensity was obtained by the conformational
746 change of fluorescent nucleotides after binding to the proteins (Supplementary Figure S2H).
747 The data provided by stopped-flow were applied to obtain the observed rate constants.
748 Dissociation rate constants or nucleotide exchange rates (k_{off} in s^{-1}) and pseudo-first-order rate
749 constants or observed rate constants (k_{obs} in s^{-1}) at the different concentrations of the protein
750 were obtained by non-linear curve fitting using Origin software (version 2021b). The slopes
751 obtained from plotting k_{obs} against respective concentrations of proteins were used as the
752 second-order association rate constants (k_{on} in $\mu M^{-1}s^{-1}$). The equilibrium constant of
753 dissociation (K_d in µM) was calculated from the ratio of k_{off}/k_{on}. In order to investigate the
754 intrinsic GTP-hydrolysis rate of TTN5 variants, the HPLC method is used as described (Eberth
755 and Ahmadian 2009). As an accurate strategy, HPLC provides the nucleotide contents over
756 time. The GTPase reaction rates were determined by mixing 100 µM nucleotide-free GTPase
757 and 100 µM GTP at 25°C in a standard buffer without GDP. The GTP contents were measured

758 at different times and the data were fitted with Origin software to get the observed rate
759 constant.
760

761 ***Nicotiana benthamiana* leaf infiltration**

762 *N. benthamiana* leaf infiltration was performed with the Agrobacterium (*Agrobacterium*
763 *radiobacter*) strain C58 (GV3101) carrying the respective constructs for confocal microscopy.
764 Agrobacteria cultures were grown overnight at 28°C, centrifuged for 5 min at 4°C at 5000*g*,
765 resuspended in infiltration solution (5 % sucrose, a pinch of glucose, 0.01 % Silwet Gold,
766 150 µM Acetosyringone) and incubated for 1 hour at room temperature. Bacterial suspension
767 was set to an OD_{600} = 0.4 and infiltrated into the abaxial side of *N. benthamiana* leaves.

768

769 **Subcellular localization of fluorescent protein fusions**

770 Cloning of YFP-tagged TTN5 constructs is described in the paragraph 'Arabidopsis plant
771 material and growth conditions'. Localization studies were carried out by laser-scanning
772 confocal microscopy (LSM 780 or LSM880, Zeiss) with a 40x C-Apochromat water immersion
773 objective. YFP constructs and Alexa Fluor 488 stainings were excited at 488 nm and detected
774 at 491-560 nm. mCherry, Alexa 555 or FM4-64 fluorescence was excited at 561 nm and
775 detected at 570-633 nm.

776 Wortmannin (10 µM, Sigma-Aldrich), BFA (36 µM Sigma-Aldrich) and plasma membrane
777 dyes FM4-64 (165 µM, ThermoFisher Scientific) were infiltrated into *N. benthamiana* leaves.
778 FM4-64 was detected after 5 min incubation. Wortmannin and BFA were incubated for 25 min
779 before checking the treatment effect. Plasmolysis was induced by incubating leaf discs in 1 M
780 mannitol solution for 15 min. Signal intensities were increased for better visibility.
781

782 **Whole-mount Immunostaining**

783 Whole-mount immunostaining by immunofluorescence was performed according to the
784 protocol described by (Pasternak et al. 2015). Briefly, Arabidopsis seedlings were grown in the
785 standard condition in Hoagland media for 4-6 days. Methanol or Formaldehyde (4 %) was used
786 to fix the seedlings. The seedlings were transferred to a glass slide and resuspended in 1x
787 microtubule-stabilizing buffer (MTSB). Seedlings were digested with 2 % Driselase dissolved
788 in 1x MTSB at 37°C for 40 mins. Following digestion, permeabilization step was performed by
789 treating the seedlings with permeabilization buffer (3 % IGEPAL C630, 10 % dimethylsulfoxide
790 (DMSO) in 1x MTSB buffer) at 37°C for 20 mins. Then blocking was performed with a buffer
791 consisting of 5 % BSA for 30 min at room temperature. They were incubated overnight with
792 different primary antibodies (detailed information are listed below). After two washes with 1x
793 MTSB, seedlings were incubated with a respective Alexa Fluor secondary antibody for 2 hours
794 at 37°C. After five steps of washing with 1x PBS, coverslips were mounted on slides with the
795 antifade reagent (Prolong glass Antifade Mountant with NucBlue Stain, Invitrogen).
796 Fluorescence microscopy was conducted as described in the previous section.

797 Immunodetection was conducted with following antibody combinations: HA detection was
798 performed using α-HA antibody (1:100 dilution, rabbit Abcam ab9110 or chicken AGRISERA,
799 AS204463) followed by Alexa Fluor 488 or Alexa Fluor 555-labeled secondary antibodies
800 (1:200 α-rabbit, Thermo Scientific, A32731 and AGRISERA, AS204463). ATPase (PM marker)
801 was detected using primary chicken α-AHA antibody (1:200 Agrisera, AS132671), while ARF1
802 (Golgi and TGN marker) was detected using primary chicken α-ARF1 antibody (1:200 Agrisera,
803 AS08325), both in combination with Alexa Fluor™ Plus 555-labeled secondary antibody (1:500
804 α-Chicken for ATPase, Thermo Scientific A32932).

805 For obtention of BFA bodies, seedlings were first treated with BFA (72 µM, Sigma-Aldrich)
806 and fixable plasma membrane dye FM4-64 FX (10 mM, Thermo Scientific, F34653) for 1 hour,
807 before formaldehyde fixation.
808

809 **Immunoblot detection**

810 Total protein extraction from Arabidopsis plants grown for 6 days or in the 2-week system,
811 sample separation on SDS-PAGE and immunodetection were performed as previously
812 described (Le et al. 2015). In short, plant material was grinded under liquid nitrogen and
813 proteins were extracted with SDG buffer (62 mM Tris-HCl, pH 8.6, 2.5 % SDS, 2 % DTT, 10 %
814 glycerol). Samples were separated on 12 % SDS-PAGE gels. Following electrophoresis, the
815 proteins were transferred to a Protran nitrocellulose membrane (Amersham).
816 Membranes were blocked for 1 hour in 5 % milk-TBST solution (20 mM Tris-HCl, pH 7.4,
817 180 mM NaCl and 0.1 % Tween 20), followed by 1 hour antibody incubation (α-GFP,
818 monoclonal mouse antibody, Roche, catalog no. 11814460001, 1:1000). After three washes
819 with TBST for 10 min each, membranes were incubated in secondary antibody (α-mouse-HRP,
820 polyclonal goat antibody, SigmaAldrich, cat. no. SAB3701159, 1:5000) for 1 hour. HA detection
821 was performed with a directly coupled α-HA antibody (α-HA-HRP, high-affinity monoclonal rat
822 antibody, 3F10, Roche, catalog no. 12013819001, 1:1000). Immunodetection was performed
823 after three washes with TBST for 10 min each, using the enhanced chemiluminescence
824 system (GE Healthcare) and the FluorChem Q System for quantitative Western blot imaging
825 (ProteinSimple) with the AlphaView software.

826

827 **JACoP based colocalization analysis**
828 Colocalization analysis was carried out with the ImageJ (Schneider et al. 2012) Plugin Just
829 Another Colocalization Plugin (JACoP) (Bolte and Cordelières 2006) and a comparison of
830 Pearson's and Overlap coefficients and Li's intensity correlation quotient (ICQ) was performed.
831 Object-based analysis was done for punctate structures, adapted by (Ivanov et al. 2014).
832 Colocalization for both channels was calculated based on the distance between geometrical
833 centers of signals and presented as percentage. Analysis was done in three replicates each
834 (n = 3).

835

836 **Structure prediction**
837 TTN5 structure prediction was performed by AlphaFold (Jumper et al. 2021). The molecular
838 graphic was edited with UCSF ChimeraX (1.2.5, (Goddard et al. 2018), developed by the
839 Resource for Biocomputing, Visualization and Informatics at the University of California, San
840 Francisco, with support from the National Institutes of Health R01-GM129325 and the Office
841 of Cyber Infrastructure and Computational Biology, National Institute of Allergy and Infectious
842 Diseases.
843

844 ***In silico* tool for gene expression analysis**
845 RNA-seq data relies on published data and was visualized with the AtGenExpress eFP at
846 bar.utoronto.ca/eplant (Waese et al. 2017).
847

848 **Statistical analysis**

One-way ANOVA was used for statistical analysis and performed in OriginPro 2019. Fisher LSD or Tukey was chosen as a post-hoc test with $p < 0.05$.

ACCESSION NUMBERS

Sequence data from this article can be found in the TAIR and GenBank data libraries under accession numbers: *ARA7* (TAIR: AT4G19640), *ARF1* (TAIR: AT1G23490), *GmMan1* (Uniprot: Q0PKY2) and *TTN5* (TAIR: AT2G18390).

Acknowledgements

We thank Gintaute Matthäi and Elke Wieneke for their excellent technical assistance. We are thankful to Dr. Anna Sergeeva for advice and help with whole-mount immunolocalization. We thank Dr. Ksenia Krooß for microscopy help and advice and Natalie Köhler for experimental assistance. We are thankful for the assistance from Stefanie Weidtkamp-Peters and Sebastian Hänsch, members of the Center for Advanced Imaging (CAi) at Heinrich Heine University. We would like to sincerely thank Dr. Madhumita Narasimhan for her help with immunolocalization experiments. We are greatful to Dr. Alexander Hertle for many fruitful discussions and advices on immunolocalization and fluorescence microscopy. RFP-ARA7 clones were a gift from Dr. Thierry Gaude.

This work was supported by the Deutsche Forschungsgemeinschaft (DFG, German Research Foundation) Project no. 267205415–SFB 1208, project B05 to P.B.; Ba1610/7-2 to P.B.; Germany´s Excellence Strategy – EXC-2048/1 – project ID 390686111. Support was provided by DFG AH 92/8-3 to A.M. and M.R.A.. Funding for instrumentation: Zeiss LSM780 + 4channel FLIM extension (Picoquant): DFG- INST 208/551-1 FUGG and Zeiss LSM 880 Airyscan Fast DFG- INST 208/746-1 FUGG.

Figure legends

Figure 1: TTN5 is predicted to be a functional small ARF-like GTPase with nucleotide exchange capacity. (A), Sequence alignment of TTN5 with its human homolog ARL2, Arabidopsis, human ARF1 and human HRAS created with Jalview (Waterhouse et al. 2009). The conserved G-motifs (G1-G5; indicated by red lines) are defined for the TTN5 and HRAS sequence. The secondary structure of TTN5 is depicted by black lines and corresponding cartoon (α-helix in green; β-sheet in orange). Here mentioned conserved residues in ARF/ARL proteins are highlighted by boxes; Gly-2, and mutated Thr-30 and Gln-70. $TTN5^{T30N}$ is expected to have a low nucleotide exchange capacity, while $TTN5^{Q70L}$ is expected to have a low GTPase hydrolysis activity. (B), Model of the predicted GTPase nucleotide exchange and hydrolysis cycle of TTN5. TTN5 switches from an inactive GDP-loaded form to an active GTP-loaded one. GDP to GTP nucleotide exchange and GTP hydrolysis may be aided by a guanidine exchange factor (GEF) and a GTPase-activating protein (GAP). (C), Predicted protein structural model of TTN5; magenta, marks the GTP-binding pocket; N-terminal amphipathic helix is highlighted in orange; conserved Gly-2 in green; T30 and Q70, mutagenized in this study, shown in sticks. The model was generated with AlphaFold (Jumper et al. 2021), and adaptation was done with UCSF ChimeraX 1.2.5 (Goddard et al. 2018).

Figure 2: Biochemical properties of TTN5 proteins suggest that TTN5 is present in a GTP-loaded active form in cells. (A), Schematic illustration of the stopped-flow fluorescence

895 device for monitoring the nucleotide-binding kinetics of the purified TTN5 protein
896 heterologously expressed in bacteria (Supplementary Figure S2A-D). It consists of two
897 motorized, thermostated syringes, a mixing chamber and a fluorescence detector. Two
898 different reagents 1 and 2 are rapidly mixed and transferred to a fluorescence detection cell
899 within 4 ms. One of the reagents must contain a fluorescent reporter group. Here, mdGDP and
900 mGppNHp were used to mimic GDP and GTP. (B), Schematic illustration of the nucleotide
901 association. Nucleotide-free TTN5 (reagent 1; preparation see Supplementary Figure S2E)
902 was rapidly mixed with mdGDP (reagent 2). A fluorescence increase is expected upon
903 association of mdGDP with TTN5. Similar measurements are performed with mGppNHp
904 instead of mdGDP. (C), Schematic illustration of the intrinsic nucleotide dissociation. mdGDP-
905 bound TTN5 (reagent 1) is mixed with a molar excess of GDP (reagent 2). A fluorescence
906 decrease is expected upon mdGDP dissociation from TTN5 and binding of free GDP. Similar
907 measurements are performed with mGppNHp. (D-E), Kinetics of association and dissociation
908 of fluorescent nucleotides mdGDP (D) or mGppNHp (E) with TTN5 proteins (WT, $TTN5^{T30N}$,
909 $TTN5^{Q70L}$) are illustrated as bar charts. The association of mdGDP (0.1 µM) or mGppNHp
910 (0.1 µM) with increasing concentration of $TTN5^{WT}$, $TTN5^{T30N}$ and $TTN5^{Q70L}$ was measured
911 using a stopped-flow device (see A, B; data see Supplementary Figure S3A-F, S4A-E).
912 Association rate constants (k_{on} in $\mu M^{-1}s^{-1}$) were determined from the plot of increasing observed
913 rate constants (k_{obs} in s^{-1}) against the corresponding concentrations of the TTN5 proteins.
914 Intrinsic dissociation rates (k_{off} in s^{-1}) were determined by rapidly mixing 0.1 µM mdGDP-bound
915 or mGppNHp-bound TTN5 proteins with the excess amount of unlabeled GDP (see A, C, data
916 see Supplementary Figure S3G-I, S4F-H). The nucleotide affinity (dissociation constant or K_d
917 in µM) of the corresponding TTN5 proteins was calculated by dividing k_{off} by k_{on}. When mixing
918 mGppNHp with nucleotide-free $TTN5^{T30N}$, no binding was observed (n.b.o.) under these
919 experimental conditions. (F-G), GTP hydrolysis of TTN5 proteins determined by HPLC. (F),
920 Schematic illustration of the GTP hydrolysis measurement. (G), GTP-bound TTN5 proteins
921 (100 µM) were incubated at room temperature at different time points before injecting them on
922 a reversed-phase HPLC system. Evaluated data (data see Supplementary Figure S5) resulted
923 in the determination of the GTP hydrolysis rates (k_{cat} in s^{-1}) illustrated as bar charts. (H), TTN5
924 accumulated in a GTP-loaded active form. GST-$TTN5^{WT}$ (46.5 kDa) was purified from bacterial
925 cell lysates at three different volumes in the presence of 0.1 µM unbound free GppNHp using
926 glutathione beads. The nucleotide contents and the protein purities were determined by HPLC
927 and Coomassie Blue-stained SDS-polyacrylamide gel electrophoresis. The presence of much
928 higher amounts of GppNHp-bound versus GDP-bound GST-TTN5 protein indicates that TTN5
929 rapidly exchanged bound nucleotide und accumulated in this state.

930

931 **Figure 3: TTN5 may be present in punctate structures in seedlings.** Microscopic
932 observations of YFP fluorescence signals were made in a plane underneath the plasma
933 membrane at the cell peripheries. (A), Schematic representation of an Arabidopsis seedling.
934 Images were taken at three different positions of the seedlings and imaged areas are indicated
935 by a red rectangle. (B-J), Analysis of YFP-TTN5, YFP-$TTN5^{T30N}$ and YFP-$TTN5^{Q70L}$
936 Arabidopsis seedlings *via* fluorescent confocal microscopy. (B-D), Fluorescence signals
937 observed in stomata (indicated by empty white arrowhead) and in the epidermis of cotyledons
938 in punctate structures (indicated by filled white arrowhead). (E-G), Localization in the
939 hypocotyls showed the same pattern of punctate structures. (H-J), Signals were present in
940 punctate structures in the root hair zone and in root hairs (indicated by filled magenta
941 arrowhead). (K), Schematic representation of a *N. benthamiana* plant, used for leaf infiltration
942 for transient expression. Imaged area is indicated by a red rectangle. (L-N), YFP fluorescence

943 signals in *N. benthamiana* leaf epidermal cells expressing YFP-TTN5, YFP-TTN5^{T30N} and YFP-
944 TTN5^{Q70L}. Signals were present in punctate structures (indicated by white arrowheads) and in
945 the nucleus (indicated by empty magenta arrowheads). Scale bar 50 µm. (O), Root length
946 measurement of HA_3-TTN5, HA_3-TTN5^{T30N} and HA_3-TTN5^{Q70L} Arabidopsis lines in comparison
947 with non-transgenic wild type (WT). Seedlings were grown for 10 days on Hoagland plates.
948 Only HA_3-TTN5^{T30N} showed a slightly reduced root length compared to WT, whereas HA_3-
949 TTN5 and HA_3-TTN5^{Q70L} did not have a divergent phenotype. Analysis was conducted in
950 replicates (n = 14). One-way ANOVA with Tukey post-hoc test was performed. Different letters
951 indicate statistical significance ($p < 0.05$). (P), Two representative images of whole-mount
952 immunostaining of HA_3-TTN5 seedling roots in the root differentiation zone (rabbit α-HA
953 primary antibody, Alexa-488-labeled secondary α-rabbit antibody). Alexa-488 signals were
954 present in punctate structures in root cells (indicated by filled white arrowhead) and in root
955 hairs (indicated by filled magenta arrowhead) comparable to YFP signals (Figure 3H-J).
956 Images are presented in a maximum intensity projection of several z-layers for a better
957 visualization. Scale bar 50 µm.

958

959 **Figure 4. Whole-mount Immunolocalization analysis of HA_3-TTN5 in Arabidopsis**
960 **including colocalization with Golgi marker and localization in BFA bodies.**
961 (A-B), Representative images showing whole-mount immunostaining of HA_3-TTN5 seedlings
962 with different types of markers for colocalization analysis. (A), Detection of HA_3-TTN5 (chicken
963 α-HA primary antibody, Alexa 555-labeled secondary α-chicken antibody) with Golgi and TGN
964 marker ARF1 (rabbit α-ARF1 primary antibody, Alexa-488-labeled secondary α-rabbit
965 antibody). Both fluorescence signals were detected in vesicle-like structures in root cells in
966 close proximity to each other but mostly not colocalizing. The experiment was repeated twice
967 with three seedlings. (B) Detection of HA_3-TTN5 (rabbit α-HA primary antibody, Alexa-488-
968 labeled secondary α-rabbit antibody) and staining with lipid membrane dye FM4-64 after
969 brefeldin A (BFA) treatment (72 µM, 1 h). Alexa-488 signals colocalized with FM4-64 in BFA
970 bodies in root cells. The experiment was repeated three times with three seedlings. (C), in
971 comparison, YFP fluorescence in YFP-TTN5 seedlings, co-analyzed with FM4-64 after BFA
972 treatment (36 µM, 30 min). YFP fluorescence signals colocalized with FM4-64 in BFA bodies
973 similar as in (B). The experiment was performed once with three independent YFP-TTN5 lines.
974 Colocalizing signals in the two channels are indicated by filled white arrowheads, whereas
975 signals that do not colocalize in the two channels are indicated by empty white arrowheads.
976 Scale bar overview: 50 µm, close-up: 10 µm.

977

978 **Figure 5: TTN5 may be associated with the endomembrane system in *N. benthamiana***
979 **leaf epidermal cells.** YFP fluorescence signals were localized in *N. benthamiana* leaf
980 epidermal cells transiently transformed to express YFP-TTN5, YFP-TTN5^{T30N} and YFP-
981 TTN5^{Q70L} *via* fluorescent confocal microscopy. Specific markers indicating the endomembrane
982 system were used. (A), Schematic representation of GmMan1 localization at the *cis*-Golgi site.
983 (B-D), Partial colocalization of YFP signal with the Golgi marker GmMan1-mCherry at *cis*-Golgi
984 stacks (filled white arrowheads). Additionally, YFP fluorescent signals were detected in non-
985 colocalizing punctate structures with depleted fluorescence in the center (empty white
986 arrowheads). (E), Schematic representation of GmMan1 localization at the ER upon brefeldin
987 A (BFA) treatment. BFA blocks ARF-GEF proteins which leads to a loss of Golgi *cis*-cisternae
988 and the formation of BFA-induced compartments due to an accumulation of Golgi stacks up to
989 a redistribution of the Golgi to the ER by fusion of the Golgi with the ER (Renna and Brandizzi

990 2020). (F-H), Redistribution of Golgi stacks was induced by BFA treatment (36 μM, 30 min).
991 GmMan1-mCherry and YFP fluorescence signals were present in the ER and in colocalizing
992 punctate structures. (I), Schematic representation of ARA7 localization at the *trans*-Golgi
993 network (TGN) and multi-vesicular bodies (MVBs). (J-L), Colocalization of YFP fluorescence
994 signal with the MVB marker RFP-ARA7. (M), Schematic representation of ARA7 localization
995 in swollen MVBs upon wortmannin treatment. Wortmannin inhibits phosphatidylinositol-3-
996 kinase (PI3K) function leading to the fusion of TGN/EE to swollen MVBs (Renna and Brandizzi
997 2020). (N-P), MVB swelling was obtained by wortmannin treatment (10 μM, 30 min). ARA7-
998 RFP was colocalizing with YFP signal in these swollen MVBs. Chemical treatment-induced
999 changes were imaged after 25 min incubation. Colocalization is indicated with filled
1000 arrowheads, YFP signal only with empty ones. Corresponding colocalization analysis data is
1001 presented in Supplementary Figure S8. Scale bar 10 μm.

1002

1003 **Figure 6. TTN5 may colocalize with endocytosed plasma membrane material.** (A),
1004 Schematic representation of progressive stages of FM4-64 localization and internalization in
1005 a cell. FM4-64 is a lipophilic substance. After infiltration, it first localizes in the plasma
1006 membrane, at later stages it localizes to intracellular vesicles and membrane compartments.
1007 This localization pattern reflects the endocytosis process (Bolte et al. 2004). (B-J), YFP
1008 fluorescence signals were localized in *N. benthamiana* leaf epidermal cells together with the
1009 plasma membrane dye FM4-64 *via* fluorescent confocal microscopy, following transient
1010 transformation to express YFP-tagged TTN5, YFP-TTN5^{T30N} and YFP-TTN5^{Q70L}. (B-D), YFP
1011 signals colocalized with FM4-64 at the plasma membrane. (E-G), Plasma membrane
1012 localization of YFP fluorescence was evaluated after mannitol-induced (1 M) plasmolysis. The
1013 formation of Hechtian strands is a sign of plasma membrane material and fluorescence staining
1014 there is indicated with filled arrowheads. (H-J), Internalized FM4-64 was present in vesicle-like
1015 structures that showed YFP signals. Colocalization is indicated with filled arrowheads. Scale
1016 bar 10 μm.

1017

1018 **Figure 7: Schematic models summarize TTN5 kinetic GTPase activities and potential**
1019 **localization within the cell.** (A), Model of the predicted GTPase nucleotide exchange and
1020 hydrolysis cycle mechanism of TTN5 based on the biochemical investigation. TTN5 affinity to
1021 mGppNHp was 9.2-fold higher compared to mGDP resulting in a fast switching from an inactive
1022 GDP-loaded form to an active GTP-loaded one. mGppNHp dissociation was 8-fold faster as
1023 GTP hydrolysis but both processes were much slower than nucleotide association. TTN5
1024 kinetics identified it as a non-classical GTPase which tended to stay in a GTP-loaded form
1025 even under resting conditions. (B), Presumed TTN5 locations within the cell. TTN5 (green
1026 square) can be present at the plasma membrane (PM) similar as FM4-64 (red circle) or in the
1027 endomembrane compartments of the *trans*-Golgi network (TGN) or multivesicular body (MVB)
1028 as found by colocalization with ARA7 (red hexagon). Additionally TTN5 might colocalize with
1029 GmMan1-positive (red square) Golgi stacks.

1030

1031 **Supplementary Figure S1. Visualization of *TTN5* gene expression levels during plant**
1032 **development based on transcriptome data.** Expression levels in (A), different types of aerial
1033 organs at different developmental stages; from left to right and bottom to top are represented
1034 different seed and plant growth stages, flower development stages, different leaves, vegetative
1035 to inflorescence shoot apex, embryo and silique development stages; (B), seedling root tissues

1036 based on single cell analysis represented in form of a uniform manifold approximation and
1037 projection plot; (C), successive stages of embryo development. As shown in (A) to (C), *TTN5*
1038 is ubiquitously expressed in these different plant organs and tissues. In particular, it should be
1039 noted that *TTN5* transcripts were detectable in the epidermis cell layer of roots that we used
1040 for localization of tagged TTN5 protein in this study. In accordance with the embryo-lethal
1041 phenotype, the ubiquitous expression of *TTN5* highlights its importance for plant growth.
1042 Original data were derived from (Nakabayashi et al. 2005, Schmid et al. 2005) (A); (Ryu et al.
1043 2019) (B); (Waese et al. 2017) (C). Gene expression levels are indicated by local maximum
1044 color code, ranging from the minimum (no expression) in yellow to the maximum (highest
1045 expression) in red.

1046

1047 **Supplementary Figure S2. Heterologous expression and purification of TTN5 protein as**
1048 **well as preparation of its nucleotide-free form.** (A), Overview of protein purification and
1049 preparation of nucleotide-free form of TTN5 in the presence of excess GDP. (B-C), The
1050 chromatograms represent the GST-affinity chromatography to obtain GST-TTN5 and TTN5
1051 variants, before and after GST-cleavage by thrombin. (D), Coomassie Blue SDS-PAGE of
1052 GST-TTN5 (left panel; 46.5 kDa) and TTN5 after GST-cleavage by thrombin and a second
1053 GST-affinity chromatography (right panel; 21 kDa). (E), Schematic illustration of nucleotide-
1054 free TTN5 preparation. In the first step, the purified GDP-bound TTN5 is incubated with alkaline
1055 phosphatase in the presence of 1.5-fold molar excess of Gpp(CH_2)p, which is a non-
1056 hydrolyzable GTP analog and, unlike GDP, resistant to alkaline phosphatase. After GDP is
1057 completely degraded, phosphodiesterase is added to the reaction to degrade Gpp(CH_2)p to
1058 GMP, G and Pi. The nucleotide content is monitored in each step by HPLC. The solution with
1059 nucleotide-free TTN5 is deep-frozen and thawed twice, aliquoted and stored at -80°C.

1060

1061 **Supplementary Figure S3. Kinetic measurements of mdGDP interaction with TTN5**
1062 **proteins.** (A-C), Association of mdGDP (0.1 μM) with increasing concentrations of $TTN5^{WT}$
1063 (A), $TTN5^{T30N}$ (B) and $TTN5^{Q70L}$ (C). (D-F), Association rate constant (k_{on}) is determined by
1064 plotting the k_{obs} values, obtained from the exponential fits of the mdGDP association data (A-
1065 C) against the TTN5 (D), $TTN5^{T30N}$ (E) and $TTN5^{Q70L}$ (F) protein concentrations. (G-I),
1066 Dissociation of mdGDP from TTN5 (G), $TTN5^{T30N}$ (H) and $TTN5^{Q70L}$ (I) proteins (0.1 μM) is
1067 determined in the presence of excess amounts of unlabeled GDP (20 μM). The dissociation
1068 rates (k_{off}) are obtained from the exponential fitting of the data by Origin software. All results
1069 are shown as bar charts in Figure 2D. The principles of the assays are illustrated in Figure 2A-
1070 C.

1071

1072 **Supplementary Figure S4. Kinetic measurements of mGppNHp interaction with TTN5**
1073 **proteins.** (A-E), Association kinetics. (A, C), Association of mGppNHp (0.1 μM) with increasing
1074 concentrations of $TTN5^{WT}$ (A) and $TTN5^{Q70L}$ (C). (B) When mixing mGppNHp with nucleotide-
1075 free $TTN5^{T30N}$, no binding was observed under these experimental conditions. Instead,
1076 association of mGppNHp (0.1 μM) with two different titrations of 0.5 μM $TTN5^{T30N}$ was
1077 measured, indicated by arrows, to confirm the fast binding of $TTN5^{T30N}$ with mGppNHp by
1078 increasing fluorescence intensity, determined by fluorimeter. (D-E), Association rate constant
1079 (k_{on}) is determined by plotting the k_{obs} values, obtained from the exponential fits of the
1080 mGppNHp association data (left panels) against the $TTN5^{WT}$ (D) and $TTN5^{Q70L}$ (E) protein
1081 concentrations. Note that $TTN5^{T30N}$ did not show association with mGppNHp, therefore middle

space is left empty. (F-H), Dissociation of mGppNHp from $TTN5^{WT}$ (F), $TTN5^{T30N}$ (G) and $TTN5^{Q70L}$ (H) proteins (0.1 μM) is determined in the presence of excess amounts of unlabeled GppNHp (20 μM). The dissociation rates (k_{off}) are obtained from the exponential fitting of the data by Origin software. All results are shown as bar charts in Figure 2E. The principles of the assays are illustrated in Figure 2A-C.

Supplementary Figure S5. GTP hydrolysis reaction rates of the TTN5 proteins. (A-C), The GTP hydrolysis reaction rates (k_{cat}) of $TTN5^{WT}$ (A), $TTN5^{T30N}$ (B) and $TTN5^{Q70L}$ (C) proteins (100 μM) were measured at 25°C. Aliquots of the reaction mixture at the indicated time points were analyzed by HPLC as described in Materials and Methods. The obtained results are shown as bar charts in Figure 2G. The principle of the assay is illustrated in Figure 2F.

Supplementary Figure S6. YFP fluorescence signal localization in YFP-TTN5 and -TTN5 mutant Arabidopsis seedlings. Microscopic YFP fluorescence observations were made in a plane across the centers of most cells. (A), Schematic representation of an Arabidopsis seedling. Images were taken at four different positions of the seedlings and imaged areas are indicated by a red rectangle. (B-M), Fluorescent YFP signals in Arabidopsis seedlings *via* fluorescent confocal microscopy. (B–D), YFP signal localization was observed in the epidermis of cotyledons. Fluorescence signals were present in nucleus (indicated by empty white arrowhead) and cytoplasm and at or in close proximity to the plasma membrane (indicated by filled white arrowhead) in the epidermis of cotyledons of YFP-TTN5, YFP-$TTN5^{T30N}$ and YFP-$TTN5^{Q70L}$ seedlings. (E-G), Fluorescence localization in the hypocotyls showed clear presence in the cytoplasm (indicated by empty magenta arrowhead), next to nuclear and plasma membrane-related localization. (H-J), Fluorescence signals were present in nuclei, cytoplasm, at or close to the plasma membrane in the root hair zone and in root hairs (indicated by filled magenta arrowhead) with clear cytoplasmic localization of YFP-TTN5, YFP-$TTN5^{T30N}$ and YFP-$TTN5^{Q70L}$ seedlings. (K-M), Fluorescence signal localization at the root tip showed clear expression in nuclei and cytoplasm, visible due to the smaller size of the vacuoles. (N), Schematic representation of a *N. benthamiana* plant, used for leaf infiltration for transient expression of YFP-TTN5, YFP-$TTN5^{T30N}$ and YFP-$TTN5^{Q70L}$. Imaged areas are indicated by a red rectangle. (O-Q), Fluorescent signals in *N. benthamiana* leaf epidermal cells *via* fluorescent confocal microscopy. Signals were present in nucleus and cytoplasm and at or in close proximity to the plasma membrane. Scale bar 50 μm.

Supplementary Figure S7. Phenotypes of *ttn5-1* T-DNA insertion line and root length of HA_3-TTN5 lines. (A), Schematic representation of the *TTN5* exon-intron structure and T-DNA insertion in the *ttn5-1* allele. The numbers below the exon numbers indicate base pairs (bp). (B), Early embryo arrest phenotype of a homozygous *ttn5-1*$^{-/-}$ seed on the left in comparison with a wild type (WT) seed of the same silique on the right; arrowheads, indicate enlarged nuclei in the arrested embryo (filled) and endosperm (empty). Early embryo arrest phenotypes were previously shown by (Mayer et al. 1999, McElver et al. 2000). Scale bar 1 cm. (C), Western blot control of YFP-TTN5 protein expressed in stable transgenic plant lines. α-GFP primary plus secondary antibody treatment detected a strong band at the correct size of 48 kDa for YFP-TTN5 and three additional smaller sized weak bands 26-35 kDa. Plants were grown for 6 days. (D), Western blot control of HA_3-TTN5 protein expressed in stable transgenic plant lines. One single band was detected by α-HA-HRP antibody treatment at the correct size of

1128 28 kDa for HA_3-TTN5 protein. Plants were grown in the two-week system. (E), Siliques of
1129 heterozygous *ttn5-1*$^{+/-}$ plants, containing ca. 25 % white seeds with arrested embryos (empty
1130 arrowheads) and ca. 75 % regular green seeds (filled arrowheads). HA_3-TTN5 line crossed to
1131 *ttn5-1*$^{+/-}$ was able to rescue embryo lethal seed phenotype.

1132

1133 **Supplementary Figure S8. Colocalization analysis of YFP fluorescent signal with**
1134 **GmMan1-mCherry and mRFP-ARA7 signals in YFP-TTN5, YFP-TTN5^{T30N} and YFP-**
1135 **TTN5^{Q70L} seedlings.** Colocalization analyses were conducted with specific markers using
1136 ImageJ (Schneider et al. 2012). (A), JACoP-based colocalization analysis (Bolte and
1137 Cordelières 2006). Comparison of Pearson's and Overlap coefficients for *cis*-Golgi-located
1138 GmMan1-mCherry with the YFP fluorescence signals of three YFP-TTN5 seedlings in vesicle-
1139 like structures. Fluorescent signals colocalized similarly with the *cis*-Golgi marker in YFP-
1140 TTN5, YFP-TTN5^{T30N} and YFP-TTN5^{Q70L} seedlings. (B), Object-based analysis was performed
1141 for vesicle-like structures based on distance between geometrical centers of signals. YFP
1142 fluorescent signal-positive structures overlapped most with GmMan1-mCherry-positive Golgi
1143 stacks in YFP-TTN5 compared to YFP-TTN5^{T30N} and YFP-TTN5^{Q70L} seedlings. GmMan1-
1144 mCherry-positive Golgi stacks overlapped most with YFP-TTN5^{Q70L}-positive structures
1145 followed by YFP-TTN5 and YFP-TTN5^{T30N} signals. (C), JACoP-based colocalization analysis
1146 (Bolte and Cordelières 2006). Comparison of Pearson's and Overlap coefficients for
1147 TGN/MVB-located mRFP-ARA7 with YFP fluorescence signals of YFP-TTN5, YFP-TTN5^{T30N}
1148 and YFP-TTN5^{Q70L} seedlings in vesicle-like structures. YFP fluorescence signals in YFP-TTN5
1149 and YFP-TTN5^{Q70L} seedlings colocalized similarly with mRFP-ARA7, whereas YFP signals
1150 tended to colocalize less in YFP-TTN5^{T30N} seedlings. (D), Object-based analysis was
1151 performed for vesicle-like structures based on distance between geometrical centers of
1152 signals. More than half of signals corresponding to all YFP-TTN5-positive structures
1153 overlapped with mRFP-ARA7-positive structures, in the order YFP-TTN5^{T30N}, YFP-TTN5 and
1154 best YFP-TTN5^{Q70L}. mRFP-ARA7-positive structures overlapped most with YFP fluorescence
1155 signals in YFP-TTN5^{Q70L} seedlings, while signals were reduced for YFP-TTN5 and YFP-
1156 TTN5^{T30N} seedlings by ca. 3.5-fold and 2.5-fold, respectively. Analyses were conducted in
1157 three replicates each (n = 3). One-way ANOVA with Fisher-LSD post-hoc test was performed.
1158 Different letters indicate statistical significance ($p < 0.05$).

1159

1160 **Supplementary Video Material S1. YFP fluorescence signals are present in dynamic**
1161 **vesicle-like structures in YFP-TTN5 seedlings.** (A-O), Time series of YFP fluorescent
1162 signals in dynamic vesicle-like structures of YFP-TTN5, YFP-TTN5^{T30N} and YFP-TTN5^{Q70L}
1163 Arabidopsis seedlings (A-L), or *N. benthamiana* leaf epidermal cells (M-O) recorded *via*
1164 fluorescence confocal microscopy. (A-C), Fluorescence signals were present in dynamic
1165 vesicle-like structures in epidermal cotyledon cells and stomata and in (D-F), in the hypocotyls,
1166 Note that mobility of fluorescence signal of YFP-TTN5^{T30N} (E) seedlings differed by a slower or
1167 aborted motion in half of the cells compared to (D) YFP-TTN5 and (F) YFP-TTN5^{Q70L}. (G-I),
1168 YFP fluorescence signals were present in the dynamic vesicle-like structures in the root hair
1169 zone and in root hairs as well. (J-L), but no clear mobility or vesicle-like structures were
1170 deciphered in the root tips of YFP-TTN5, YFP-TTN5^{T30N} or YFP-TTN5^{Q70L} seedlings. (M-O),
1171 Time series of YFP fluorescence signals together with *cis*-Golgi marker GmMan1-mCherry.
1172 GmMan1-positive Golgi stacks showed movement in *N. benthamiana* epidermal cells together
1173 with YFP fluorescence upon transient transformation with YFP-TTN5 (M), YFP-TTN5^{T30N} (N)
1174 and YFP-TTN5^{Q70L} (O) constructs. GmMan1 is described with a stop-and-go directed

movement mediated by the actino-myosin system (Nebenführ 1999) and similarly it might be the case for YFP-TTN5 signals based on the colocalization. Note that mobility of YFP fluorescence and GmMan1-mCherry signal in YFP-TTN5^{T30N} (N) transformed leaf discs differed by a slower or aborted motion compared to YFP-TTN5 (M) and YFP-TTN5^{Q70L} (O). Hence fluorescence signals were present in a comparable manner to Arabidopsis seedlings. Scale bar 50 µm.

References

Adarska, P., L. Wong-Dilworth and F. Bottanelli (2021). "ARF GTPases and Their Ubiquitous Role in Intracellular Trafficking Beyond the Golgi." Frontiers in cell and developmental biology **9**: 679046-679046.

Ahmadi, Y., A. Ghorbanihaghjo and H. Argani (2017). "The balance between induction and inhibition of mevalonate pathway regulates cancer suppression by statins: A review of molecular mechanisms." Chem Biol Interact **273**: 273-285.

Antoshechkin, I. and M. Han (2002). "The *C. elegans* evl-20 Gene Is a Homolog of the Small GTPase ARL2 and Regulates Cytoskeleton Dynamics during Cytokinesis and Morphogenesis." Developmental Cell **2**(5): 579-591.

Aspenström, P. (2020). "Fast-cycling Rho GTPases." Small GTPases **11**(4): 248-255.

Beck, R., F. Adolf, C. Weimer, B. Bruegger and F. T. Wieland (2009). "ArfGAP1 Activity and COPI Vesicle Biogenesis." Traffic **10**(3): 307-315.

Beck, R., S. Prinz, P. Diestelkötter-Bachert, S. Röhling, F. Adolf, K. Hoehner, S. Welsch, P. Ronchi, B. Brügger, J. A. G. Briggs and F. Wieland (2011). "Coatomer and dimeric ADP ribosylation factor 1 promote distinct steps in membrane scission." The Journal of cell biology **194**(5): 765-777.

Bensmihen, S., A. To, G. Lambert, T. Kroj, J. Giraudat and F. Parcy (2004). "Analysis of an activated ABI5 allele using a new selection method for transgenic Arabidopsis seeds." FEBS Lett **561**(1-3): 127-131.

Bhamidipati, A., S. A. Lewis and N. J. Cowan (2000). "ADP ribosylation factor-like protein 2 (Arl2) regulates the interaction of tubulin-folding cofactor D with native tubulin." Journal of Cell Biology **149**(5): 1087-1096.

Boisson, B., C. Giglione and T. Meinnel (2003). "Unexpected Protein Families Including Cell Defense Components Feature in the N-Myristoylome of a Higher Eukaryote." Journal of Biological Chemistry **278**(44): 43418-43429.

Bolte, S. and F. P. Cordelières (2006). "A guided tour into subcellular colocalization analysis in light microscopy." J Microsc **224**(Pt 3): 213-232.

Bolte, S., C. Talbot, Y. Boutte, O. Catrice, N. D. Read and B. Satiat-Jeunemaitre (2004). "FM-dyes as experimental probes for dissecting vesicle trafficking in living plant cells." Journal of Microscopy **214**(2): 159-173.

Bos, J. L. (1988). "The ras gene family and human carcinogenesis." Mutation Research/Reviews in Genetic Toxicology **195**(3): 255-271.

Bottanelli, F., N. Kilian, A. M. Ernst, F. Rivera-Molina, L. K. Schroeder, E. B. Kromann, M. D. Lessard, R. S. Erdmann, A. Schepartz, D. Baddeley, J. Bewersdorf, D. Toomre and J. E. Rothman (2017). "A novel physiological role for ARF1 in the formation of bidirectional tubules from the Golgi." Mol Biol Cell **28**(12): 1676-1687.

Brandizzi, F. (2018). "Transport from the endoplasmic reticulum to the Golgi in plants: Where are we now?" Semin Cell Dev Biol **80**: 94-105.

Brandizzi, F., E. L. Snapp, A. G. Roberts, J. Lippincott-Schwartz and C. Hawes (2002). "Membrane Protein Transport between the Endoplasmic Reticulum and the Golgi in Tobacco Leaves Is Energy Dependent but Cytoskeleton Independent : Evidence from Selective Photobleaching." The Plant Cell **14**(6): 1293-1309.

Chang, D. D. and H. M. Colecraft (2015). "Rad and Rem are non-canonical G-proteins with respect to the regulatory role of guanine nucleotide binding in Ca(V)1.2 channel regulation." J Physiol **593**(23): 5075-5090.

Cherfils, J. and M. Zeghouf (2013). "Regulation of small GTPases by GEFs, GAPs, and GDIs." Physiol Rev **93**(1): 269-309.
Clough, S. J. and A. F. Bent (1998). "Floral dip: a simplified method for Agrobacterium-mediated transformation of Arabidopsis thaliana." Plant J **16**(6): 735-743.
Cui, Y., J. Shen, C. Gao, X. Zhuang, J. Wang and L. Jiang (2016). "Biogenesis of Plant Prevacuolar Multivesicular Bodies." Molecular Plant **9**(6): 774-786.
Der, C. J., T. Finkel and G. M. Cooper (1986). "Biological and biochemical properties of human rasH genes mutated at codon 61." Cell **44**(1): 167-176.
Dhonukshe, P., F. Aniento, I. Hwang, D. G. Robinson, J. Mravec, Y.-D. Stierhof and J. Friml (2007). "Clathrin-Mediated Constitutive Endocytosis of PIN Auxin Efflux Carriers in Arabidopsis." Current Biology **17**(6): 520-527.
Eberth, A. and M. R. Ahmadian (2009). "In Vitro GEF and GAP Assays." Current Protocols in Cell Biology **43**(1): 14.19.11-14.19.25.
Ebine, K., M. Fujimoto, Y. Okatani, T. Nishiyama, T. Goh, E. Ito, T. Dainobu, A. Nishitani, T. Uemura, M. H. Sato, H. Thordal-Christensen, N. Tsutsumi, A. Nakano and T. Ueda (2011). "A membrane trafficking pathway regulated by the plant-specific RAB GTPase ARA6." Nat Cell Biol **13**(7): 853-859.
ElMaghloob, Y., B. Sot, M. J. McIlwraith, E. Garcia, T. Yelland and S. Ismail (2021). "ARL3 activation requires the co-GEF BART and effector-mediated turnover." Elife **10**.
Emans, N., S. Zimmermann and R. Fischer (2002). "Uptake of a fluorescent marker in plant cells is sensitive to brefeldin A and wortmannin." Plant Cell **14**(1): 71-86.
Erickson, J. W., R. A. Cerione and M. J. Hart (1997). "Identification of an actin cytoskeletal complex that includes IQGAP and the Cdc42 GTPase." J Biol Chem **272**(39): 24443-24447.
Esposito, A., V. Ventura, M. V. Petoukhov, A. Rai, D. I. Svergun and M. A. Vanoni (2019). "Human MICAL1: Activation by the small GTPase Rab8 and small-angle X-ray scattering studies on the oligomerization state of MICAL1 and its complex with Rab8." Protein Sci **28**(1): 150-166.
Fansa, E. K. and A. Wittinghofer (2016). "Sorting of lipidated cargo by the Arl2/Arl3 system." Small GTPases **7**(4): 222-230.
Fasano, G., V. Muto, F. C. Radio, M. Venditti, N. Mosaddeghzadeh, S. Coppola, G. Paradisi, E. Zara, F. Bazgir, A. Ziegler, G. Chillemi, L. Bertuccini, A. Tinari, A. Vetro, F. Pantaleoni, S. Pizzi, L. A. Conti, S. Petrini, A. Bruselles, I. G. Prandi, C. Mancini, B. Chandramouli, M. Barth, C. Bris, D. Milani, A. Selicorni, M. Macchiaiolo, M. V. Gonfiantini, A. Bartuli, R. Mariani, C. J. Curry, R. Guerrini, A. Slavotinek, M. Iascone, B. Dallapiccola, M. R. Ahmadian, A. Lauri and M. Tartaglia (2022). "Dominant ARF3 variants disrupt Golgi integrity and cause a neurodevelopmental disorder recapitulated in zebrafish." Nat Commun **13**(1): 6841.
Fidyk, N., J. B. Wang and R. A. Cerione (2006). "Influencing cellular transformation by modulating the rates of GTP hydrolysis by Cdc42." Biochemistry **45**(25): 7750-7762.
Fiegen, D., L. C. Haeusler, L. Blumenstein, U. Herbrand, R. Dvorsky, I. R. Vetter and M. R. Ahmadian (2004). "Alternative splicing of Rac1 generates Rac1b, a self-activating GTPase." J Biol Chem **279**(6): 4743-4749.
Fisher, S., D. Kuna, T. Caspary, R. A. Kahn and E. Sztul (2020). "ARF family GTPases with links to cilia." Am J Physiol Cell Physiol **319**(2): C404-c418.
Fleming, J. A., L. R. Vega and F. Solomon (2000). "Function of tubulin binding proteins in vivo." Genetics **156**(1): 69-80.
Ghosh, P. M., N. Ghosh-Choudhury, M. L. Moyer, G. E. Mott, C. A. Thomas, B. A. Foster, N. M. Greenberg and J. I. Kreisberg (1999). "Role of RhoA activation in the growth and morphology of a murine prostate tumor cell line." Oncogene **18**(28): 4120-4130.
Goddard, T. D., C. C. Huang, E. C. Meng, E. F. Pettersen, G. S. Couch, J. H. Morris and T. E. Ferrin (2018). "UCSF ChimeraX: Meeting modern challenges in visualization and analysis." Protein Sci **27**(1): 14-25.
Gremer, L., T. Merbitz-Zahradnik, R. Dvorsky, I. C. Cirstea, C. P. Kratz, M. Zenker, A. Wittinghofer and M. R. Ahmadian (2011). "Germline KRAS mutations cause aberrant biochemical and physical properties leading to developmental disorders." Hum Mutat **32**(1): 33-43.

Haeusler, L. C., L. Hemsath, D. Fiegen, L. Blumenstein, U. Herbrand, P. Stege, R. Dvorsky and M. R. Ahmadian (2006). "Purification and biochemical properties of Rac1, 2, 3 and the splice variant Rac1b." Methods Enzymol **406**: 1-11.

Hall, A. (1990). "The cellular functions of small GTP-binding proteins." Science **249**(4969): 635-640.

Hanton, S. L., L. A. Matheson, L. Chatre and F. Brandizzi (2009). "Dynamic organization of COPII coat proteins at endoplasmic reticulum export sites in plant cells." The Plant Journal **57**(6): 963-974.

Hanzal-Bayer, M., M. Linari and A. Wittinghofer (2005). "Properties of the interaction of Arf-like protein 2 with PDEdelta." J Mol Biol **350**(5): 1074-1082.

Hemsath, L. and M. R. Ahmadian (2005). "Fluorescence approaches for monitoring interactions of Rho GTPases with nucleotides, regulators, and effectors." Methods **37**(2): 173-182.

Heucken, N. and R. Ivanov (2018). "The retromer, sorting nexins and the plant endomembrane protein trafficking." J Cell Sci **131**(2).

Hillig, R. C., M. Hanzal-Bayer, M. Linari, J. Becker, A. Wittinghofer and L. Renault (2000). "Structural and biochemical properties show ARL3-GDP as a distinct GTP binding protein." Structure **8**(12): 1239-1245.

Hodge, R. G., A. Schaefer, S. V. Howard and C. J. Der (2020). "RAS and RHO family GTPase mutations in cancer: twin sons of different mothers?" Crit Rev Biochem Mol Biol **55**(4): 386-407.

Huang, X., Y. Shen, Y. Zhang, L. Wei, Y. Lai, J. Wu, X. Liu and X. Liu (2013). "Rac1 mediates laminar shear stress-induced vascular endothelial cell migration." Cell Adh Migr **7**(6): 462-468.

Ismail, S. A., Y. X. Chen, A. Rusinova, A. Chandra, M. Bierbaum, L. Gremer, G. Triola, H. Waldmann, P. I. Bastiaens and A. Wittinghofer (2011). "Arl2-GTP and Arl3-GTP regulate a GDI-like transport system for farnesylated cargo." Nat Chem Biol **7**(12): 942-949.

Ito, E., T. Uemura, T. Ueda and A. Nakano (2016). "Distribution of RAB5-positive multivesicular endosomes and the trans-Golgi network in root meristematic cells of *Arabidopsis thaliana*." Plant biotechnology (Tokyo, Japan) **33**(4): 281-286.

Ivanov, R., T. Brumbarova, A. Blum, A.-M. Jantke, C. Fink-Straube and P. Bauer (2014). "SORTING NEXIN1 is required for modulating the trafficking and stability of the Arabidopsis IRON-REGULATED TRANSPORTER1." The Plant cell **26**(3): 1294-1307.

Ivanov, R. and G. Vert (2021). "Endocytosis in plants: Peculiarities and roles in the regulated trafficking of plant metal transporters." Biology of the Cell **113**(1): 1-13.

Jaillais, Y., I. Fobis-Loisy, C. Miège and T. Gaude (2008). "Evidence for a sorting endosome in Arabidopsis root cells." The Plant Journal **53**(2): 237-247.

Jaiswal, M., E. K. Fansa, R. Dvorsky and M. R. Ahmadian (2013). "New insight into the molecular switch mechanism of human Rho family proteins: shifting a paradigm." Biol Chem **394**(1): 89-95.

Jian, X., J. M. Gruschus, E. Sztul and P. A. Randazzo (2012). "The pleckstrin homology (PH) domain of the Arf exchange factor Brag2 is an allosteric binding site." J Biol Chem **287**(29): 24273-24283.

Jumper, J., R. Evans, A. Pritzel, T. Green, M. Figurnov, O. Ronneberger, K. Tunyasuvunakool, R. Bates, A. Žídek, A. Potapenko, A. Bridgland, C. Meyer, S. A. A. Kohl, A. J. Ballard, A. Cowie, B. Romera-Paredes, S. Nikolov, R. Jain, J. Adler, T. Back, S. Petersen, D. Reiman, E. Clancy, M. Zielinski, M. Steinegger, M. Pacholska, T. Berghammer, S. Bodenstein, D. Silver, O. Vinyals, A. W. Senior, K. Kavukcuoglu, P. Kohli and D. Hassabis (2021). "Highly accurate protein structure prediction with AlphaFold." Nature **596**(7873): 583-589.

Jung, A. and H. Rösner (2002). "RAC1-dependent regulation of cholinergically induced lamellar protrusive activity is independent of MAPKinase and attenuated by active p-JNK." Neuroreport **13**(18): 2443-2446.

Just, W. W. and J. Peränen (2016). "Small GTPases in peroxisome dynamics." Biochimica et Biophysica Acta (BBA) - Molecular Cell Research **1863**(5): 1006-1013.

Kahn, R. A., J. Cherfils, M. Elias, R. C. Lovering, S. Munro and A. Schurmann (2006). "Nomenclature for the human Arf family of GTP-binding proteins: ARF, ARL, and SAR proteins." The Journal of cell biology **172**(5): 645-650.

Kahn, R. A., C. J. Der and G. M. Bokoch (1992). "The ras superfamily of GTP-binding proteins: guidelines on nomenclature." The FASEB Journal **6**(8): 2512-2513.

Kapoor, S., E. K. Fansa, S. Möbitz, S. A. Ismail, R. Winter, A. Wittinghofer and K. Weise (2015). "Effect of the N-Terminal Helix and Nucleotide Loading on the Membrane and Effector Binding of Arl2/3." Biophys J **109**(8): 1619-1629.

Karimi, M., B. De Meyer and P. Hilson (2005). "Modular cloning in plant cells." Trends in Plant Science **10**(3): 103-105.

Karnoub, A. E. and R. A. Weinberg (2008). "Ras oncogenes: split personalities." Nat Rev Mol Cell Biol **9**(7): 517-531.

Klein, S., M. Franco, P. Chardin and F. Luton (2006). "Role of the Arf6 GDP/GTP cycle and Arf6 GTPase-activating proteins in actin remodeling and intracellular transport." J Biol Chem **281**(18): 12352-12361.

Kondo, Y., A. Hanai, W. Nakai, Y. Katoh, K. Nakayama and H. W. Shin (2012). "ARF1 and ARF3 are required for the integrity of recycling endosomes and the recycling pathway." Cell Struct Funct **37**(2): 141-154.

Kotzer, A. M., F. Brandizzi, U. Neumann, N. Paris, I. Moore and C. Hawes (2004). "AtRabF2b (Ara7) acts on the vacuolar trafficking pathway in tobacco leaf epidermal cells." Journal of Cell Science **117**(26): 6377-6389.

Kuemmerle, J. F. and H. Zhou (2002). "Insulin-like growth factor-binding protein-5 (IGFBP-5) stimulates growth and IGF-I secretion in human intestinal smooth muscle by Ras-dependent activation of p38 MAP kinase and Erk1/2 pathways." J Biol Chem **277**(23): 20563-20571.

Latijnhouwers, M., C. Hawes, C. Carvalho, K. Oparka, A. K. Gillingham and P. Boevink (2005). "An Arabidopsis GRIP domain protein locates to the trans-Golgi and binds the small GTPase ARL1." The Plant Journal **44**(3): 459-470.

Le, C. T. T., T. Brumbarova, R. Ivanov, C. Stoof, E. Weber, J. Mohrbacher, C. Fink-Straube and P. Bauer (2015). "ZINC FINGER OF ARABIDOPSIS THALIANA12 (ZAT12) Interacts with FER-LIKE IRON DEFICIENCY-INDUCED TRANSCRIPTION FACTOR (FIT) Linking Iron Deficiency and Oxidative Stress Responses " Plant Physiology **170**(1): 540-557.

Lee, G. J., E. J. Sohn, M. H. Lee and I. Hwang (2004). "The Arabidopsis rab5 homologs rha1 and ara7 localize to the prevacuolar compartment." Plant Cell Physiol **45**(9): 1211-1220.

Lee, M. C., L. Orci, S. Hamamoto, E. Futai, M. Ravazzola and R. Schekman (2005). "Sar1p N-terminal helix initiates membrane curvature and completes the fission of a COPII vesicle." Cell **122**(4): 605-617.

Li, C.-C., T.-S. Wu, C.-F. Huang, L.-T. Jang, Y.-T. Liu, S.-T. You, G.-G. Liou and F.-J. S. Lee (2012). "GTP-Binding-Defective ARL4D Alters Mitochondrial Morphology and Membrane Potential." PLOS ONE **7**(8): e43552.

Lloyd, J. and D. Meinke (2012). "A comprehensive dataset of genes with a loss-of-function mutant phenotype in Arabidopsis." Plant Physiol **158**(3): 1115-1129.

Macia, E., F. Luton, M. Partisani, J. Cherfils, P. Chardin and M. Franco (2004). "The GDP-bound form of Arf6 is located at the plasma membrane." J Cell Sci **117**(Pt 11): 2389-2398.

Matsumoto, S., H. Taniguchi-Tamura, M. Araki, T. Kawamura, R. Miyamoto, C. Tsuda, F. Shima, T. Kumasaka, Y. Okuno and T. Kataoka (2021). "Oncogenic mutations Q61L and Q61H confer active form-like structural features to the inactive state (state 1) conformation of H-Ras protein." Biochem Biophys Res Commun **565**: 85-90.

Mayer, U., U. Herzog, F. Berger, D. Inzé and G. Jürgens (1999). "Mutations in the PILZ group genes disrupt the microtubule cytoskeleton and uncouple cell cycle progression from cell division in Arabidopsis embryo and endosperm." European Journal of Cell Biology **78**(2): 100-108.

McElver, J., D. Patton, M. Rumbaugh, C.-m. Liu, L. J. Yang and D. Meinke (2000). "The TITAN5 Gene of Arabidopsis Encodes a Protein Related to the ADP Ribosylation Factor Family of GTP Binding Proteins." The Plant Cell **12**(8): 1379-1392.

Memon, A. R. (2004). "The role of ADP-ribosylation factor and SAR1 in vesicular trafficking in plants." Biochim Biophys Acta **1664**(1): 9-30.

Mori, R. and T. Toda (2013). "The dual role of fission yeast Tbc1/cofactor C orchestrates microtubule homeostasis in tubulin folding and acts as a GAP for GTPase Alp41/Arl2." Molecular biology of the cell **24**(11): 1713-S1718.

Nakabayashi, K., M. Okamoto, T. Koshiba, Y. Kamiya and E. Nambara (2005). "Genome-wide profiling of stored mRNA in Arabidopsis thaliana seed germination: epigenetic and genetic regulation of transcription in seed." Plant J **41**(5): 697-709.

Nakai, W., Y. Kondo, A. Saitoh, T. Naito, K. Nakayama and H. W. Shin (2013). "ARF1 and ARF4 regulate recycling endosomal morphology and retrograde transport from endosomes to the Golgi apparatus." Mol Biol Cell **24**(16): 2570-2581.

Nassar, N., K. Singh and M. Garcia-Diaz (2010). "Structure of the dominant negative S17N mutant of Ras." Biochemistry **49**(9): 1970-1974.

Nelson, B. K., X. Cai and A. Nebenführ (2007). "A multicolored set of in vivo organelle markers for co-localization studies in Arabidopsis and other plants." The Plant Journal **51**(6): 1126-1136.

Newman, L. E., C. J. Zhou, S. Mudigonda, A. L. Mattheyses, E. Paradies, C. M. Marobbio and R. A. Kahn (2014). "The ARL2 GTPase is required for mitochondrial morphology, motility, and maintenance of ATP levels." PLoS One **9**(6): e99270.

Nielsen, E. (2020). "The Small GTPase Superfamily in Plants: A Conserved Regulatory Module with Novel Functions." Annual Review of Plant Biology **71**(1): 247-272.

Niu, F., C. Ji, Z. Liang, R. Guo, Y. Chen, Y. Zeng and L. Jiang (2022). "ADP-ribosylation factor D1 modulates Golgi morphology, cell plate formation, and plant growth in Arabidopsis." Plant Physiol **190**(2): 1199-1213.

Pasternak, T., O. Tietz, K. Rapp, M. Begheldo, R. Nitschke, B. Ruperti and K. Palme (2015). "Protocol: an improved and universal procedure for whole-mount immunolocalization in plants." Plant Methods **11**(1): 50.

Radcliffe, P. A., L. Vardy and T. Toda (2000). "A conserved small GTP-binding protein Alp41 is essential for the cofactor-dependent biogenesis of microtubules in fission yeast." FEBS Letters **468**(1): 84-88.

Radhakrishna, H., O. Al-Awar, Z. Khachikian and J. G. Donaldson (1999). "ARF6 requirement for Rac ruffling suggests a role for membrane trafficking in cortical actin rearrangements." J Cell Sci **112 (Pt 6)**: 855-866.

Renna, L. and F. Brandizzi (2020). "The mysterious life of the plant trans-Golgi network: advances and tools to understand it better." Journal of Microscopy **278**(3): 154-163.

Ritzenthaler, C., A. Nebenführ, A. Movafeghi, C. Stussi-Garaud, L. Behnia, P. Pimpl, L. A. Staehelin and D. G. Robinson (2002). "Reevaluation of the effects of brefeldin A on plant cells using tobacco Bright Yellow 2 cells expressing Golgi-targeted green fluorescent protein and COPI antisera." The Plant cell **14**(1): 237-261.

Robinson, D. G., D. Scheuring, S. Naramoto and J. Friml (2011). "ARF1 Localizes to the Golgi and the Trans-Golgi Network." The Plant Cell **23**(3): 846-849.

Ryu, K. H., L. Huang, H. M. Kang and J. Schiefelbein (2019). "Single-Cell RNA Sequencing Resolves Molecular Relationships Among Individual Plant Cells." Plant Physiol **179**(4): 1444-1456.

Scheffzek, K., M. R. Ahmadian, W. Kabsch, L. Wiesmüller, A. Lautwein, F. Schmitz and A. Wittinghofer (1997). "The Ras-RasGAP Complex: Structural Basis for GTPase Activation and Its Loss in Oncogenic Ras Mutants." Science **277**(5324): 333-339.

Schmid, M., T. S. Davison, S. R. Henz, U. J. Pape, M. Demar, M. Vingron, B. Schölkopf, D. Weigel and J. U. Lohmann (2005). "A gene expression map of Arabidopsis thaliana development." Nat Genet **37**(5): 501-506.

Schneider, C. A., W. S. Rasband and K. W. Eliceiri (2012). "NIH Image to ImageJ: 25 years of image analysis." Nature Methods **9**(7): 671-675.

Sharer, J. D. and R. A. Kahn (1999). "The ARF-like 2 (ARL2)-binding protein, BART. Purification, cloning, and initial characterization." J Biol Chem **274**(39): 27553-27561.

Sharer, J. D., J. F. Shern, H. Van Valkenburgh, D. C. Wallace and R. A. Kahn (2002). "ARL2 and BART Enter Mitochondria and Bind the Adenine Nucleotide Transporter." Molecular Biology of the Cell **13**(1): 71-83.

Shirazi, F., R. J. Jones, R. K. Singh, J. Zou, I. Kuiatse, Z. Berkova, H. Wang, H. C. Lee, S. Hong, L. Dick, N. Chattopadhyay and R. Z. Orlowski (2020). "Activating KRAS, NRAS, and BRAF mutants enhance proteasome capacity and reduce endoplasmic reticulum stress in multiple myeloma." Proc Natl Acad Sci U S A **117**(33): 20004-20014.

Singh, M. K., S. Richter, H. Beckmann, M. Kientz, Y.-D. Stierhof, N. Anders, F. Fäßler, M. Nielsen, C. Knöll, A. Thomann, M. Franz-Wachtel, B. Macek, K. Skriver, P. Pimpl and G. Jürgens (2018). "A single class of ARF GTPase activated by several pathway-specific ARF-GEFs regulates essential membrane traffic in Arabidopsis." PLOS Genetics **14**(11): e1007795.

Singh, M. K., S. Richter, H. Beckmann, M. Kientz, Y. D. Stierhof, N. Anders, F. Fäßler, M. Nielsen, C. Knöll, A. Thomann, M. Franz-Wachtel, B. Macek, K. Skriver, P. Pimpl and G. Jürgens (2018). "A single class of ARF GTPase activated by several pathway-specific ARF-GEFs regulates essential membrane traffic in Arabidopsis." PLoS Genet **14**(11): e1007795.

Soh, U. J. and B. C. Low (2008). "BNIP2 extra long inhibits RhoA and cellular transformation by Lbc RhoGEF via its BCH domain." J Cell Sci **121**(Pt 10): 1739-1749.

Sohn, E. J., E. S. Kim, M. Zhao, S. J. Kim, H. Kim, Y. W. Kim, Y. J. Lee, S. Hillmer, U. Sohn, L. Jiang and I. Hwang (2003). "Rha1, an Arabidopsis Rab5 homolog, plays a critical role in the vacuolar trafficking of soluble cargo proteins." Plant Cell **15**(5): 1057-1070.

Stefano, G., L. Renna, S. L. Hanton, L. Chatre, T. A. Haas and F. Brandizzi (2006). "ARL1 plays a role in the binding of the GRIP domain of a peripheral matrix protein to the Golgi apparatus in plant cells." Plant Mol Biol **61**(3): 431-449.

Stierhof, Y. D. and F. El Kasmi (2010). "Strategies to improve the antigenicity, ultrastructure preservation and visibility of trafficking compartments in Arabidopsis tissue." Eur J Cell Biol **89**(2-3): 285-297.

Sugawara, R., H. Ueda and R. Honda (2019). "Structural and functional characterization of fast-cycling RhoF GTPase." Biochem Biophys Res Commun **513**(2): 522-527.

Suo, Y., F. Hu, H. Zhu, D. Li, R. Qi, J. Huang and W. Wu (2021). "BIG3 and BIG5 Redundantly Mediate Vesicle Trafficking in Arabidopsis." Biomolecules **11**(5).

Sztul, E., P.-W. Chen, J. E. Casanova, J. Cherfils, J. B. Dacks, D. G. Lambright, F.-J. S. Lee, P. A. Randazzo, L. C. Santy, A. Schürmann, I. Wilhelmi, M. E. Yohe and R. A. Kahn (2019). "ARF GTPases and their GEFs and GAPs: concepts and challenges." Molecular biology of the cell **30**(11): 1249-1271.

Tichá, M., H. Richter, M. Ovečka, N. Maghelli, M. Hrbáčková, P. Dvořák, J. Šamaj and O. Šamajová (2020). "Advanced Microscopy Reveals Complex Developmental and Subcellular Localization Patterns of ANNEXIN 1 in Arabidopsis." Front Plant Sci **11**: 1153.

Tzafrir, I., J. A. McElver, C.-m. Liu Cm, L. J. Yang, J. Q. Wu, A. Martinez, D. A. Patton and D. W. Meinke (2002). "Diversity of TITAN functions in Arabidopsis seed development." Plant physiology **128**(1): 38-51.

Ueda, T., M. Yamaguchi, H. Uchimiya and A. Nakano (2001). "Ara6, a plant-unique novel type Rab GTPase, functions in the endocytic pathway of *Arabidopsis thaliana*." The EMBO Journal **20**(17): 4730-4741.

Valencia, J. P., K. Goodman and M. S. Otegui (2016). "Endocytosis and Endosomal Trafficking in Plants." Annual Review of Plant Biology **67**(1): 309-335.

Van Valkenburgh, H., J. F. Shern, J. D. Sharer, X. Zhu and R. A. Kahn (2001). "ADP-ribosylation factors (ARFs) and ARF-like 1 (ARL1) have both specific and shared effectors: characterizing ARL1-binding proteins." J Biol Chem **276**(25): 22826-22837.

Vanoni, M., R. Bertini, E. Sacco, L. Fontanella, M. Rieppi, S. Colombo, E. Martegani, V. Carrera, A. Moroni, C. Bizzarri, V. Sabbatini, M. Cattozzo, A. Colagrande and L. Alberghina (1999). "Characterization and properties of dominant-negative mutants of the ras-specific guanine nucleotide exchange factor CDC25(Mm)." J Biol Chem **274**(51): 36656-36662.

Veltel, S., A. Kravchenko, S. Ismail and A. Wittinghofer (2008). "Specificity of Arl2/Arl3 signaling is mediated by a ternary Arl3-effector-GAP complex." FEBS Letters **582**(17): 2501-2507.

Vernoud, V., A. C. Horton, Z. Yang and E. Nielsen (2003). "Analysis of the small GTPase gene superfamily of Arabidopsis." Plant Physiol **131**(3): 1191-1208.

Volpicelli-Daley, L. A., Y. Li, C. J. Zhang and R. A. Kahn (2005). "Isoform-selective effects of the depletion of ADP-ribosylation factors 1-5 on membrane traffic." Mol Biol Cell **16**(10): 4495-4508.

Waese, J., J. Fan, A. Pasha, H. Yu, G. Fucile, R. Shi, M. Cumming, L. A. Kelley, M. J. Sternberg, V. Krishnakumar, E. Ferlanti, J. Miller, C. Town, W. Stuerzlinger and N. J. Provart (2017). "ePlant: Visualizing and Exploring Multiple Levels of Data for Hypothesis Generation in Plant Biology." The Plant Cell **29**(8): 1806-1821.

Walsh, T. G., Y. Li, A. Wersäll and A. W. Poole (2019). "Small GTPases in platelet membrane trafficking." Platelets **30**(1): 31-40.

Wang, J., Y. Cai, Y. Miao, S. K. Lam and L. Jiang (2009). "Wortmannin induces homotypic fusion of plant prevacuolar compartments*." Journal of Experimental Botany **60**(11): 3075-3083.

Wang, J. B., W. J. Wu and R. A. Cerione (2005). "Cdc42 and Ras cooperate to mediate cellular transformation by intersectin-L." J Biol Chem **280**(24): 22883-22891.

Wang, Y., F. Liu, Y. Ren, Y. Wang, X. Liu, W. Long, D. Wang, J. Zhu, X. Zhu, R. Jing, M. Wu, Y. Hao, L. Jiang, C. Wang, H. Wang, Y. Bao and J. Wan (2016). "GOLGI TRANSPORT 1B Regulates Protein Export from the Endoplasmic Reticulum in Rice Endosperm Cells." The Plant Cell **28**(11): 2850-2865.

Waterhouse, A. M., J. B. Procter, D. M. Martin, M. Clamp and G. J. Barton (2009). "Jalview Version 2--a multiple sequence alignment editor and analysis workbench." Bioinformatics **25**(9): 1189-1191.

Wittmann, T., G. M. Bokoch and C. M. Waterman-Storer (2003). "Regulation of leading edge microtubule and actin dynamics downstream of Rac1." J Cell Biol **161**(5): 845-851.

Wright, J., R. A. Kahn and E. Sztul (2014). "Regulating the large Sec7 ARF guanine nucleotide exchange factors: the when, where and how of activation." Cellular and Molecular Life Sciences **71**(18): 3419-3438.

Zhang, C. J., A. G. Rosenwald, M. C. Willingham, S. Skuntz, J. Clark and R. A. Kahn (1994). "Expression of a dominant allele of human ARF1 inhibits membrane traffic in vivo." J Cell Biol **124**(3): 289-300.

Zhang, H., Z. Yang, T. Lin, Y. Wu, T. Zou, J. yang and Y. Zhang (2018). "ARL2 regulates trafficking and expression of isoprenylated proteins and is crucial for development of photoreceptor outer segments." Investigative Ophthalmology & Visual Science **59**(9): 963-963.

Zhou, C., L. Cunningham, A. I. Marcus, Y. Li and R. A. Kahn (2006). "Arl2 and Arl3 regulate different microtubule-dependent processes." Mol Biol Cell **17**(5): 2476-2487.

Figures

Characterization of the small *Arabidopsis thaliana* GTPase and ADP-ribosylation factor-like 2 protein TITAN 5

Inga Mohr[1], Amin Mirzaiebadizi[2], Sibaji K. Sanyal[1], Pichaporn Chuenban[1], Mohammad R. Ahmadian[2], Rumen Ivanov[1] and Petra Bauer[1,3]

[1]Institute of Botany, Heinrich Heine University, 40225 Düsseldorf, Germany.
[2]Institute of Biochemistry and Molecular Biology II, Medical Faculty and University Hospital Düsseldorf, Heinrich Heine University, Düsseldorf, Germany
[3]Cluster of Excellence on Plant Sciences, Heinrich Heine University, 40225 Düsseldorf,
Germany

Figure 1

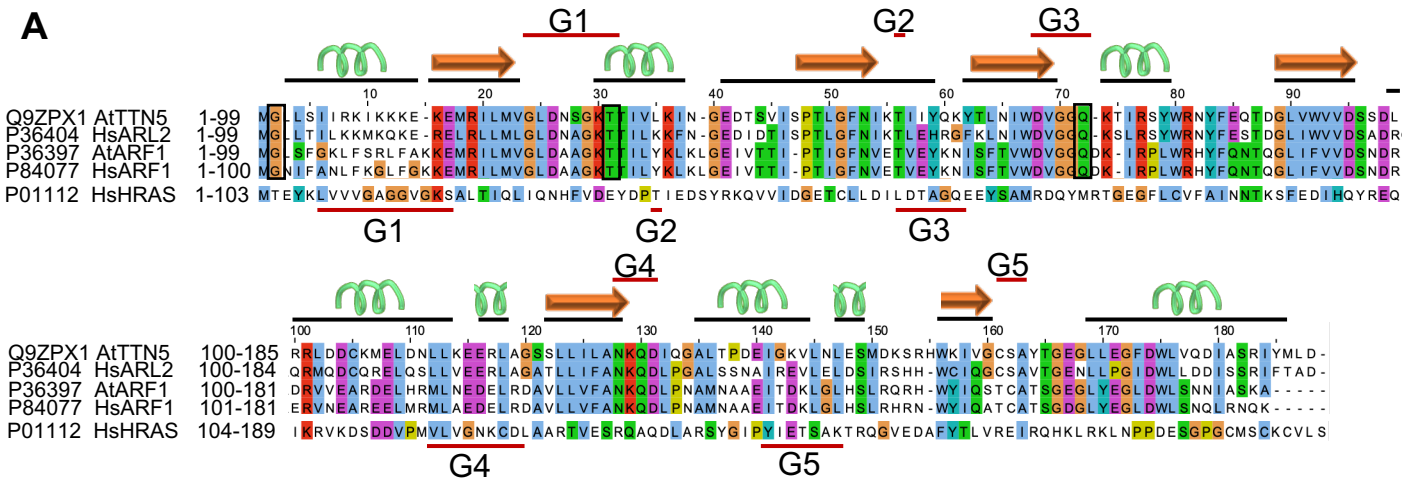
A
G1
G2
G3
G4
G5
Q9ZPX1 AtTTN5 1-99
P36404 HsARL2 1-99
P36397 AtARF1 1-99
P84077 HsARF1 1-100
P01112 HsHRAS 1-103
Q9ZPX1 AtTTN5 100-185
P36404 HsARL2 100-184
P36397 AtARF1 100-181
P84077 HsARF1 101-181
P01112 HsHRAS 104-189

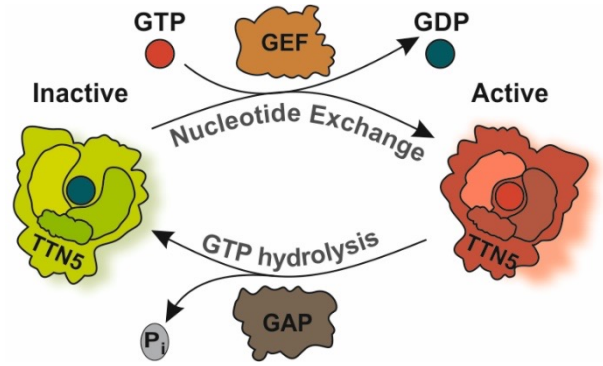
B
GTP
GEF
GDP
Inactive
Active
Nucleotide Exchange
TTN5
TTN5
GTP hydrolysis
GAP
Pi

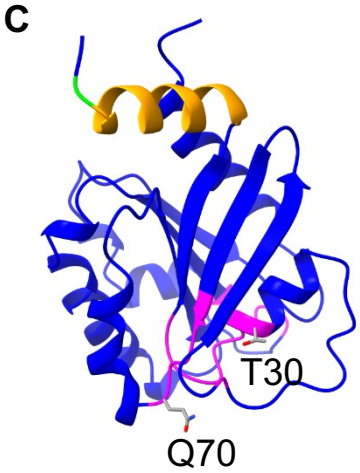
C
T30
Q70

Figure 1: TTN5 is predicted to be a functional small ARF-like GTPase with nucleotide exchange capacity. (A), Sequence alignment of TTN5 with its human homolog ARL2, Arabidopsis, human ARF1 and human HRAS created with Jalview (Waterhouse et al., 2009). The conserved G-motifs (G1-G5; indicated by red lines) are defined for the TTN5 and HRAS sequence. The secondary structure of TTN5 is depicted by black lines and corresponding cartoon (α-helix in green; β-sheet in orange). Here mentioned conserved residues in ARF/ARL proteins are highlighted by boxes; Gly-2, and mutated Thr-30 and Gln-70. $TTN5^{T30N}$ is expected to have a low nucleotide exchange capacity, while $TTN5^{Q70L}$ is expected to have a low GTPase hydrolysis activity. (B), Model of the predicted GTPase nucleotide exchange and hydrolysis cycle of TTN5. TTN5 switches from an inactive GDP-loaded form to an active GTP-loaded one. GDP to GTP nucleotide exchange and GTP hydrolysis may be aided by a guanidine exchange factor (GEF) and a GTPase-activating protein (GAP). (C), Predicted protein structural model of TTN5; magenta, marks the GTP-binding pocket; N-terminal amphipathic helix is highlighted in orange; conserved Gly-2 in green; T30 and Q70, mutagenized in this study, shown in sticks. The model was generated with AlphaFold (Jumper et al., 2021), and adaptation was done with UCSF ChimeraX 1.2.5 (Goddard et al., 2018).

Figure 2

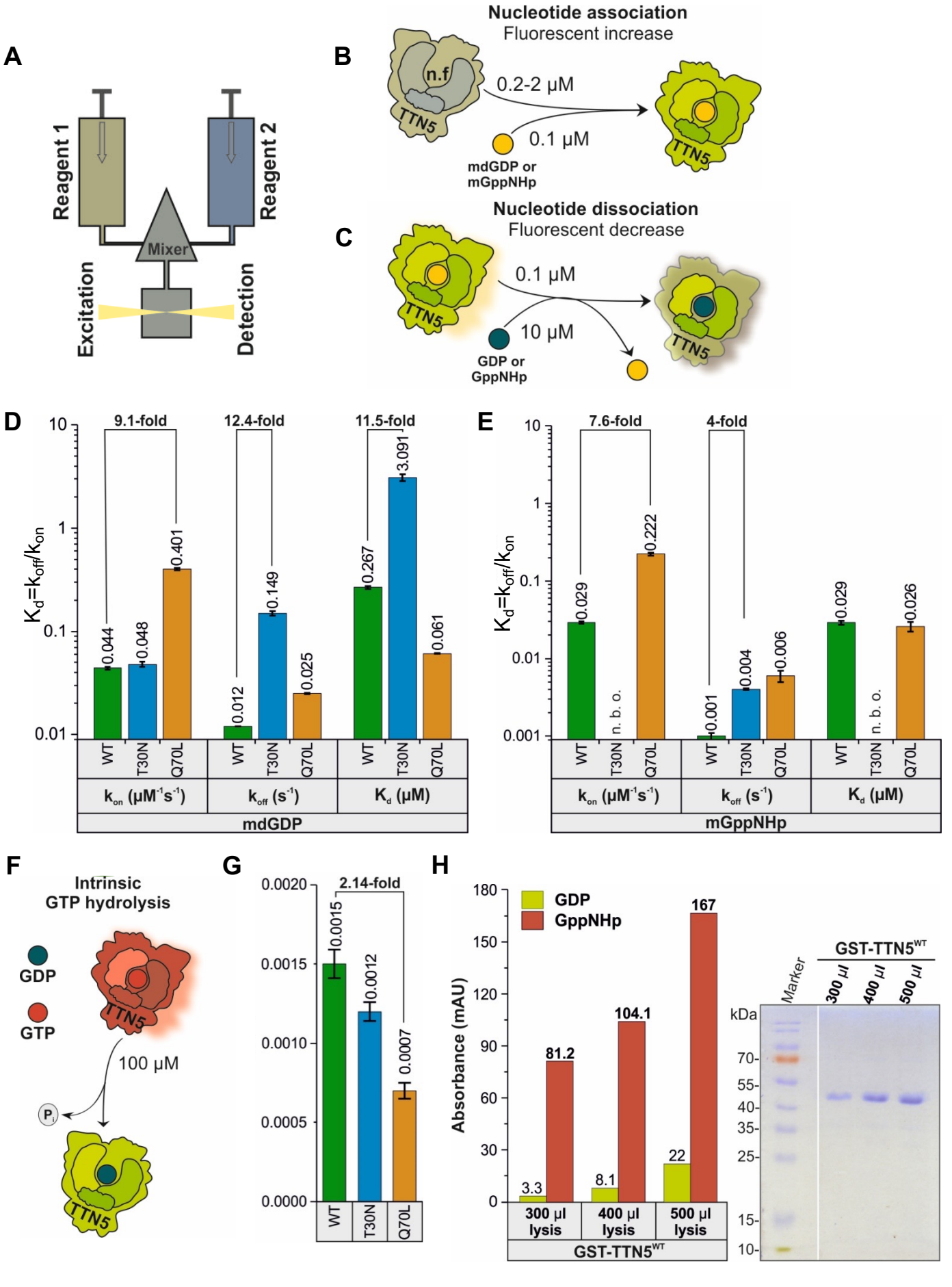
A
Reagent 1
Reagent 2
Mixer
Excitation
Detection
B
Nucleotide association
Fluorescent increase
n.f
TTN5
0.2-2 µM
0.1 µM
mdGDP or
mGppNHp
C
Nucleotide dissociation
Fluorescent decrease
0.1 µM
10 µM
GDP or
GppNHp
D
9.1-fold
12.4-fold
11.5-fold
$K_d=k_{off}/k_{on}$
0.044
0.048
0.401
0.012
0.149
0.025
0.267
3.091
0.061
WT
T30N
Q70L
k_{on} (µM^{-1}s^{-1})
k_{off} (s^{-1})
K_d (µM)
mdGDP
E
7.6-fold
4-fold
0.029
n. b. o.
0.222
0.001
0.004
0.006
0.029
n. b. o.
0.026
mGppNHp
F
Intrinsic
GTP hydrolysis
GDP
GTP
100 µM
P_i
G
2.14-fold
0.0015
0.0012
0.0007
H
GDP
GppNHp
Absorbance (mAU)
3.3
81.2
8.1
104.1
22
167
300 µl lysis
400 µl lysis
500 µl lysis
GST-TTN5^{WT}
Marker
kDa
70-
55-
40-
35-
25-
15-
10-

Figure 2: Biochemical properties of TTN5 proteins suggest that TTN5 is present in a GTP-loaded active form in cells. (A), Schematic illustration of the stopped-flow fluorescence device for monitoring the nucleotide-binding kinetics of the purified TTN5 protein heterologously expressed in bacteria (Supplementary Figure S2A-D). It consists of two motorized, thermostated syringes, a mixing chamber and a fluorescence detector. Two different reagents 1 and 2 are rapidly mixed and transferred to a fluorescence detection cell within 4 ms. One of the reagents must contain a fluorescent reporter group. Here, mdGDP and mGppNHp were used to mimic GDP and GTP. (B), Schematic illustration of the nucleotide association. Nucleotide-free TTN5 (reagent 1; preparation see Supplementary Figure S2E) was rapidly mixed with mdGDP (reagent 2). A fluorescence increase is expected upon association of mdGDP with TTN5. Similar measurements are performed with mGppNHp instead of mdGDP. (C), Schematic illustration of the intrinsic nucleotide dissociation. mdGDP-bound TTN5 (reagent 1) is mixed with a molar excess of GDP (reagent 2). A fluorescence decrease is expected upon mdGDP dissociation from TTN5 and binding of free GDP. Similar measurements are performed with mGppNHp. (D-E), Kinetics of association and dissociation of fluorescent nucleotides mdGDP (D) or mGppNHp (E) with TTN5 proteins (WT, $TTN5^{T30N}$, $TTN5^{Q70L}$) are illustrated as bar charts. The association of mdGDP (0.1 µM) or mGppNHp (0.1 µM) with increasing concentration of $TTN5^{WT}$, $TTN5^{T30N}$ and $TTN5^{Q70L}$ was measured using a stopped-flow device (see A, B; data see Supplementary Figure S3A-F, S4A-E). Association rate constants (k_{on} in $\mu M^{-1}s^{-1}$) were determined from the plot of increasing observed rate constants (k_{obs} in s^{-1}) against the corresponding concentrations of the TTN5 proteins. Intrinsic dissociation rates (k_{off} in s^{-1}) were determined by rapidly mixing 0.1 µM mdGDP-bound or mGppNHp-bound TTN5 proteins with the excess amount of unlabeled GDP (see A, C, data see Supplementary Figure S3G-I, S4F-H). The nucleotide affinity (dissociation constant or K_d in µM) of the corresponding TTN5 proteins was calculated by dividing k_{off} by k_{on}. When mixing mGppNHp with nucleotide-free $TTN5^{T30N}$, no binding was observed (n.b.o.) under these experimental conditions. (F-G), GTP hydrolysis of TTN5 proteins determined by HPLC. (F), Schematic illustration of the GTP hydrolysis measurement. (G), GTP-bound TTN5 proteins (100 µM) were incubated at room temperature at different time points before injecting them on a reversed-phase HPLC system. Evaluated data (data see Supplementary Figure S5) resulted in the determination of the GTP hydrolysis rates (k_{cat} in s^{-1}) illustrated as bar charts. (H), TTN5 accumulated in a GTP-loaded active form. GST-$TTN5^{WT}$ (46.5 kDa) was purified from bacterial cell lysates at three different volumes in the presence of 0.1 µM unbound free GppNHp using glutathione beads. The nucleotide contents and the protein purities were determined by HPLC and Coomassie Blue-stained SDS-polyacrylamide gel electrophoresis. The presence of much higher amounts of GppNHp-bound versus GDP-bound GST-TTN5 protein indicates that TTN5 rapidly exchanged bound nucleotide und accumulated in this state.

Figure 3

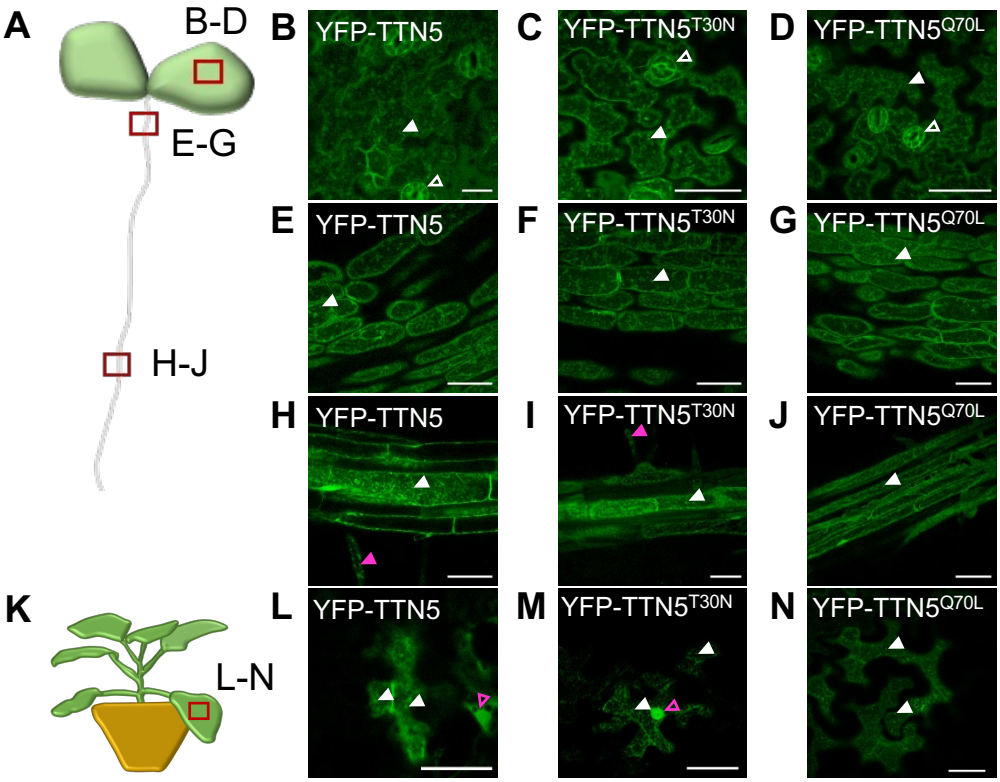
A
B-D
E-G
H-J
K
L-N
B
YFP-TTN5
C
YFP-TTN5T30N
D
YFP-TTN5Q70L
E
YFP-TTN5
F
YFP-TTN5T30N
G
YFP-TTN5Q70L
H
YFP-TTN5
I
YFP-TTN5T30N
J
YFP-TTN5Q70L
L
YFP-TTN5
M
YFP-TTN5T30N
N
YFP-TTN5Q70L

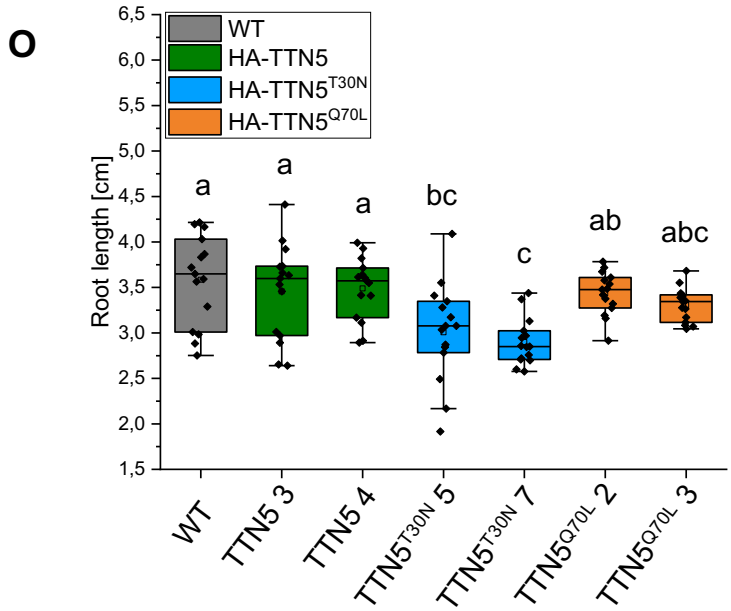
O
WT
HA-TTN5
HA-TTN5T30N
HA-TTN5Q70L
Root length [cm]
6,5
6,0
5,5
5,0
4,5
4,0
3,5
3,0
2,5
2,0
1,5
a
a
a
bc
c
ab
abc
WT
TTN5 3
TTN5 4
TTN5T30N 5
TTN5T30N 7
TTN5Q70L 2
TTN5Q70L 3

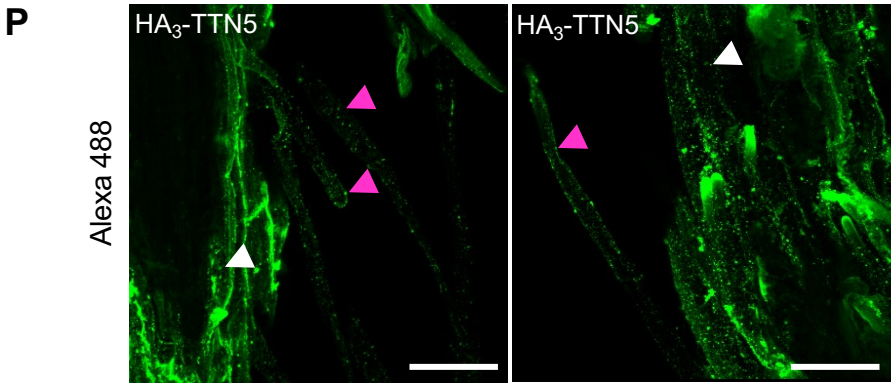
P
Alexa 488
HA3-TTN5
HA3-TTN5

Figure 3: TTN5 may be present in punctate structures in seedlings. Microscopic observations of YFP fluorescence signals were made in a plane underneath the plasma membrane at the cell peripheries. (A), Schematic representation of an Arabidopsis seedling. Images were taken at three different positions of the seedlings and imaged areas are indicated by a red rectangle. (B-J), Analysis of YFP-TTN5, YFP-TTN5^{T30N} and YFP-TTN5^{Q70L} Arabidopsis seedlings *via* fluorescent confocal microscopy. (B-D), Fluorescence signals observed in stomata (indicated by empty white arrowhead) and in the epidermis of cotyledons in punctate structures (indicated by filled white arrowhead). (E-G), Localization in the hypocotyls showed the same pattern of punctate structures. (H-J), Signals were present in punctate structures in the root hair zone and in root hairs (indicated by filled magenta arrowhead). (K), Schematic representation of a *N. benthamiana* plant, used for leaf infiltration for transient expression. Imaged area is indicated by a red rectangle. (L-N), YFP fluorescence signals in *N. benthamiana* leaf epidermal cells expressing YFP-TTN5, YFP-TTN5^{T30N} and YFP-TTN5^{Q70L}. Signals were present in punctate structures (indicated by white arrowheads) and in the nucleus (indicated by empty magenta arrowheads). Scale bar 50 µm. (O), Root length measurement of HA_3-TTN5, HA_3-TTN5^{T30N} and HA_3-TTN5^{Q70L} Arabidopsis lines in comparison with non-transgenic wild type (WT). Seedlings were grown for 10 days on Hoagland plates. Only HA_3-TTN5^{T30N} showed a slightly reduced root length compared to WT, whereas HA_3-TTN5 and HA_3-TTN5^{Q70L} did not have a divergent phenotype. Analysis was conducted in replicates (n= 14). One-way ANOVA with Tukey post-hoc test was performed. Different letters indicate statistical significance ($p < 0.05$). (P), Two representative images of whole-mount immunostaining of HA_3-TTN5 seedling roots in the root differentiation zone (rabbit α-HA primary antibody, Alexa-488-labeled secondary α-rabbit antibody). Alexa-488 signals were present in punctate structures in root cells (indicated by filled white arrowhead) and in root hairs (indicated by filled magenta arrowhead) comparable to YFP signals (Figure 3H-J). Images are presented in a maximum intensity projection of several z-layers for a better visualization. Scale bar 50 µm.

Figure 4

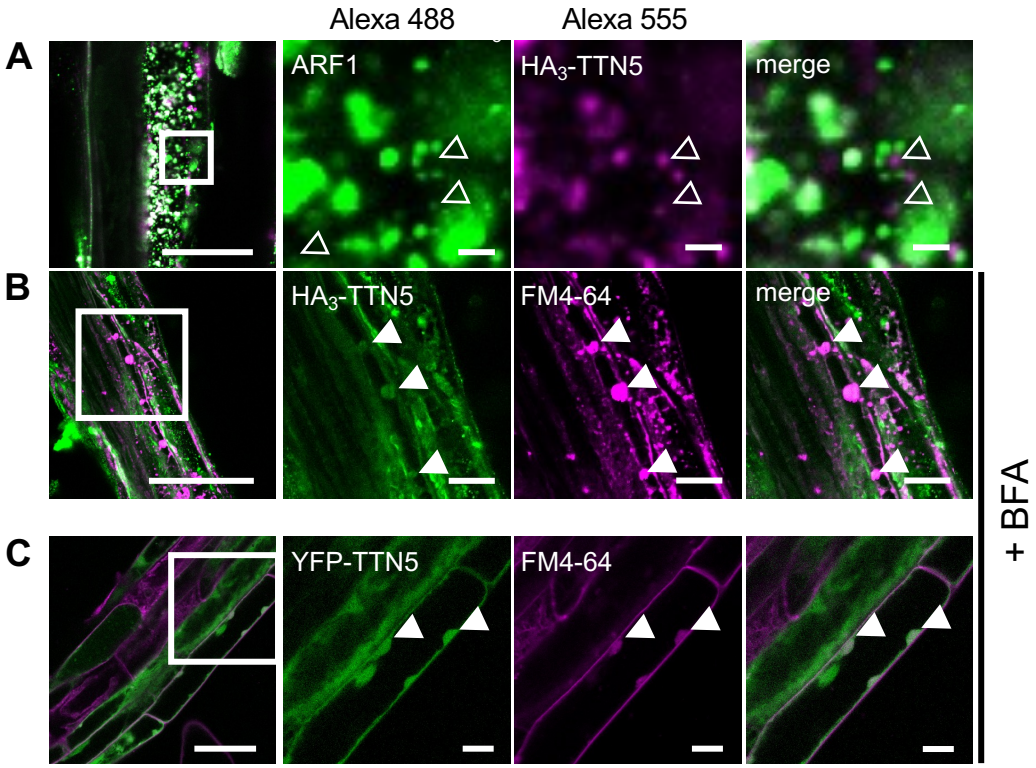
Alexa 488
Alexa 555
A
ARF1
HA3-TTN5
merge
B
HA3-TTN5
FM4-64
merge
C
YFP-TTN5
FM4-64
+ BFA

Figure 4. Whole-mount Immunolocalization analysis of HA_3-TTN5 in Arabidopsis including colocalization with Golgi marker and localization in BFA bodies.

(A-B), Representative images showing whole-mount immunostaining of HA_3-TTN5 seedlings with different types of markers for colocalization analysis. (A), Detection of HA_3-TTN5 (chicken α-HA primary antibody, Alexa 555-labeled secondary α-chicken antibody) with Golgi and TGN marker ARF1 (rabbit α-ARF1 primary antibody, Alexa-488-labeled secondary α-rabbit antibody). Both fluorescence signals were detected in vesicle-like structures in root cells in close proximity to each other but mostly not colocalizing. The experiment was repeated twice with three seedlings. (B) Detection of HA_3-TTN5 (rabbit α-HA primary antibody, Alexa-488-labeled secondary α-rabbit antibody) and staining with lipid membrane dye FM4-64 after brefeldin A (BFA) treatment (72 μM, 1 h). Alexa-488 signals colocalized with FM4-64 in BFA bodies in root cells. The experiment was repeated three times with three seedlings. (C), in comparison, YFP fluorescence in YFP-TTN5 seedlings, co-analyzed with FM4-64 after BFA treatment (36 μM, 30 min). YFP fluorescence signals colocalized with FM4-64 in BFA bodies similar as in (B). The experiment was performed once with three independent YFP-TTN5 lines.

Colocalizing signals in the two channels are indicated by filled white arrowheads, whereas signals that do not colocalize in the two channels are indicated by empty white arrowheads. Scale bar overview: 50 μm, close-up: 10 μm.

Figure 5

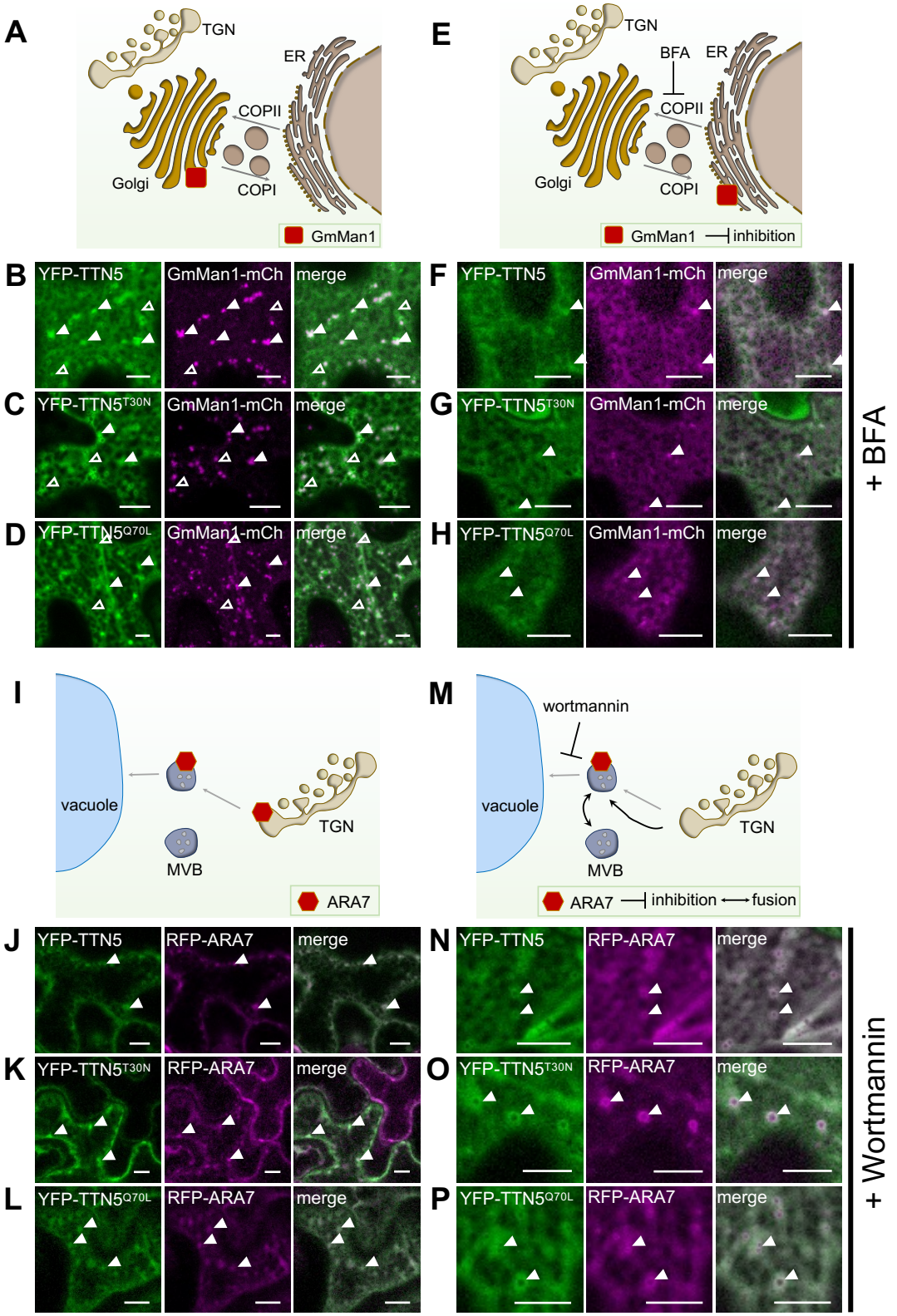
A
TGN
ER
COPII
Golgi
COPI
GmMan1
E
TGN
BFA
ER
COPII
Golgi
COPI
GmMan1
inhibition
B
YFP-TTN5
GmMan1-mCh
merge
C
YFP-TTN5T30N
GmMan1-mCh
merge
D
YFP-TTN5Q70L
GmMan1-mCh
merge
F
YFP-TTN5
GmMan1-mCh
merge
G
YFP-TTN5T30N
GmMan1-mCh
merge
H
YFP-TTN5Q70L
GmMan1-mCh
merge
+ BFA
I
vacuole
TGN
MVB
ARA7
M
wortmannin
vacuole
TGN
MVB
ARA7
inhibition
fusion
J
YFP-TTN5
RFP-ARA7
merge
K
YFP-TTN5T30N
RFP-ARA7
merge
L
YFP-TTN5Q70L
RFP-ARA7
merge
N
YFP-TTN5
RFP-ARA7
merge
O
YFP-TTN5T30N
RFP-ARA7
merge
P
YFP-TTN5Q70L
RFP-ARA7
merge
+ Wortmannin

Figure 5: TTN5 may be associated with the endomembrane system in *N. benthamiana* leaf epidermal cells. YFP fluorescence signals were localized in *N. benthamiana* leaf epidermal cells transiently transformed to express YFP-TTN5, YFP-TTN5^{T30N} and YFP-TTN5^{Q70L} *via* fluorescent confocal microscopy. Specific markers indicating the endomembrane system were used. (A), Schematic representation of GmMan1 localization at the *cis*-Golgi site. (B-D), Partial colocalization of YFP signal with the Golgi marker GmMan1-mCherry at *cis*-Golgi stacks (filled white arrowheads). Additionally, YFP fluorescent signals were detected in non-colocalizing punctate structures with depleted fluorescence in the center (empty white arrowheads). (E), Schematic representation of GmMan1 localization at the ER upon brefeldin A (BFA) treatment. BFA blocks ARF-GEF proteins which leads to a loss of Golgi *cis*-cisternae and the formation of BFA-induced compartments due to an accumulation of Golgi stacks up to a redistribution of the Golgi to the ER by fusion of the Golgi with the ER (Renna and Brandizzi 2020). (F-H), Redistribution of Golgi stacks was induced by BFA treatment (36 µM, 30 min). GmMan1-mCherry and YFP fluorescence signals were present in the ER and in colocalizing punctate structures. (I), Schematic representation of ARA7 localization at the *trans*-Golgi network (TGN) and multi-vesicular bodies (MVBs). (J-L), Colocalization of YFP fluorescence signal with the MVB marker RFP-ARA7. (M), Schematic representation of ARA7 localization in swollen MVBs upon wortmannin treatment. Wortmannin inhibits phosphatidylinositol-3-kinase (PI3K) function leading to the fusion of TGN/EE to swollen MVBs (Renna and Brandizzi 2020). (N-P), MVB swelling was obtained by wortmannin treatment (10 µM, 30 min). ARA7-RFP was colocalizing with YFP signal in these swollen MVBs. Chemical treatment-induced changes were imaged after 25 min incubation. Colocalization is indicated with filled arrowheads, YFP signal only with empty ones. Corresponding colocalization analysis data is presented in Supplementary Figure S8. Scale bar 10 µm.

Figure 6

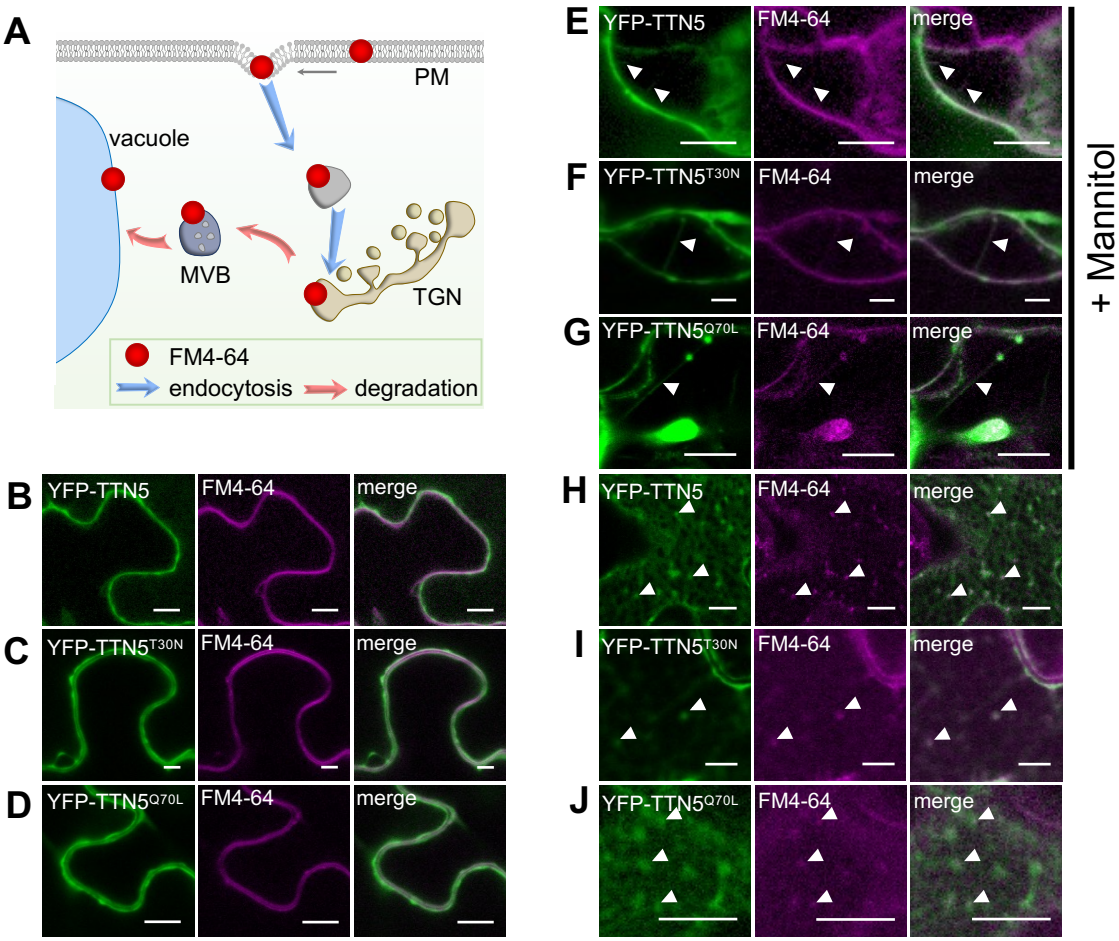
A
PM
vacuole
MVB
TGN
FM4-64
endocytosis
degradation
B
YFP-TTN5
FM4-64
merge
C
YFP-TTN5T30N
FM4-64
merge
D
YFP-TTN5Q70L
FM4-64
merge
E
YFP-TTN5
FM4-64
merge
F
YFP-TTN5T30N
FM4-64
merge
G
YFP-TTN5Q70L
FM4-64
merge
H
YFP-TTN5
FM4-64
merge
I
YFP-TTN5T30N
FM4-64
merge
J
YFP-TTN5Q70L
FM4-64
merge
+ Mannitol

Figure 6. TTN5 may colocalize with endocytosed plasma membrane material. (A), Schematic representation of progressive stages of FM4-64 localization and internalization in a cell. FM4-64 is a lipophilic substance. After infiltration, it first localizes in the plasma membrane, at later stages it localizes to intracellular vesicles and membrane compartments. This localization pattern reflects the endocytosis process (Bolte et al., 2004). (B-J), YFP fluorescence signals were localized in *N. benthamiana* leaf epidermal cells together with the plasma membrane dye FM4-64 *via* fluorescent confocal microscopy, following transient transformation to express YFP-tagged TTN5, YFP-TTN5^{T30N} and YFP-TTN5^{Q70L}. (B-D), YFP signals colocalized with FM4-64 at the plasma membrane. (E-G), Plasma membrane localization of YFP fluorescence was evaluated after mannitol-induced (1 M) plasmolysis. The formation of Hechtian strands is a sign of plasma membrane material and fluorescence staining there is indicated with filled arrowheads. (H-J), Internalized FM4-64 was present in vesicle-like structures that showed YFP signals. Colocalization is indicated with filled arrowheads. Scale bar 10 µm.

Figure 7

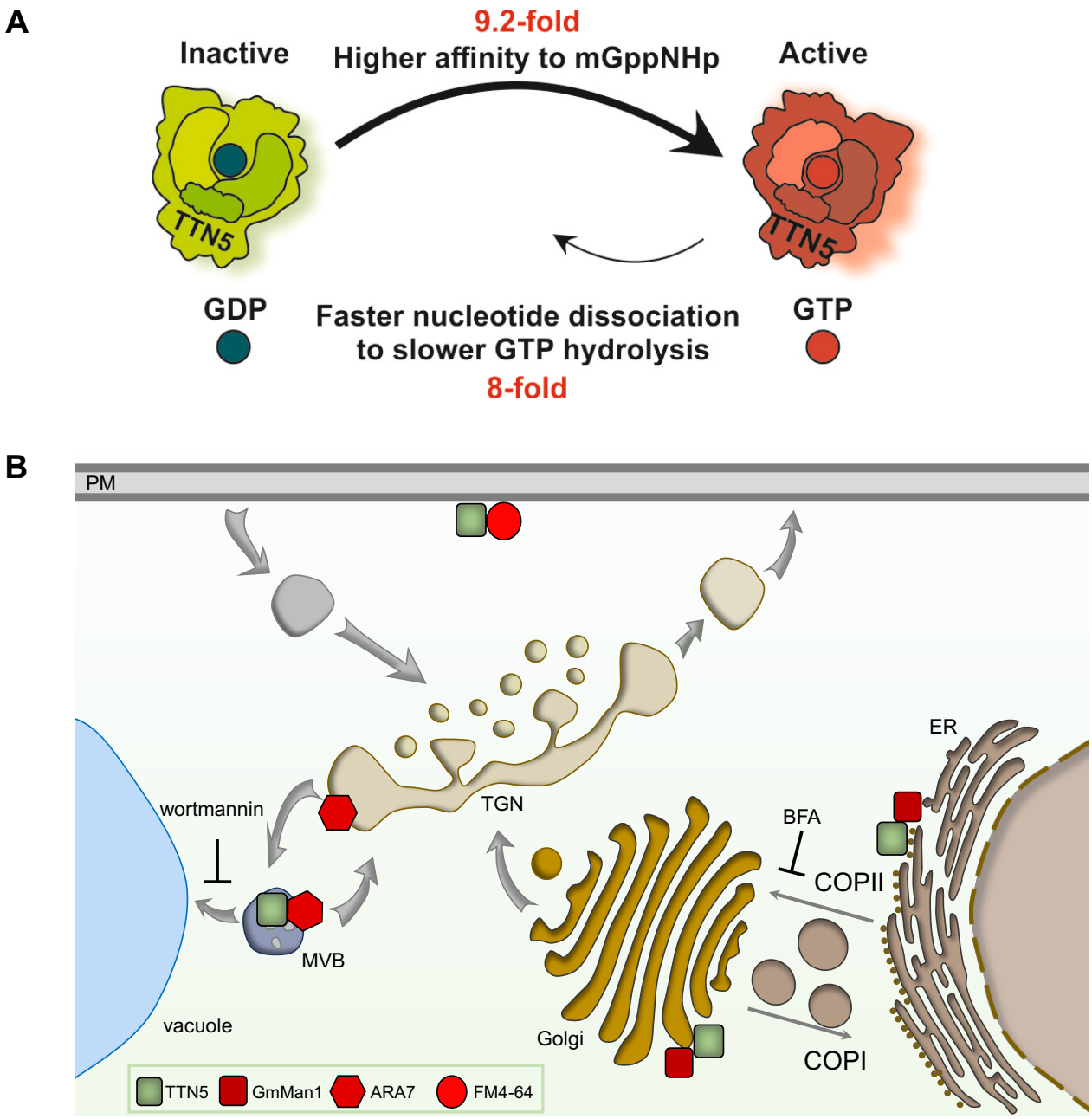
A
Inactive
9.2-fold
Higher affinity to mGppNHp
Active
TTN5
TTN5
GDP
Faster nucleotide dissociation
to slower GTP hydrolysis
8-fold
GTP
B
PM
TGN
wortmannin
MVB
vacuole
Golgi
BFA
COPII
COPI
ER
TTN5
GmMan1
ARA7
FM4-64

Figure 7: Schematic models summarize TTN5 kinetic GTPase activities and potential localization within the cell.
(A), Model of the predicted GTPase nucleotide exchange and hydrolysis cycle mechanism of TTN5 based on the biochemical investigation. TTN5 affinity to mGppNHp was 9.2-fold higher compared to mGDP resulting in a fast switching from an inactive GDP-loaded form to an active GTP-loaded one. mGppNHp dissociation was 8-fold faster as GTP hydrolysis but both processes were much slower than nucleotide association. TTN5 kinetics identified it as a non-classical GTPase which tended to stay in a GTP-loaded form even under resting conditions. (B), Presumed TTN5 locations within the cell. TTN5 (green square) can be present at the plasma membrane (PM) similar as FM4-64 (red circle) or in the endomembrane compartments of the *trans*-Golgi network (TGN) or multivesicular body (MVB) as found by colocalization with ARA7 (red hexagon). Additionally TTN5 might colocalize with GmMan1-positive (red square) Golgi stacks.

Supplementary figures

Characterization of the small *Arabidopsis thaliana* GTPase and ADP-ribosylation factor-like 2 protein TITAN 5

Inga Mohr[1], Amin Mirzaiebadizi[2], Sibaji K. Sanyal[1], Pichaporn Chuenban[1], Mohammad R. Ahmadian[2], Rumen Ivanov[1] and Petra Bauer[1,3]

[1]Institute of Botany, Heinrich Heine University, 40225 Düsseldorf, Germany.
[2]Institute of Biochemistry and Molecular Biology II, Medical Faculty and University Hospital Düsseldorf, Heinrich Heine University, Düsseldorf, Germany
[3]Cluster of Excellence on Plant Sciences, Heinrich Heine University, 40225 Düsseldorf,
Germany

Supplementary Figure S1

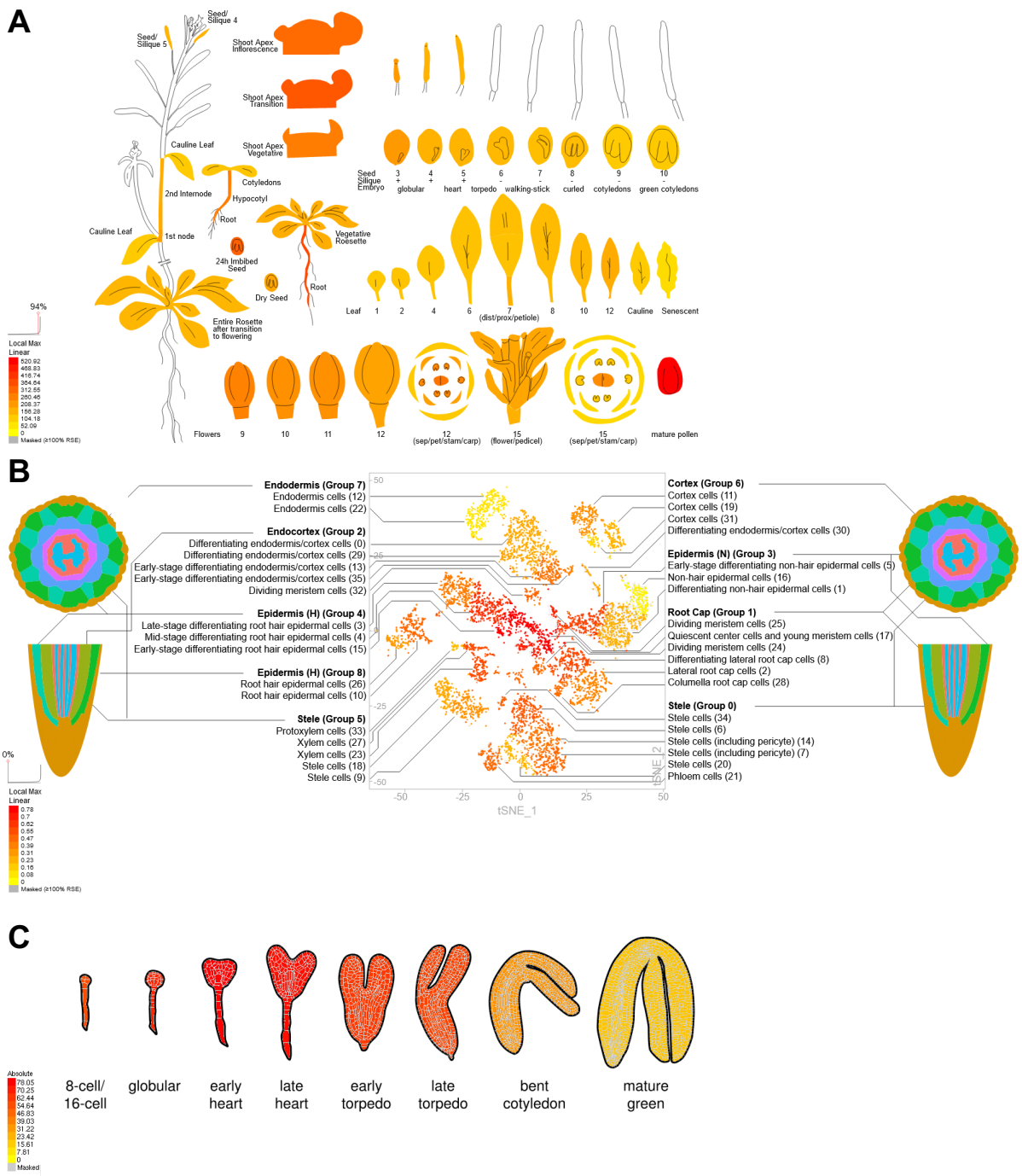

Supplementary Figure S1. Visualization of *TTN5* gene expression levels during plant development based on transcriptome data. Expression levels in (A), different types of aerial organs at different developmental stages; from left to right and bottom to top are represented different seed and plant growth stages, flower development stages, different leaves, vegetative to inflorescence shoot apex, embryo and silique development stages; (B), seedling root tissues based on single cell analysis represented in form of a uniform manifold approximation and projection plot; (C), successive stages of embryo development. As shown in (A) to (C), *TTN5* is ubiquitously expressed in these different plant organs and tissues. In particular, it should be noted that *TTN5* transcripts were detectable in the epidermis cell layer of roots that we used for localization of tagged TTN5 protein in this study. In accordance with the embryo-lethal phenotype, the ubiquitous expression of *TTN5* highlights its importance for plant growth. Original data were derived from Schmid et al., 2005 and Nakabayashi et al., 2005 (A); Ryu et al., 2019 (B); Waese et al., 2017 (C). Gene expression levels are indicated by local maximum color code, ranging from the minimum (no expression) in yellow to the maximum (highest expression) in red.

Supplementary Figure S2

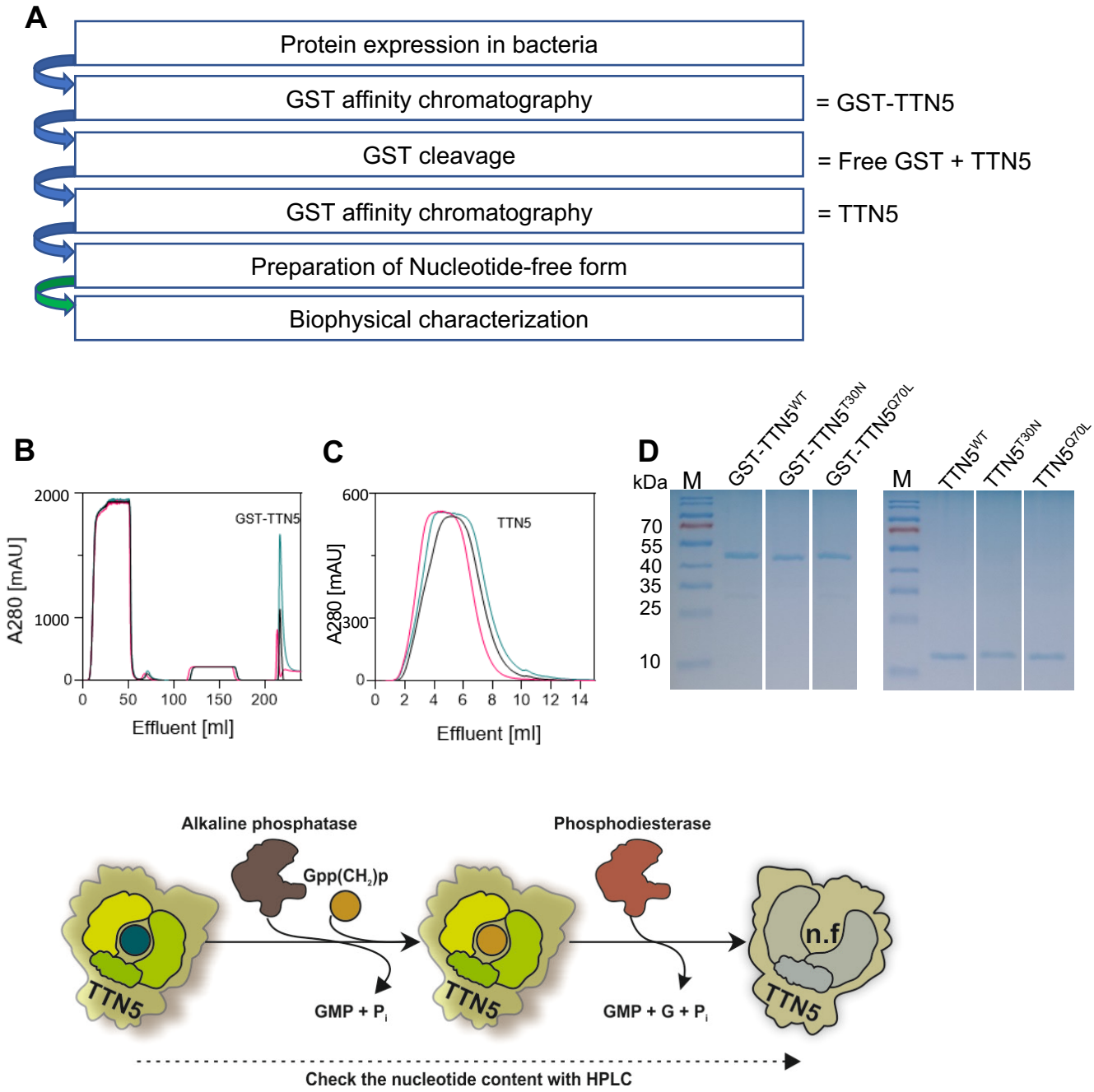

Supplementary Figure S2. Heterologous expression and purification of TTN5 protein as well as preparation of its nucleotide-free form. (A), Overview of protein purification and preparation of nucleotide-free form of TTN5 in the presence of excess GDP. (B-C), The chromatograms represent the GST-affinity chromatography to obtain GST-TTN5 and TTN5 variants, before and after GST-cleavage by thrombin. (D), Coomassie Blue SDS-PAGE of GST-TTN5 (left panel; 46.5 kDa) and TTN5 after GST-cleavage by thrombin and a second GST-affinity chromatography (right panel; 21 kDa). (E), Schematic illustration of nucleotide-free TTN5 preparation. In the first step, the purified GDP-bound TTN5 is incubated with alkaline phosphatase in the presence of 1.5-fold molar excess of Gpp(CH_2)p, which is a non-hydrolyzable GTP analog and, unlike GDP, resistant to alkaline phosphatase. After GDP is completely degraded, phosphodiesterase is added to the reaction to degrade Gpp(CH_2)p to GMP, G and Pi. The nucleotide content is monitored in each step by HPLC. The solution with nucleotide-free TTN5 is deep-frozen and thawed twice, aliquoted and stored at -80°C.

Supplementary Figure S3

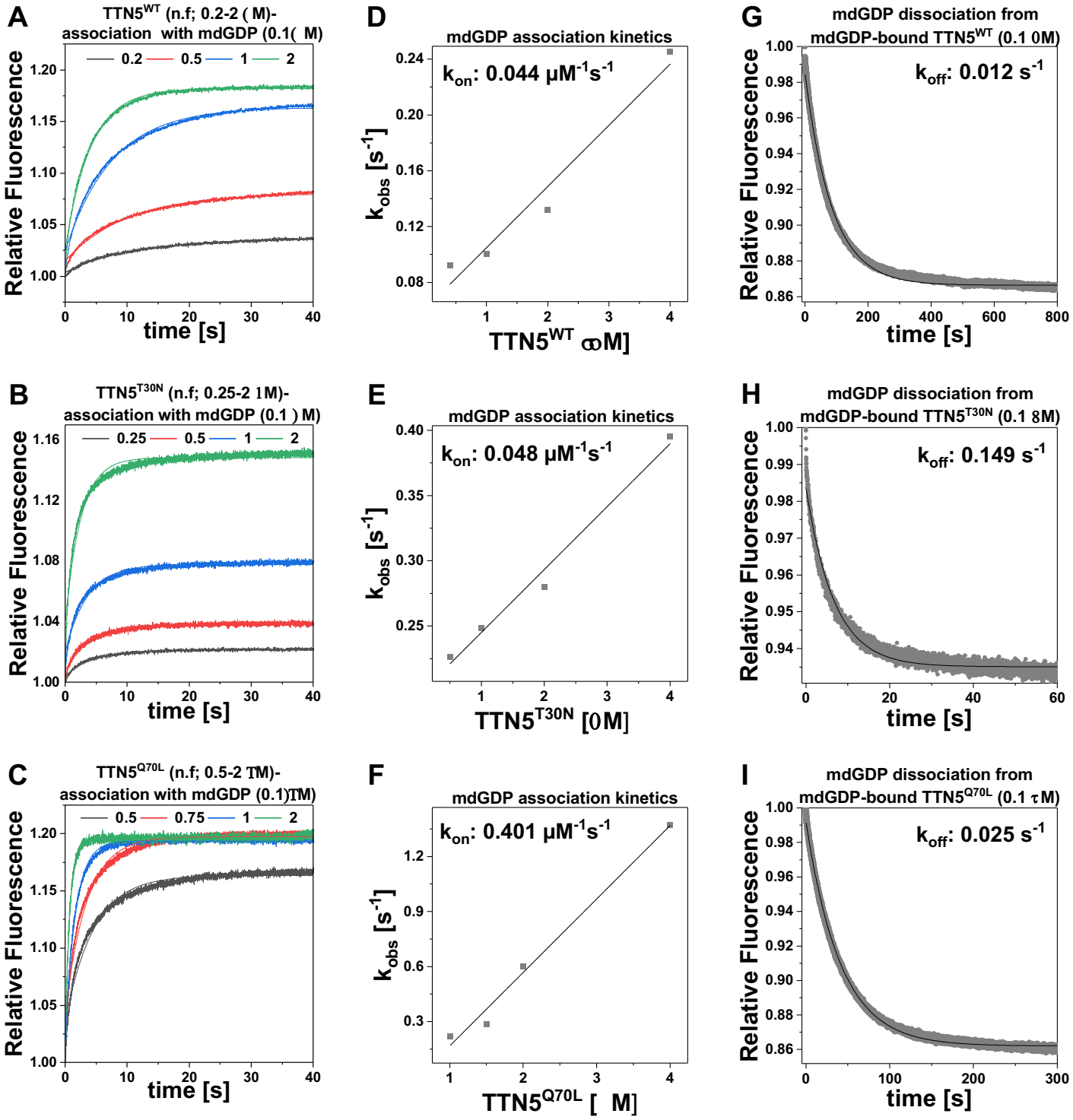

Supplementary Figure S3. Kinetic measurements of mdGDP interaction with TTN5 proteins. (A-C), Association of mdGDP (0.1 μM) with increasing concentrations of $TTN5^{WT}$ (A), $TTN5^{T30N}$ (B) and $TTN5^{Q70L}$ (C). (D-F), Association rate constant (k_{on}) is determined by plotting the k_{obs} values, obtained from the exponential fits of the mdGDP association data (A-C) against the TTN5 (D), $TTN5^{T30N}$ (E) and $TTN5^{Q70L}$ (F) protein concentrations. (G-I), Dissociation of mdGDP from TTN5 (G), $TTN5^{T30N}$ (H) and $TTN5^{Q70L}$ (I) proteins (0.1 μM) is determined in the presence of excess amounts of unlabeled GDP (20 μM). The dissociation rates (k_{off}) are obtained from the exponential fitting of the data by Origin software. All results are shown as bar charts in Figure 2D. The principles of the assays are illustrated in Figure 2A-C.

Supplementary Figure S4

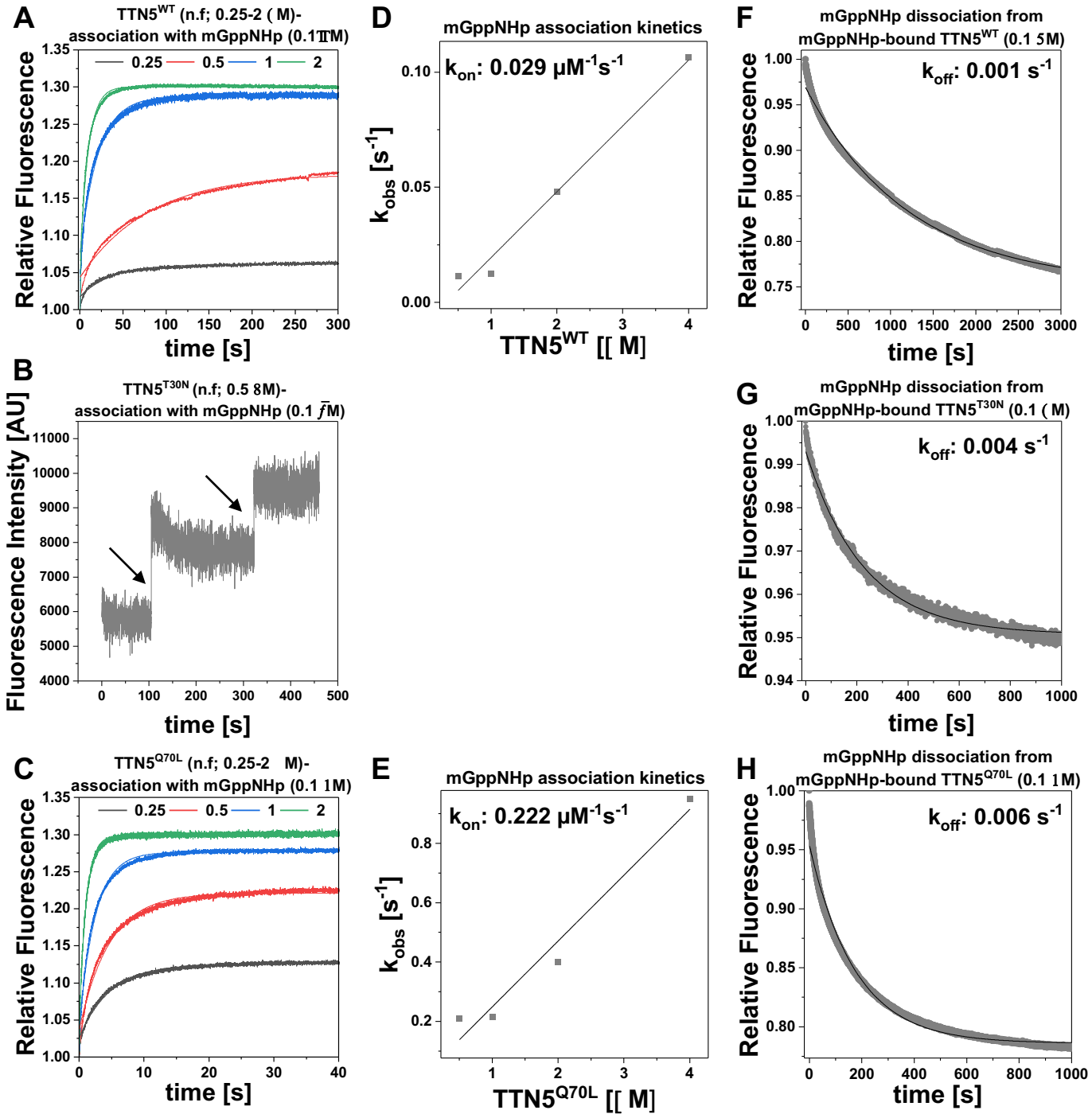

Supplementary Figure S4. Kinetic measurements of mGppNHp interaction with TTN5 proteins. (A-E), Association kinetics. (A, C), Association of mGppNHp (0.1 μM) with increasing concentrations of $TTN5^{WT}$ (A) and $TTN5^{Q70L}$ (C). (B) When mixing mGppNHp with nucleotide-free $TTN5^{T30N}$, no binding was observed under these experimental conditions. Instead, association of mGppNHp (0.1 μM) with two different titrations of 0.5 μM $TTN5^{T30N}$ was measured, indicated by arrows, to confirm the fast binding of $TTN5^{T30N}$ with mGppNHp by increasing fluorescence intensity, determined by fluorimeter. (D-E), Association rate constant (k_{on}) is determined by plotting the k_{obs} values, obtained from the exponential fits of the mGppNHp association data (left panels) against the $TTN5^{WT}$ (D) and $TTN5^{Q70L}$ (E) protein concentrations. Note that $TTN5^{T30N}$ did not show association with mGppNHp, therefore middle space is left empty. (F-H), Dissociation of mGppNHp from $TTN5^{WT}$ (F), $TTN5^{T30N}$ (G) and $TTN5^{Q70L}$ (H) proteins (0.1 μM) is determined in the presence of excess amounts of unlabeled GppNHp (20 μM). The dissociation rates (k_{off}) are obtained from the exponential fitting of the data by Origin software. All results are shown as bar charts in Figure 2E. The principles of the assays are illustrated in Figure 2A-C.

Supplementary Figure S5

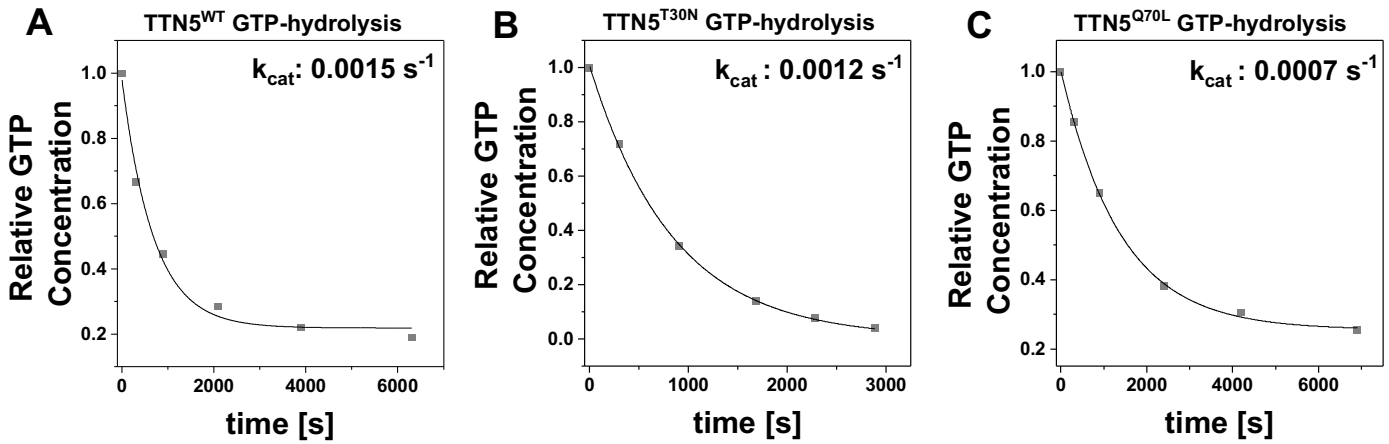

Supplementary Figure S5. GTP hydrolysis reaction rates of the TTN5 proteins. (A-C), The GTP hydrolysis reaction rates (k_{cat}) of $TTN5^{WT}$ (A), $TTN5^{T30N}$ (B) and $TTN5^{Q70L}$ (C) proteins (100 μM) were measured at 25°C. Aliquots of the reaction mixture at the indicated time points were analyzed by HPLC as described in Materials and Methods. The obtained results are shown as bar charts in Figure 2G. The principle of the assay is illustrated in Figure 2F.

Supplementary Figure S6

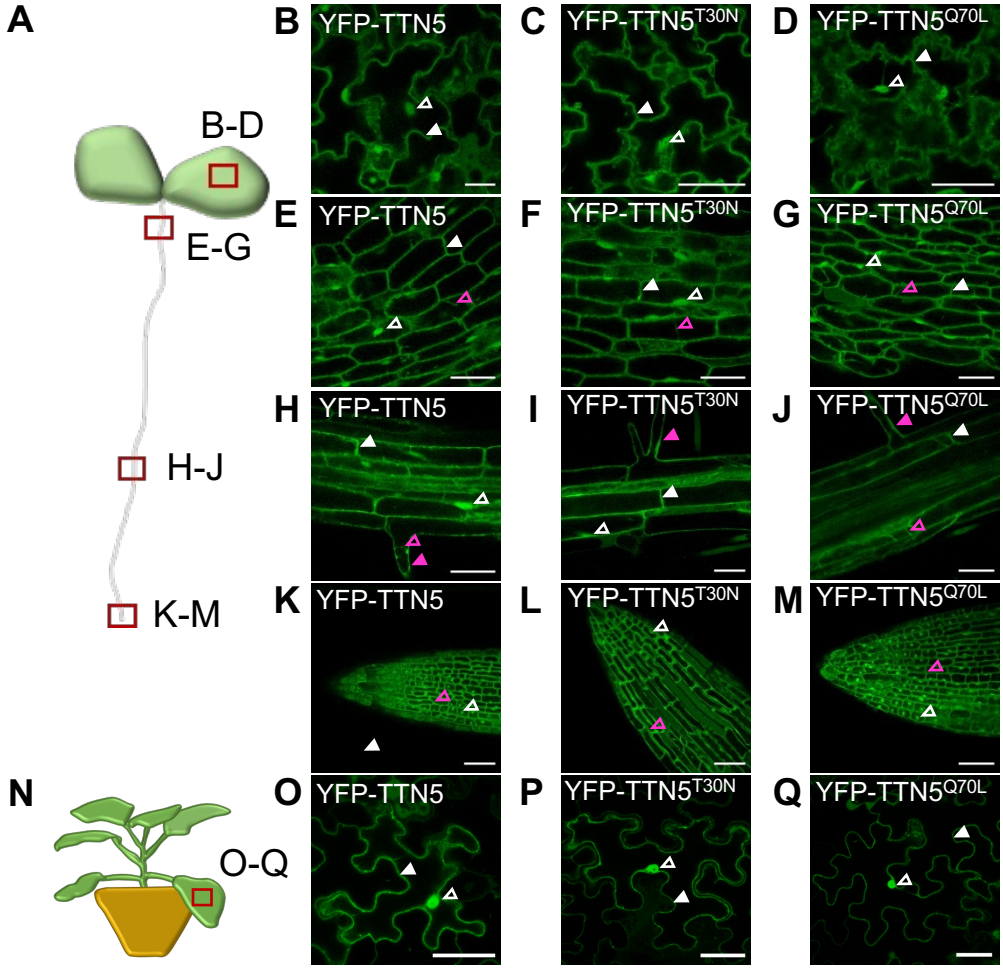

Supplementary Figure S6. YFP fluorescence signal localization in YFP-TTN5 and -TTN5 mutant Arabidopsis seedlings. Microscopic YFP fluorescence observations were made in a plane across the centers of most cells. (A), Schematic representation of an Arabidopsis seedling. Images were taken at four different positions of the seedlings and imaged areas are indicated by a red rectangle. (B-M), Fluorescent YFP signals in Arabidopsis seedlings *via* fluorescent confocal microscopy. (B–D), YFP signal localization was observed in the epidermis of cotyledons. Fluorescence signals were present in nucleus (indicated by empty white arrowhead) and cytoplasm and at or in close proximity to the plasma membrane (indicated by filled white arrowhead) in the epidermis of cotyledons of YFP-TTN5, YFP-TTN5^{T30N} and YFP-TTN5^{Q70L} seedlings. (E-G), Fluorescence localization in the hypocotyls showed clear presence in the cytoplasm (indicated by empty magenta arrowhead), next to nuclear and plasma membrane-related localization. (H-J), Fluorescence signals were present in nuclei, cytoplasm, at or close to the plasma membrane in the root hair zone and in root hairs (indicated by filled magenta arrowhead) with clear cytoplasmic localization of YFP-TTN5, YFP-TTN5^{T30N} and YFP-TTN5^{Q70L} seedlings. (K-M), Fluorescence signal localization at the root tip showed clear expression in nuclei and cytoplasm, visible due to the smaller size of the vacuoles. (N), Schematic representation of a *N. benthamiana* plant, used for leaf infiltration for transient expression of YFP-TTN5, YFP-TTN5^{T30N} and YFP-TTN5^{Q70L}. Imaged areas are indicated by a red rectangle. (O-Q), Fluorescent signals in *N. benthamiana* leaf epidermal cells *via* fluorescent confocal microscopy. Signals were present in nucleus and cytoplasm and at or in close proximity to the plasma membrane. Scale bar 50 µm.

Supplementary Figure S7

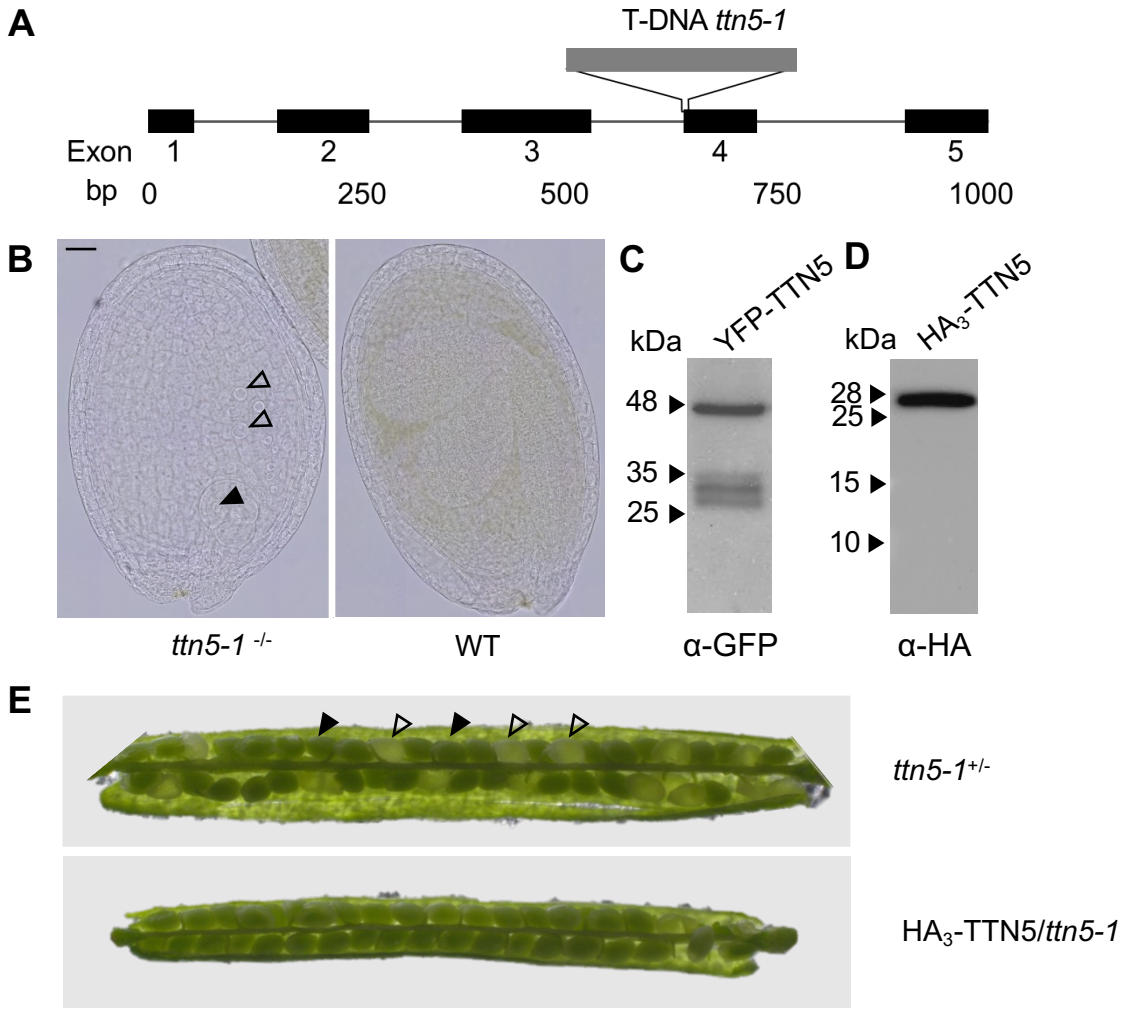

Supplementary Figure S7. Phenotypes of *ttn5-1* T-DNA insertion line and root length of HA_3-TTN5 lines. (A), Schematic representation of the *TTN5* exon-intron structure and T-DNA insertion in the *ttn5-1* allele. The numbers below the exon numbers indicate base pairs (bp). (B), Early embryo arrest phenotype of a homozygous *ttn5-1*$^{-/-}$ seed on the left in comparison with a wild type (WT) seed of the same silique on the right; arrowheads, indicate enlarged nuclei in the arrested embryo (filled) and endosperm (empty). Early embryo arrest phenotypes were previously shown by (Mayer et al., 1999; McElver et al., 2000). Scale bar 1 cm. (C), Western blot control of YFP-TTN5 protein expressed in stable transgenic plant lines. α-GFP primary plus secondary antibody treatment detected a strong band at the correct size of 48 kDa for YFP-TTN5 and three additional smaller sized weak bands 26-35 kDa. Plants were grown for 6 days. (D), Western blot control of HA_3-TTN5 protein expressed in stable transgenic plant lines. One single band was detected by α-HA-HRP antibody treatment at the correct size of 28 kDa for HA_3-TTN5 protein. Plants were grown in the two-week system. (E), Siliques of heterozygous *ttn5-1*$^{+/-}$ plants, containing ca. 25 % white seeds with arrested embryos (empty arrowheads) and ca. 75 % regular green seeds (filled arrowheads). HA_3-TTN5 line crossed to *ttn5-1*$^{+/-}$ was able to rescue embryo lethal seed phenotype.

Supplementary Figure S8

A

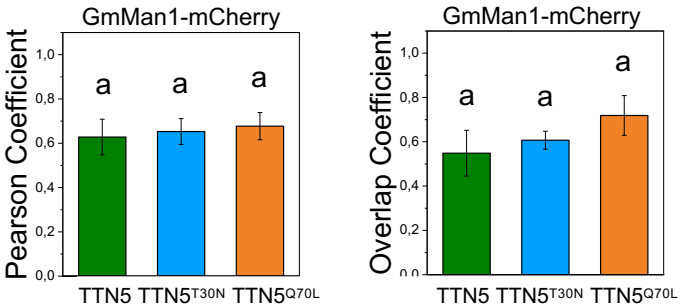

B

Channel		Colocalization	
YFP	mCherry	YFP/mCh	mCh/YFP
YFP-TTN5	GmMan1-mCherry	23.85±22.77	42.62±21.85
YFP-TTN5^{T30N}	GmMan1-mCherry	15.83±10.21	31.25±14.88
YFP-TTN5^{Q70L}	GmMan1-mCherry	14.81±6.79	47.82±35.04

C

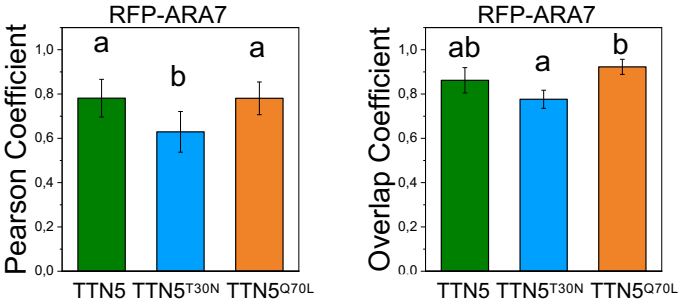

D

Channel		Colocalization	
YFP	mRFP	YFP/mRFP	mRFP/YFP
YFP-TTN5	mRFP-ARA7	58.75±15.69	28.94±11.96
YFP-TTN5^{T30N}	mRFP-ARA7	51.79±8.12	21.21±11.76
YFP-TTN5^{Q70L}	mRFP-ARA7	64.90±6.15	75.05±10.66

Supplementary Figure S8. Colocalization analysis of YFP fluorescent signal with GmMan1-mCherry and mRFP-ARA7 signals in YFP-TTN5, YFP-TTN5^{T30N} and YFP-TTN5^{Q70L} seedlings. Colocalization analyses were conducted with specific markers using ImageJ (Schneider et al., 2012). (A), JACoP-based colocalization analysis (Bolte and Cordelières, 2006). Comparison of Pearson's and Overlap coefficients for *cis*-Golgi-located GmMan1-mCherry with the YFP fluorescence signals of three YFP-TTN5 seedlings in vesicle-like structures. Fluorescent signals colocalized similarly with the *cis*-Golgi marker in YFP-TTN5, YFP-TTN5^{T30N} and YFP-TTN5^{Q70L} seedlings. (B), Object-based analysis was performed for vesicle-like structures based on distance between geometrical centers of signals. YFP fluorescent signal-positive structures overlapped most with GmMan1-mCherry-positive Golgi stacks in YFP-TTN5 compared to YFP-TTN5^{T30N} and YFP-TTN5^{Q70L} seedlings. GmMan1-mCherry-positive Golgi stacks overlapped most with YFP-TTN5^{Q70L}-positive structures followed by YFP-TTN5 and YFP-TTN5^{T30N} signals. (C), JACoP-based colocalization analysis (Bolte and Cordelières, 2006). Comparison of Pearson's and Overlap coefficients for TGN/MVB-located mRFP-ARA7 with YFP fluorescence signals of YFP-TTN5, YFP-TTN5^{T30N} and YFP-TTN5^{Q70L} seedlings in vesicle-like structures. YFP fluorescence signals in YFP-TTN5 and YFP-TTN5^{Q70L} seedlings colocalized similarly with mRFP-ARA7, whereas YFP signals tended to colocalize less in YFP-TTN5^{T30N} seedlings. (D), Object-based analysis was performed for vesicle-like structures based on distance between geometrical centers of signals. More than half of signals corresponding to all YFP-TTN5-positive structures overlapped with mRFP-ARA7-positive structures, in the order YFP-TTN5^{T30N}, YFP-TTN5 and best YFP-TTN5^{Q70L}. mRFP-ARA7-positive structures overlapped most with YFP fluorescence signals in YFP-TTN5^{Q70L} seedlings, while signals were reduced for YFP-TTN5 and YFP-TTN5^{T30N} seedlings by ca. 3.5-fold and 2.5-fold, respectively. Analyses were conducted in three replicates each (n=3). One-way ANOVA with Fisher-LSD post-hoc test was performed. Different letters indicate statistical significance ($p < 0.05$).

Supplementary Video Material S1. YFP fluorescence signals are present in dynamic vesicle-like structures in YFP-TTN5 seedlings. (A-O), Time series of YFP fluorescent signals in dynamic vesicle-like structures of YFP-TTN5, YFP-TTN5^{T30N} and YFP-TTN5^{Q70L} Arabidopsis seedlings (A-L), or *N. benthamiana* leaf epidermal cells (M-O) recorded *via* fluorescence confocal microscopy. (A-C), Fluorescence signals were present in dynamic vesicle-like structures in epidermal cotyledon cells and stomata and in (D-F), in the hypocotyls, Note that mobility of fluorescence signal of YFP-TTN5^{T30N} (E) seedlings differed by a slower or aborted motion in half of the cells compared to (D) YFP-TTN5 and (F) YFP-TTN5^{Q70L}. (G-I), YFP fluorescence signals were present in the dynamic vesicle-like structures in the root hair zone and in root hairs as well. (J-L), but no clear mobility or vesicle-like structures were deciphered in the root tips of YFP-TTN5, YFP-TTN5^{T30N} or YFP-TTN5^{Q70L} seedlings. (M-O), Time series of YFP fluorescence signals together with *cis*-Golgi marker GmMan1-mCherry. GmMan1-positive Golgi stacks showed movement in *N. benthamiana* epidermal cells together with YFP fluorescence upon transient transformation with YFP-TTN5 (M), YFP-TTN5^{T30N} (N) and YFP-TTN5^{Q70L} (O) constructs. GmMan1 is described with a stop-and-go directed movement mediated by the actino-myosin system (Nebenführ 1999) and similarly it might be the case for YFP-TTN5 signals based on the colocalization. Note that mobility of YFP fluorescence and GmMan1-mCherry signal in YFP-TTN5^{T30N} (N) transformed leaf discs differed by a slower or aborted motion compared to YFP-TTN5 (M) and YFP-TTN5^{Q70L} (O). Hence fluorescence signals were present in a comparable manner to Arabidopsis seedlings. Scale bar 50 µm.